# The study of Drosophila melanogaster blue cheese (bchs) function in the involvement of autophagy in neurodegenerative disorders

Sim, Joan Poh Ling

2014

Sim, J. P. L. (2014). The study of Drosophila melanogaster blue cheese (bchs) function in the involvement of autophagy in neurodegenerative disorders. Doctoral thesis, Nanyang Technological University, Singapore.

https://hdl.handle.net/10356/64797

https://doi.org/10.32657/10356/64797

# The Study of *Drosophila melanogaster blue cheese* (*bchs*) Function in the Involvement of Autophagy in Neurodegenerative Disorders

**Sim Poh Ling Joan**

**SCHOOL OF BIOLOGICAL SCIENCES**

A thesis submitted to the Nanyang Technological University in partial fulfillment of the requirement for the degree of Doctor of Philosophy

**2014**

## Acknowledgements

I will like to express my sincere gratitude to my supervisor, Associate Professor Rachel Susan Kraut, for her patient guidance and support. I am also grateful to the post-Doc, Dr. Kathleen Amy Osborne, for the *bchs* mutant fly lines provided in this study. I will like to thank Xu Weixin, George Boo, Yip Kai Lup Bruno, Lim Hong Hwee and Nur Liyanah Zaffre who were undergraduate students for their diligent assistance in this project and joy spread. Last but not least, I am grateful to my parents for their emotional support and forbearance.

## Table of Contents

# List of Figures

## Introduction



## Materials and Methods



## Results

## List of Tables

## Abbreviations

| | |
|---|---|
| aCC | anterior Corner Cell |
| ALFY | Autophagy-linked FYVE |
| AMBRA1 | Activating molecule in Beclin1-regulated autophagy |
| Atg | Autophagy-related |
| Bchs | Blue cheese |
| BEACH | Beige and Chediak Higashi |
| CMA | Chaperone-mediated autophagy |
| CyO | Curly of Oster |
| Elav | Embryonic lethal abnormal vision |
| ESCRT | Endosomal sorting complex required for transport |
| FKBP12 | FK506-binding protein 12 |
| FYVE | Fab1p, YOTB, Vac1p and EEA1 |
| HDAC6 | Histone deacetylase 6 |
| HRP | Horseradish peroxidase |
| Htt | Huntingtin |
| LAMP | Lysosome-associated membrane protein |
| LC3 | Microtubule-associated light chain 3 |
| LIR | LC3-interacting region |
| LRBA | LPS-responsive and beige-like anchor |
| LYST | Lysosomal trafficking regulator |
| NBEA | Neurobeachin |
| NBR1 | Neighbor of BRCA1 gene 1 |
| PAS | Phagophore assembly site |

| | |
|---|---|
| PB1 | Phox and Bem1 |
| PH | Pleckstrin homology |
| PI3K | Phosphatidylinositol 3-kinase |
| PI3P | Phosphatidylinositol 3-phosphate |
| Rab | Ras-related in brain |
| Raptor | Regulatory associated protein of TOR |
| Ref(2)P | Refractory to sigma P |
| Rheb | Ras homologue enriched in brain |
| Rictor | Rapamycin-insensitive companion of TOR |
| RP2 | Raw prawn 2 |
| Sco | Scutoid |
| SNARE | Soluble N-ethylmaleimide-sensitive factor attachment protein receptor |
| SQSTM1 | Sequestosome 1 |
| TOR | Target of rapamycin |
| TSC1/2 | Tuberous sclerosis complex 1/2 |
| UAS | Upstream activation sequence |
| UBA | Ubiquitin-associated |
| ULK1 | Unc51-like kinase 1 |
| Unc | Uncoordinated |
| UPS | Ubiquitin-proteasome system |
| UVRAG | UV irradiation resistance-associated gene |
| Vps | Vacuolar protein sorting |
| yw | yellow white |

## Abstract

Neurodegenerative disorders are becoming an increasing concern in today's aging society whereby cognitive, postural and memory abilities are impaired in sporadic and familial forms of the disorders. Extensive research over the years has generated insights into the patho-physiological mechanisms of proteins implicated in the etiology of these diseases. A common pathological hallmark is the accumulation of cytotoxic protein aggregates in the brain that accompanies neuronal dysfunction and atrophy. The intracellular protein quality control system consists of three main components: chaperone-mediated folding, the ubiquitin-proteasome system, and autophagy. In this study, it is shown that autophagy function is impaired in *Drosophila melanogaster* neurodegenerative mutants in the gene *blue cheese* (*bchs*), and conversely that augmenting autophagy is sufficient to rescue the degeneration. We show this by rescuing neuronal atrophy through rapamycin feeding and *atg7* over-expression. Rapamycin feeding also alleviates the accumulation of ubiquitinated aggregates in neuronal termini of *bchs* motor neurons. Autophagy inhibitors wortmannin and 3-methyladenine in contrast exacerbate neuronal death in *bchs* mutants. In the absence of Bchs protein, Atg5-positive and Atg8-positive autophagic vacuoles are not able to be recruited to ubiquitinated aggregates. Colocalization analysis and live imaging on primary neurons show that Bchs dissociates from Rab11 and associates with Atg5 during Huntingtin Q93 expression. However, there is no effect on the association of Bchs with Atg8 or Spinster, a late endolysosomal marker, in response to the induction of aggrephagy. These findings suggest that Bchs is involved in the early steps of autophagosome formation and recognition of target substrates, in a similar manner as the human homologue Autophagy Linked FYVE (ALFY) protein. Bchs is unlikely to be a motor protein adaptor mediating cargo assembly due to the absence of interaction with dynein or kinesin compared to APP-like interacting protein 1 (Aplip1). Therefore, this study demonstrates that Bchs functions as an adaptor bridging the autophagy machinery to aggregate-prone proteins using a neurodegenerative disease model in *Drosophila melanogaster*.

# 1. Introduction

## 1.1 Aggregate formation in neurodegenerative disorders

The accumulation of cytotoxic protein aggregates intraneuronally is a pathological hallmark observed in many familial early-onset, as well as sporadic age-related neurodegenerative diseases. These include Lewy bodies, which are comprised predominantly of α-synuclein protein, in Parkinson's disease (Spillantini et al., 1998), the observation of neurofibrillary tangles (NFTs) and extracellular amyloid plaques in post-mortem brains of patients with Alzheimer's disease (Price et al., 1991), ubiquitinated inclusion bodies in amyotrophic lateral sclerosis (Bruijn et al., 1998), and expanded poly-glutamine huntingtin aggregates in Huntington's disease (Scherzinger et al., 1997). There are also other examples of the pathological settings in which the development of intracellular aggregates lead to neuronal dysfunction, possibly due to the impairment of normal intracellular trafficking, sequestering of essential metabolites and oxidative damage (Martinez-Vicente and Cuervo, 2007; Wong and Cuervo, 2010). The importance of which protein turnover plays in maintaining the cellular homeostasis cannot be emphasized more in the context of the nervous system, where post-mitotic neurons by virtue of their terminally differentiated state cannot reduce protein load by cell division. Therefore, disorders of protein degradation and misfolding are more frequently seen in the nervous system than anywhere else in the organism. With the increasingly aging population, more people will be susceptible to the debilitating effects of neurodegenerative disorders which inflict one in fifty people over the age of 65 years (Brookmeyer et al., 1998).

## 1.2 Two intracellular proteolytic systems for protein turnover

There are two major proteolytic systems within the cell that are responsible for eliminating damaged or misfolded proteins and organelles, thereby maintaining cellular homeostasis and a dynamic equilibrium of protein levels through degradation **(Figure 1)** (Nedelsky et al., 2008). These are the ubiquitin-proteasome system (UPS) and autophagy, both of which are intracellular catabolic processes with different substrate selectivity and mechanisms of degradation. However, they play an important complementary relationship in coordinating the

cellular response towards stress caused by aberrant protein accumulation (Iwata et al., 2005; Pandey et al., 2007). The UPS is primarily responsible for the degradation of soluble, short-lived proteins and thus provides for the fine-tuning of the steady-state levels of many regulatory proteins (Ciechanover et al., 2000). The UPS also contributes significantly to the degradation of defective misfolded proteins (Glickman and Ciechanover, 2002).

On the other hand, autophagy has been previously considered as an in-bulk catabolic process where cytoplasmic constituents, including insoluble, long-lived proteins and organelles, are delivered to the lysosomes for degradation by hydrolases and cathepsins (Kundu and Thompson, 2008; Levine and Klionsky, 2004). However, this view has since been challenged by evidences which support selectivity in the recognition of autophagic cargo. The first evidence is given by the observation that lysine63-linked polyubiquitinated proteins may serve as the signal to be routed to autophagy for degradation, instead of the conventional lysine48-linked polyubiquitinated proteins for degradation by the UPS (Kirkin et al., 2009b; Tan et al., 2008). The second evidence is provided by the presence of cargo receptors which are able to bind to specific motifs or modifications on substrates and recruit the autophagy machinery in a spatially controlled manner, thus acting as a mechanistic link for selective degradation.

An example is p62, also known as SQSTM1 (sequestosome 1) which binds to polyubiquitinated proteins through the UBA (ubiquitin-associated) domain (Vadlamudi et al., 1996) and promotes their aggregation into p62-positive inclusion bodies through homo-polymerization of the PB1 (Phox and Bem1) domain of p62 (Clausen et al., 2010; Lamark et al., 2003). In addition, p62 is able to recruit LC3 (microtubule-associated light chain 3; mammalian homologue of Atg8), a component of the autophagy machinery, through the LIR (LC3-interacting region) (Pankiv et al., 2007). Another example is NBR1 (neighbor of BRCA1 gene 1) that functions similarly to p62 in facilitating the autophagic degradation of ubiquitinated substrates (Kirkin et al., 2009a; Lamark et al., 2009).

Autophagy plays essential physiological functions in various tissues in the organism and during differentiation and development (Mizushima and Komatsu, 2011; Mizushima et al., 2008). Autophagy can be viewed as an analogy to the remodeling or renewal of cells and it has evolved from a simple adaptive mechanism in response to amino acids deprivation in unicellular yeast

(Noda and Ohsumi, 1998) to a medley of sophisticated roles in higher eukaryotes, including the removal of cytotoxic constituents and invasive pathogens (Birmingham et al., 2006; Bukau et al., 2006), regulation of cell growth and proliferation (Sarbassov et al., 2005), maintenance of genomic stability (Mathew et al., 2007b; Zhao et al., 2012), programmed cell death (Maiuri et al., 2007; Yu et al., 2004), adaptation to metabolic (nutrients and energy) stress (Lum et al., 2005) and lymphocyte development and self-tolerance (Levine et al., 2011). To put it simply, these functions are related to the general health and longevity of the organism and some researchers in the field have touted it to be the elixir against aging (Eisenberg et al., 2009; Rubinsztein et al., 2011). An example can be given by studies of calorie restriction conducted on nematodes, fruit-flies and mice models which extended life-span, and one of the proposed mechanisms is through autophagy (Jia and Levine, 2007; Kapahi et al., 2010). Indeed, other studies have shown that dysregulation of autophagy function contributes to the progression of neurodegenerative disorders, tumorigenesis and resistance to chemotherapy, infectious diseases and other organ-specific proteinopathies (Levine and Kroemer, 2008; Massey et al., 2006; Mizushima and Komatsu, 2011).

### 1.3 Three main categories of autophagy

There are three main categories of autophagy, distinguished by the mode of cargo delivery to the lysosomes. They are macroautophagy, microautophagy and chaperone-mediated autophagy (CMA) **(Figure 1)**. Macroautophagy is characterized by the initial formation of an isolation membrane (also known as phagophore) which surrounds the target cargo, and subsequently seals to form a double membrane vesicle called the autophagosome, thereby sequestering the cytosolic cargo (Dunn, 1990; Mizushima et al., 2001). The autophagosomes later fuse with lysosomes for cargo degradation and this process is important for the recycling of essential metabolites and generation of energy, especially during nutrient deprivation. In addition, macroautophagy helps to eliminate misfolded, aggregated proteins and damaged organelles. Microautophagy also sequesters a portion of the cytosolic region, albeit in a more spatially restricted manner by direct invaginations of the lysosomal membrane which "pinch off" the surrounding cytoplasmic components into the lysosomal lumen. Studies have shown

that microautophagy is responsible for the degradation of peroxisomes (Farre and Subramani, 2004) and like macroautophagy, also participates in constitutive basal levels of autophagy that is important for the maintenance of cellular homeostasis under physiological conditions (Mortimore et al., 1988).

In the case of chaperone-mediated autophagy (CMA), cargos with specific lysosomal targeting motif of the penta-peptide sequence KFERQ (Dice, 1990) are recognized by a complex of cytosolic chaperones, including hsc70 (heat shock cognate 70) (Agarraberes and Dice, 2001), which unfolds and mediates the delivery of these autophagic substrates to the lysosomal membrane receptor, such as LAMP-2A (lysosome-associated membrane protein 2A) (Cuervo and Dice, 1996). The substrate gains access to the lysosomal lumen through a translocation complex formed by several LAMP-2A, thus limiting CMA to soluble proteins which can undergo complete unfolding (Bandyopadhyay et al., 2008). Pathogenic α-synuclein mutations implicated in Parkinson's disease have been linked to the impairment of CMA function (Cuervo et al., 2004), while defective macroautophagy has been linked to several neurodegenerative diseases whereby one of the distinguished morphologies is the accumulation of autophagosomes in the brains of these patients (Rajawat and Bossis, 2008). Interestingly, both of the activities of CMA and macroautophagy decrease with age and when macroautophagy is lacking, CMA activity gets up-regulated as a compensatory mechanism (Cuervo et al., 2005; Kaushik et al., 2008).

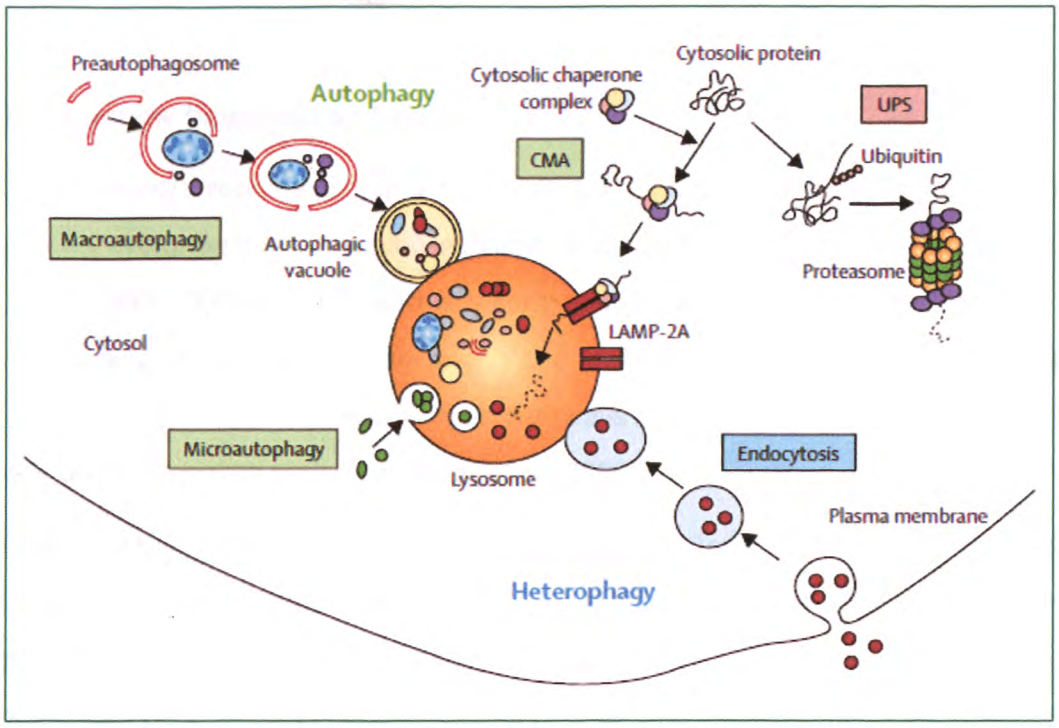


*Reprinted from The Lancet Neurology, 2007, Volume 6, Issue 4, Marta Martinez-Vicente and Ana Maria Cuervo, Autophagy and neurodegeneration: when the cleaning crew goes on strike, Pages 352 – 361, Copyright 2013, with permission from Elsevier.*

**Figure 1.** Proteolytic systems in mammalian cells. Proteins to be delivered to the lysosomes for degradation can originate from within the cell (autophagy) or from the extracellular environment (heterophagy). An example of heterophagy is the process of endocytosis. In the case of autophagy, there are three different modes of cargo delivery to the lysosomes. These are macroautophagy, microautophagy and chaperone-mediated autophagy (CMA). Macroautophagy sequesters the cytosolic cargo through the formation of an isolation membrane that subsequently seals to form the autophagosome and fuses with the lysosome. In microautophagy, substrates are directly internalized through invaginations of the lysosomal membrane. CMA selectively delivers its substrate proteins by binding to the lysosomal membrane receptor (LAMP-2A) and then translocation into the lysosomal lumen. In addition to autophagy, there is another major intracellular proteolytic system: the ubiquitin-proteasome system (UPS). In this pathway, proteins are tagged with lysine48-linked polyubiquitin chains as a signal to be delivered to the proteasome for degradation by this protease.

### 1.4 Autophagosome biogenesis and maturation

The family of serine/threonine protein kinase target of rapamycin (TOR) is an important central effector of an evolutionarily conserved nutrient sensing pathway (Hay and Sonenberg, 2004; Schmelzle and Hall, 2000). The TOR pathway controls cellular growth through diverse metabolic outputs, including protein translation and is the main pathway which negatively regulates autophagy, although there also exists other pathways that modulate autophagy, such as the phospho-inositide signaling pathway (Sarkar et al., 2009).

The different steps in the process of macroautophagy, from induction to the fusion of autophagosome or amphisome (hybrid vesicle of autophagosome and late endosome) with lysosome, have been extensively studied. In particular, the initial organization of the core autophagy machinery at phagophore assembly site (PAS) where the components of this evolutionarily conserved system from yeast, flies, nematodes to mammals (Levine and Klionsky, 2004) have been first characterized from genetic analyses in yeast. Even within macroautophagy, there appears to be selectivity for different substrates, such as mitochondria (mitophagy), portions of the nucleus (nucleophagy), endoplasmic reticulum (reticulophagy), peroxisomes (pexophagy), ribosomes (ribophagy) and microorganisms (xenophagy) (Kundu and Thompson, 2008).

Thirty-five autophagy-related (*Atg*) genes in yeast have been discovered (Nakatogawa et al., 2009) and most of them are conserved in higher eukaryotes. The various steps in macroautophagy (hereafter referred to as autophagy) consist of initiation by signaling kinases, nucleation of the isolation membrane, elongation, closure of the autophagosome, maturation by acidification, fusion with lysosome to form the autolysosome and lastly, cargo degradation **(Figure 2)** (Kawamata et al., 2008; Mizushima et al., 2011; Xie and Klionsky, 2007).

### 1.4.1 Initiation

When insulin signaling is active, the phosphatidylinositol 3-kinase (PI3K) class I phosphorylates phosphatidylinositol 4, 5-bisphosphate (PI(4, 5)$P_2$) to PI(3, 4, 5)$P_3$ which in turn recruits Akt kinase (also known as protein kinase B). Akt phosphorylates and inhibits the tuberous sclerosis complex 1/2 (TSC 1/2). This leads to the removal of inhibition on Ras homologue enriched in brain (Rheb) GTPases, thus enabling it to activate the mammalian TOR complex 1 (mTORC1) (Inoki et al., 2003). mTORC1 is a serine/threonine protein kinase that directly phosphorylates Unc51-like kinase 1 (ULK1; mammalian homologue of yeast Atg1) and another complex member Atg13, thus preventing their stable interaction and consequently causes an inhibition on autophagy (Jung et al., 2009; Kamada et al., 2010; Scott et al., 2007). The ULK1 complex in mammals consists of the serine/threonine protein kinase ULK1, Atg13, FAK family interacting protein of 200 kDa (FIP200) and Atg101 which is formed constitutively regardless of nutrient conditions (Mizushima, 2010). However, when autophagy is induced via the inhibition of mTORC1 during nutrient scarcity or metabolic stress, the ULK1 complex is stabilized through dephosphorylation and subsequently activates downstream effectors, although substrates of ULK1 are not yet conclusive (Cheong et al., 2008).

According to a hierarchical analysis of Atg proteins in the sequence order of autophagosome biogenesis, Atg1/ULK1 is at the most upstream step, indicating its importance in autophagy initiation and regulation of magnitude (Itakura and Mizushima, 2010). One evidence shows that ULK1 phosphorylates AMBRA1 which forms the PI3K class III complex together with vacuolar protein sorting 34 (Vps34), Vps15, Barkor (also known as Atg14L) and Beclin1 (also known as Atg6) (Di Bartolomeo et al., 2010). AMBRA1 interacts with Beclin1 and is required for the translocation of PI3K class III complex to the endoplasmic reticulum (ER) following autophagy induction. This proposed a model whereby ULK1 is involved in the activation of PI3K class III complex for the downstream organization of core autophagy machinery proteins at the phagophore assembly site (PAS) which is closely associated to the ER (Yla-Anttila et al., 2009). Another study shows the myosin light chain kinase (MLCK)-like protein as a substrate of ULK1 and it was hypothesized that this regulates the activation of myosin II which retrieves Atg9 from the PAS to *trans*-Golgi network (TGN) and endosomes where it binds and brings membrane

back to PAS via Atg9 transport factors (Reggiori et al., 2004; Tang et al., 2011). Both sets of evidences lend support that ULK1 is upstream of and activates PI3K class III complex, which produces PI3P, for membrane "flagging" and mediates Atg9 recycling, which is the only transmembrane protein in the autophagy machinery, for membrane recruitment at the PAS. A yeast proteomic microarray study also identifies Atg13, Atg18 (which aids Atg9 recycling) and other factors involved with vesicular transport and function as *in vitro* substrates of Atg1 (Ptacek et al., 2005).

The regulation of ULK1 complex is coordinated by mTORC1 and AMP-activated protein kinase (AMPK). mTORC1 inhibits ULK1 through phosphorylation of serine 757 while AMPK activates ULK1 through phosphorylation of serine 317 and serine 777 (Kim et al., 2011). In addition, AMPK induces autophagy by activating TSC1/2 and directly inhibiting mTORC1 through Raptor phosphorylation, thus leading to ULK1-mediated autophagy initiation (Inoki et al., 2006; Lee et al., 2010a).

### 1.4.2 Nucleation

Nucleation of the isolation membrane requires phosphatidylinositol phosphorylation and this is accomplished by the PI3K class III Vps34 which gives rise to phosphatidylinositol 3-phosphate (PI3P)-enriched sub-domains on ER called omegasomes due to the Ω-like shape and are postulated sites of nucleation (Hayashi-Nishino et al., 2009; Juhasz et al., 2008). Some studies have also shown that the source of autophagic membrane may originate from the ER based on the localization of ER proteins in autophagosomal membrane (Axe et al., 2008; Dunn, 1990). The local production of PI3P at PAS serves as an essential signal for the recruitment of downstream effectors of the autophagy machinery which includes the Atg9 recycling system for membrane supply and the two ubiquitin-like conjugation systems for membrane elongation (Noda et al., 2010b).

There are two distinct PI3K class III complexes present both in yeast and mammalian cells that may perform different functions in autophagy and vacuolar protein sorting (VPS) in yeast or endocytic trafficking in mammals (Itakura et al., 2008; Kihara et al., 2001; Zhong et al., 2009). In

yeast, the components of complex I include Vps34, Vps15, Atg6 and Atg14 and is responsible for autophagy while the complex II consisting of Vps34, Vps15, Atg6 and Vps38 is responsible for the sorting of carboxypeptidases and aminopeptidases to lytic vacuoles (Kihara et al., 2001). Similarly, the core complex in mammals that consists of Vps34, Vps15, Beclin 1 (homologue of Atg6) is able to associate with different binding partners, such as the Atg14 homologue Barkor, to induce autophagosome formation and the Vps38 homologue UVRAG (UV irradiation resistance-associated gene), for endolysosomal transport and autophagosome maturation (Itakura and Mizushima, 2009; Kang et al., 2011). Barkor (or Atg14L) localizes to ER and is required for the targeting of PI3K class III complex to ER (Matsunaga et al., 2010).

### 1.4.3 Elongation

Elongation of the phagophore occurs through two ubiquitin-like conjugation systems (Geng and Klionsky, 2008; Ohsumi, 2001). The E1-like activating enzyme Atg7 and E2-like conjugating enzyme Atg10 brings Atg12 to Atg5 (E3-like ligase) which then binds to Atg16L to form the Atg12-Atg5-Atg16L multimeric complex (Kuma et al., 2002). This E3-like ligase complex facilitates membrane dynamics through the homo-polymerization of Atg16L and the covalent modification of microtubule-associated protein light chain 3 (LC3; mammalian homologue of Atg8) with phosphatidyl-ethanolamine (PE) (Hanada et al., 2007). The Atg12-Atg5-Atg16L complex dissociates from the membrane upon formation of the autophagosome (Mizushima et al., 2003).

At the same time, unprocessed LC3-I is cleaved at its C-terminus by the cysteine protease Atg4 (Tanida et al., 2004), which then undergoes a second conjugation system by Atg7 and another E2-like conjugating enzyme Atg3 to prime LC3-I for lipidation by Atg5, thereby forming LC3-II (LC3-PE) (Ichimura et al., 2000; Kabeya et al., 2000). Subsequently, LC3-II is recruited to the autophagic membrane and contributes to its expansion (Nakatogawa et al., 2007). LC3-II remains associated with autophagosomes on both inner and outer membranes just before their fusion with lysosomes when Atg4 may cleave and release LC3 into the cytosol from PE on the

outer membrane (Kirisako et al., 2000). Therefore, Atg8/LC3 is being widely used as an autophagosomal marker (Mizushima et al., 2004).

### 1.4.4 Maturation and degradation

The maturation of autophagosomes requires acidification and their fusion with lysosomes to form autolysosomes or via an intermediate compartment amphisome (Berg et al., 1998) which arises from the fusion of autophagosome and endosome. The endosomal sorting complexes required for transport (ESCRTs) are involved in the formation of multi-vesicular bodies (MVBs) and it was found that ESCRTs are needed for the maturation of the endocytic and autophagy pathways (Slagsvold et al., 2006; Williams and Urbe, 2007). Mutation studies in ESCRTs implicate both of these pathways in the proper removal of ubiquitinated protein aggregates in neurodegenerative diseases (Fader and Colombo, 2009; Filimonenko et al., 2007; Lee et al., 2007a), suggesting that the process of autophagosome maturation and fusion with lysosomes is regulated by endocytic trafficking-dependent factors. Indeed, recent studies have shown that SNARE proteins, which mediate specific membrane fusion between different vesicles, also participate in the fusion of endosomes or lysosomes to autophagosomes (Nair et al., 2011). In particular, the SNARE protein syntaxin 17 (Stx17) was identified to localize onto the outer membrane of completed autophagosomes for the targeting to the endocytic-lysosomal pathway (Itakura et al., 2012).

In addition, for selective autophagic clearance of ubiquitinated substrates under conditions of basal (also known as quality-control) autophagy, the microtubule-associated ubiquitin-binding histone deacetylase 6 (HDAC6) is required for the recruitment of cortactin which participates in F-actin polymerization, thereby facilitating autophagosome-lysosome fusion (Lee et al., 2010b). It is interesting to note that the up-regulation of autophagy in response to proteasomal inhibition is HDAC6-dependent (Pandey et al., 2007), while HDAC6 is not required for starvation-induced autophagy (Lee et al., 2010b), further supporting the role of HDAC6 as a mediator of quality-control autophagy. After the successful delivery and fusion to lysosome, the inner membrane of autophagosome together with sequestered cargoes are degraded by

hydrolases and cathepsins present within the lysosomal lumen (Tanida et al., 2005). Essential metabolites are recycled back into the cytosol through permeases present on lysosomal membrane and the restoration of lysosome homeostasis is achieved by autophagic lysosome reformation (ALR) following starvation-induced autophagy that requires re-activation of mTOR kinase localized on lysosomes (Korolchuk et al., 2011; Rong et al., 2011).

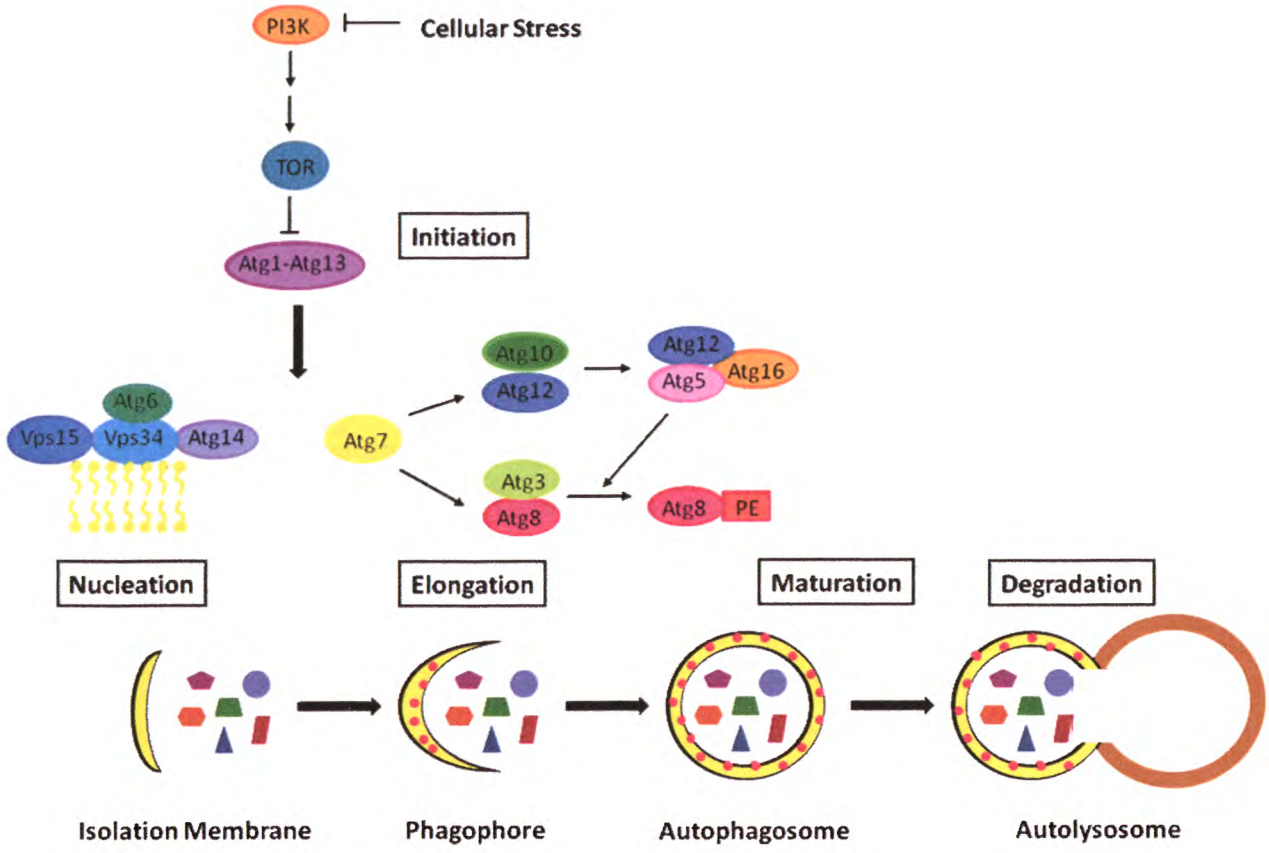


**Figure 2.** The process of autophagy. The steps involved in autophagy include initiation, nucleation, elongation, maturation and degradation. Autophagy is induced during conditions of cellular stress like starvation, oxidative stress, presence of intracellular pathogens, misfolded proteins and damaged organelles (Ginet et al., 2009). Inhibition of TOR, the main negative regulator of the rate-limiting Atg1 complex, leads to the initiation of autophagosome formation. Activation of the Vps34 complex, a PI3K class III lipid kinase, results in the production of phosphatidylinositol 3-phosphate (PI3P) which then enables nucleation of the isolation membrane. Elongation of the phagophore requires two ubiquitin-like conjugation systems. The two ubiquitin-like molecules Atg12 and Atg8 are processed by a common E1-like activating enzyme Atg7 and two E2-like conjugating enzymes Atg10 and Atg3 respectively to form the Atg12-Atg5-Atg16 E3-like ligase which can covalently attach phosphatidyl-ethanolamine (PE) to Atg8. The Atg12-Atg5-Atg16 multimeric complex and Atg8-PE contributes to membrane dynamics and elongation through Atg16 oligomerization and lipid anchor of Atg8-PE (shown by pink dots in membrane). Subsequently, the enclosed double-membrane

autophagosome carrying cytosolic cargoes matures through acidification and fusion with the lysosome, thereby leading to enzymatic lysis and metabolites turnover.

### 1.5 Selective autophagy

Once viewed as an in-bulk cellular digestion during starvation-induced autophagy to cope with metabolic stress, this conception has since changed and more studies have demonstrated that the autophagy mechanism acquires various adaptations to accommodate specialized functions in cells. Although autophagy remains as an autonomous function, it participates in the removal of cytotoxic constituents and invasive microbes (Birmingham et al., 2006; Bukau et al., 2006), regulation of cell growth and proliferation (Sarbassov et al., 2005), maintenance of genomic stability (Mathew et al., 2007b; Zhao et al., 2012), programmed cell death (Maiuri et al., 2007; Yu et al., 2004), adaptation to metabolic (nutrients and energy) stress (Lum et al., 2005) and lymphocyte development and self-tolerance (Levine et al., 2011). In order to perform all these roles, the core autophagy machinery needs to be equipped with receptors and adaptors that selectively recognize and interact with different target substrates **(Figure 3)**.

The most well-characterized example of selective autophagy is the cytoplasm-to-vacuole targeting (Cvt) pathway in *Saccharomyces cerevisiae* (Lynch-Day and Klionsky, 2010). The yeast vacuole is the equivalent of metazoan lysosome. Atg19 is the autophagy receptor for precursor aminopeptidase 1 (prApe1) that is delivered to the vacuole to be converted into the mature form (Scott et al., 2001). Besides binding to the target substrate, Atg19 also interacts with Atg8 on autophagic membrane to bring the phagophore in close proximity to the substrate (Noda et al., 2010a; Shintani et al., 2002). In addition, Atg19 interacts with the adaptor, Atg11, which associates with and recruits components of the core autophagy machinery proteins such as Atg1 and Atg9 so as to act in concert with Atg8 for the formation of autophagosomes around sequestered cargoes (He et al., 2006; Yorimitsu and Klionsky, 2005). Therefore, the autophagy receptor and adaptor function cooperatively to link the autophagy machinery to target substrates for sorting or degradation.

In yeasts, the turnover of peroxisomes and mitochondria is mediated by pexophagy and mitophagy respectively (Nakatogawa et al., 2009). The autophagy receptor responsible for binding to peroxisomes is Atg36 while that for mitochondria is Atg32 (Kanki et al., 2009; Motley et al., 2012). Both receptors also interact with Atg8 and Atg11, of which Atg11 recruits Atg1 and Atg9 that are involved in the nucleation of isolation membrane while Atg8 facilitates membrane elongation (Motley et al., 2012; Okamoto et al., 2009). As illustrated in this model system, the selectivity of organelle autophagic degradation is accomplished via different specific receptors for target ligands. Likewise, in mammalian cells, for aggregate-prone proteins such as expanded poly-glutamine Huntingtin (polyQ Htt) and hyper-phosphorylated tau in Alzheimer's disease that are modified by ubiquitination, the receptor for these cargoes is p62 (also known as SQSTM1; sequestosome 1) which is itself a target substrate for autophagy (Geetha and Wooten, 2002). In addition, p62, NDP52 (nuclear dot protein 52 kDa) and OPTN (optineurin) also bind to ubiquitinated bacteria and LC3 for the sequestration of invading microbes (Mostowy et al., 2011; von Muhlinen et al., 2012; Wild et al., 2011). Autophagy-linked FYVE (ALFY) protein has been identified as the adaptor for p62 and recruits Atg5 and PI3P to the site of autophagosome formation around ubiquitinated aggregates (Clausen et al., 2010; Filimonenko et al., 2010).

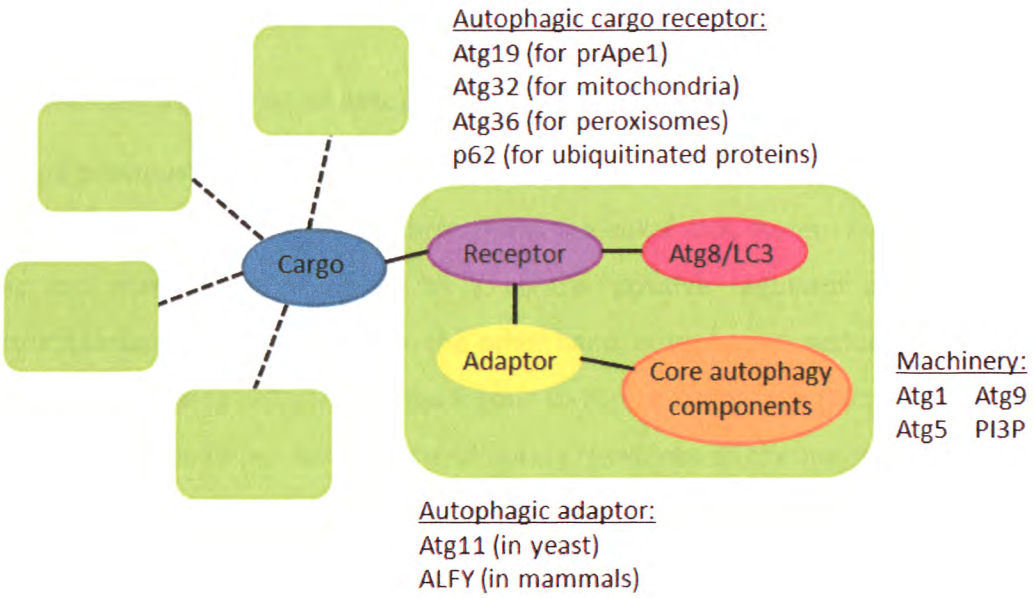


**Figure 3.** The mechanism of selective autophagy. The autophagic receptor recognizes and binds to specific motifs or modifications on cargo destined for delivery to the lysosome. In addition, the receptor interacts with Atg8/LC3 on autophagic membrane through the Atg8-family interacting motif (AIM) or LC3-interacting region (LIR) to bring the phagophore in close proximity to the sequestered cargo. In order to recruit other components of the core autophagy machinery to the site of autophagosome formation, the receptor also needs to associate with the adaptor which acts as a scaffolding protein for the organization of autophagy-related proteins and lipids. Therefore, the interactions mediated by autophagic cargo receptor and adaptor enable the autophagy machinery to function cooperatively in a targeted manner at the site of autophagosome biogenesis.

### 1.6 TOR-dependent regulation of autophagy

As described previously, the activation of TOR pathway inhibits autophagy induction and this regulation is evolutionarily conserved throughout the eukaryotic system in yeasts, nematodes, fruit flies and mammals that serves as a central positive regulator of cell growth and proliferation (Sarbassov et al., 2005). On the other hand, autophagy functions in an antagonistic role in that it suppresses cell growth (analogous to tumor-suppressing activity) and promotes cell survival (analogous to pro-tumor survival during resistance to chemotherapeutic treatment) in response to various insults (Levine and Klionsky, 2004; Mizushima et al., 2008). Thus, especially in the context of tumor initiation and progression, autophagy plays a complex dual role (Degenhardt et al., 2006; Kondo et al., 2005; Mathew et al., 2007a). The presence of extracellular growth factors, such as insulin-like growth factor (IGF), binds to their respective membrane receptors and triggers the activation of class I PI3K/Akt pathway. Akt (also known as protein kinase B) phosphorylates TSC2, thereby destabilizing the TSC1/2 heterodimer and leading to its inactivation (Inoki et al., 2002). This relieves the inhibition on Rheb which is a small GTPase, enabling the phosphorylation and activation of TORC1 (Garami et al., 2003). As a result, autophagy induction is suppressed due to the phosphorylation of Atg1-Atg13 complex which destabilizes the interaction (Chang and Neufeld, 2009).

TORC1 consists of TOR, Raptor (regulatory-associated protein of TOR) and GβL (G-protein β-subunit like protein) while TORC2 comprises TOR, Rictor (rapamycin-insensitive companion of TOR), GβL, Sin1 (SAPK-interacting protein 1) and PRR5 (proline-rich protein 5) (Wullschleger et al., 2006). In contrast to TORC1 which responds towards growth factors and nutrients, TORC2 responds towards growth factors but seems to be nutrient-insensitive (Kim and Guan, 2011). When amino acids are plentiful, this signals to the small GTPases Rag A and Rag C which in turn activate TORC1 (Kim et al., 2008; Sancak et al., 2008). Both types of TOR complexes have different downstream cellular targets. The main effects of TORC1 activation are an increase in protein synthesis through targets on the mRNA translational machinery and ribosome biogenesis, coupled with an inhibition on the autophagy pathway. On the other hand, TORC2 regulates the actin cytoskeleton through the activation of PKC (protein kinase C) and also impinges on cell growth mediated by TORC1 through the activation of Akt (Ikenoue et al., 2008;

Jacinto et al., 2004). However, it is still unclear whether TORC2 inhibits autophagy. Based on the activation of a group of AGC kinases (a family of kinases including protein kinases A, G and C), it is likely that TORC2 inhibits autophagy because PKA (cAMP-dependent protein kinase A) was found to phosphorylate and inhibit the stable assembly of Atg1-Atg13 complex, thus disrupting the localization to PAS (Budovskaya et al., 2004; Jacinto and Lorberg, 2008; Stephan et al., 2009).

In addition to the inhibitory phosphorylations on Atg1 by TORC1, it was found in *Drosophila* genetic studies that the over-expression of Atg1 inhibits TORC1 signaling while the disruption of Atg1 leads to increased TORC1 activity (Lee et al., 2007b; Scott et al., 2007). This serves as a self-reinforcing feedback loop between TORC1 and Atg1 so that the initially small changes in signaling of nutrient status can be stabilized and amplified. Interestingly, the downstream substrate of TORC1, S6K (p70 ribosomal S6 kinase) was shown to promote autophagy possibly via a positive regulation on the translation machinery for autophagy-related proteins and can provide negative feedback to the insulin signaling pathway through phosphorylation of IRS1 (insulin receptor substrate 1) (Lawrence and Brown, 1993; Shah et al., 2004). Therefore, the requirement of S6K for autophagy balance ensures that the induction of autophagy level is not excessive under conditions of prolonged TORC1 inhibition or starvation which may otherwise cause cell death and that during physiological conditions when TORC1 is activated, a basal level of autophagy is maintained.

### 1.7 TOR-independent regulation of autophagy

Despite that the TOR signaling regulatory arm of autophagy has been well-studied, other mechanisms and pathways have emerged which regulate the various steps of the autophagy process in a TOR-independent manner. The calcium-dependent cysteine protease calpain is a negative regulator of autophagy by its cleaving and activation of the G-protein $G_s$ which leads to a greater adenylyl cyclase activity and cAMP production (Williams et al., 2008). As a result, the cAMP-dependent protein kinase A (PKA) phosphorylates and inactivates the Atg1-Atg13 complex, thereby preventing its localization to the PAS (Budovskaya et al., 2004; Stephan et al., 2009). Calpain also cleaves Atg5 directly to promote apoptosis in response to cytotoxic agents (Yousefi et al., 2006). Therefore, pathways which increase inositol 1,4,5-triphosphate ($IP_3$) levels and thus elevate cytosolic calcium levels released from ER stores by binding to $IP_3$ receptors can promote calpain activity and block autophagy (Sarkar et al., 2009).

When the intracellular AMP:ATP ratio is high, AMP-activated protein kinase (AMPK) is triggered and acts as the central energy sensor in order to modulate several metabolic outputs which serve to cope with the energy demand (Hardie, 2007). One of the targets of AMPK is the autophagy pathway that can recycle essential metabolites from macromolecules for ATP production (Singh and Cuervo, 2011). This corresponds with previous reports which show that low cAMP levels and thus high AMP levels promote autophagy (Meley et al., 2006; Sarkar et al., 2009). In addition to activating TSC2 which consequently suppresses TORC1 activity, AMPK directly phosphorylates Raptor on serine 792 that will lead to TORC1 inactivation (Lee et al., 2010a). It was also found that both AMPK and TORC1 coordinately phosphorylates ULK1 (Unc51-like kinase 1; mammalian homologue of yeast Atg1) on different sites depending on nutrient conditions, resulting in varying ULK1 activity (Kim et al., 2011). Under low glucose levels, AMPK phosphorylates ULK1 on serine 317 and serine 777 which leads to ULK1 activation while during nutrient sufficiency, TORC1 phosphorylates ULK1 on serine 757 which disrupts the interaction between AMPK and ULK1.

At the 6$^{th}$ International Symposium on Autophagy (ISA, Okinawa) 2012, Dr. Beth Levine reported that the haplo-insufficient tumor suppressor and autophagy-related protein Beclin 1 (mammalian homologue of yeast Atg6) can undergo inhibitory phosphorylations by mitogenic

signals in an mTOR-independent manner. This causes alterations in the associations of Beclin 1 with positive or negative regulators of autophagy, such that oncogene-driven transformation is promoted (decreased autophagy) and resistance towards chemotherapy against these oncogenes is induced (increased autophagy). An example is given by Akt, which is upstream of mTOR and phosphorylates Beclin 1 on serine 234 and serine 295, thereby contributing to Akt-mediated tumorigenesis via autophagy suppression (unpublished data from Dr. Beth Levine). In addition, it was proposed that the interaction of Beclin 1 with the multi-partner scaffolding protein 14-3-3 renders autophagy inactive.

Autophagy not only results in protein turnover but is also involved in the regulation of lipid metabolism through macrolipophagy (Singh et al., 2009). Besides leading to the accumulation of protein aggregates, defective autophagy leads to the accumulation of lipofuscin granules and lipid droplets in hepatic cells, mainly because the liver is the major organ responsible for intracellular lipid storage (Mizushima and Komatsu, 2011; Xiong et al., 2012). Conversely, lipids in the five main classes – glycerolipids, phospholipids, fatty acids, sphingolipids and sterols – have been directly implicated in the control of autophagy at various steps in the pathway (Dall'Armi et al., 2013; Knaevelsrud and Simonsen, 2012). Predominant importance has been focused on PI3P which is required at PAS for the nucleation of isolation membrane; however studies in recent years have shed light on the role of other lipid species in signal transduction, effector recruitment, covalent modification of protein and imparting physico-chemical properties to lipid bilayers. Upon stimulation by growth factors, phosphatidylinositol 4,5-bisphosphate ($PI(4,5)P_2$) in the plasma membrane is phosphorylated into phosphatidylinositol 3,4,5-triphosphate ($PI(3,4,5)P_3$) by the class I PI3K and activates phosphoinositide-dependent kinase 1 (PDK1) which in turn suppresses autophagy through TORC1 signaling (Yang and Klionsky, 2010). On the other hand, the generation of PI3P by class III PI3K acts as a localized signal at PAS for the recruitment of downstream effectors of the autophagy machinery which organizes at these PI3P-enriched regions (Simonsen and Tooze, 2009).

The elongation of phagophore membrane requires Atg8-PE and phosphatidylethanolamine (PE) is covalently conjugated onto Atg8 by the Atg12-Atg5-Atg16 E3-like ligase complex (Hanada et al., 2007; Xie et al., 2008). In addition, PE is produced in mitochondria from phosphatidylserine

(PS) and it was proposed that one of the sources for autophagic membrane originates from the mitochondria (Hailey et al., 2010). The different shapes of lipids, such as phosphatidic acid, ceramide and lysophosphatidylcholine, facilitate membrane curvature of different dynamics so as to promote membrane fusion or budding (Haucke and Di Paolo, 2007). In the sphingolipids class, both sphingosine 1-phosphate and ceramide activates autophagy (Bedia et al., 2011). Ceramide induces autophagy by inhibiting Akt, down-regulation of nutrient transporters and promoting jun N-terminal kinase 1 (JNK1) –mediated dissociation of the Bcl 2-Beclin 1 complex, while sphingosine 1-phosphate can inhibit TORC1 directly (Guenther et al., 2008; Lavieu et al., 2006; Pattingre et al., 2009; Scarlatti et al., 2004). Cholesterol is required for the organization of microdomains within lysosomal membranes that enables the efficacy of chaperone-mediated autophagy (CMA) and autophagosome-lysosome fusion (Kaushik et al., 2006; Koga et al., 2010). However, an excessive level of cholesterol or other lipids can impair CMA function as demonstrated in hepatocytes of mice fed with a high-fat diet in a similar manner to aging, possibly due to the disruption of LAMP-2A localization on lysosomal membranes (Navarro and Cuervo, 2012; Rodriguez-Navarro et al., 2012).

### 1.8 *Drosophila melanogaster* as a model organism for neurodegenerative disorders

*Drosophila melanogaster* has helped to accelerate our understanding of human neurodegenerative diseases, although as an invertebrate organism, the complexity of its nervous system is much lower than that of other vertebrate counterparts such as the mouse model (Marsh and Thompson, 2006). The major advantages of using the fly model, in addition to its inexpensive maintenance, short life-cycle and life-span, are the small, fully-characterized, generally non-redundant genome (165 Mb, 4 chromosomes, 13890 genes) and the abundance of available genetic modification tools to investigate *in vivo* functions at both the cellular and tissue levels. The life-cycle duration lasts for 12 days at 25°C and the developmental stages comprise of embryo (1 day), first instar larva (1.5 day), second instar larva (2 days), third instar larva (2 days), early to late pupa (4.5 days) and pharate adult (1 day, prior to eclosion from pupal exoskeleton) (Ashburner et al., 2005). The life-span of adult fruit flies is approximately 40 days at 25°C. This greatly facilitates genetic screens and target validation, which in equivalent mammalian models would be prohibitively time-consuming.

Tools are available to "humanize" fruit flies through the transgenic expression of human disease proteins in specific tissues using the binary system of Gal4 transcriptional activator and UAS (upstream activation sequence) site (Rorth, 1996). Poly-glutamine repeat diseases, Alzheimer's disease, Parkinson's disease and tauopathies have been effectively investigated in *Drosophila melanogaster* model (Feany and Bender, 2000; Greeve et al., 2004; Shulman and Feany, 2003; Warrick et al., 1998). In addition, the intracellular pathways are highly conserved with vertebrates, whereby 75% of disease-associated human genes have a *Drosophila* orthologue (Reiter et al., 2001). Thus, loss-of-function mutations can also be utilized to characterize the phenotypic effects of specific genes.

### 1.9 Mutations in *bchs* lead to ubiquitinated aggregates in CNS

Previous studies presented direct evidence of progressive neuronal atrophy and accumulation of insoluble, ubiquitinated aggregates in the adult central nervous system (CNS) of *Drosophila melanogaster blue cheese* (*bchs*) mutants (Finley et al., 2003; Kraut et al., 2001). In addition, the

study performed by Finley and co-workers shows that *bchs* mutants exhibit a significantly reduced adult life-span in comparison to wild-type controls. This age-related phenomenon is also seen in human neurodegenerative disorders and therefore, the *bchs* gene provides a novel, important mechanism to study how the accumulation of inclusion bodies is generated in a pathological setting which will consequently cause a loss of neuronal homeostasis and result in cellular dysfunction using a genetically tractable model organism as a tool.

### 1.9.1 Characterization of Bchs protein

The *bchs* gene encodes a large protein of 3489 amino acids in length, with an approximate molecular weight of 390 kilo Daltons (kDa). The sequence of this gene shows evolutionary conservation from nematodes to vertebrates by exhibiting an approximate 41% identity in nearly 2500 amino acids of the N-terminus region and 60-85% identity in the last 1000 amino acids of the C-terminus region **(Figure 4)** (Finley et al., 2003; Khodosh et al., 2006). The N-terminus does not contain readily identifiable functional domains. However, this region is leucine/isoleucine rich and modeling programs have suggested the presence of leucine zippers and coiled-coil domains (Simonsen et al., 2007). The C-terminus encodes four highly conserved identifiable domains which are the PH (pleckstrin homology), BEACH (Beige and Chediak Higashi), five WD40 repeats and FYVE (Fab1p, YOTB, Vac1p and EEA1) domains.

The PH domain binds to several phosphoinositides (for example, phosphatidylinositol 4,5-bisphosphate and phosphatidylinositol 3,4,5-triphosphate) and is present in several regulatory proteins involved in the compartmentalization of downstream signaling targets to specific sites in membranes (Alberti, 1998; Ma et al., 1997). The BEACH family consists of five classes of novel, interesting proteins that play a main function in membrane trafficking, in particular lysosomal transport (De Lozanne, 2003; Wang et al., 2002). Members of this family include LYST (lysosomal trafficking regulator) (Barbosa et al., 1996; Nagle et al., 1996), LRBA (LPS-responsive and beige-like anchor) (Wang et al., 2004) and NBEA (neurobeachin) (Wang et al., 2000) in mammals, LvsB in *Dictyostelium* (Wang et al., 2002), Bchs (blue cheese) in *Drosophila* (Finley et al., 2003; Khodosh et al., 2006), and ALFY (autophagy-linked FYVE protein) in human (Simonsen

et al., 2004). The WD40 domain promotes the formation of multi-protein complexes through protein-protein interactions (Neer et al., 1994), while the FYVE domain is responsible for binding to phosphatidylinositol 3-phosphate (PI3P) implicated in vesicular trafficking (Misra et al., 2001). Expression of both *Drosophila* Bchs and murine ALFY (Wdfy3) are enriched in the CNS, but not restricted to this tissue (Khodosh et al., 2006). In addition, the subcellular localization of Bchs is found to be mostly cytoplasmic in neurons and concentrated as punctate vesicular compartments in synaptic terminals (Finley et al., 2003; Khodosh et al., 2006).

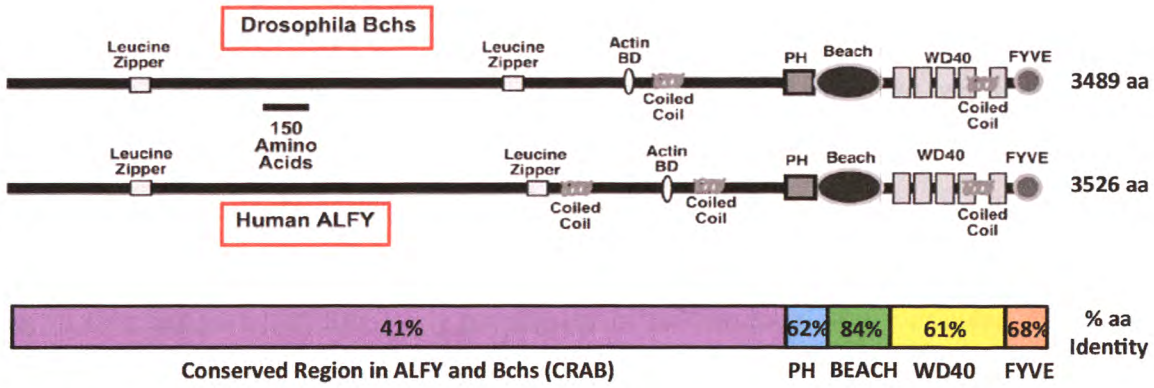


*Reproduced and modified with permission from Genetics, 2007, Volume 176, Issue 2, Anne Simonsen, Robert Cumming, Karine Lindmo, Vanessa Galaviz, Susan Cheng, Tor Erik Rusten and Kim Finley, Genetic modifiers of the Drosophila blue cheese gene link defects in lysosomal transport with decreased life span and altered ubiquitinated protein profiles, Pages 1283 – 1297.*

**Figure 4.** Evolutionary conservation of *Drosophila bchs* gene across divergent phyla. Translated amino acid sequences of the inferred *bchs* gene in *Drosophila melanogaster* and ALFY in human were aligned for comparison of the level of amino acid identity. It is noted that the overall size, identifiable protein domains located at the C-terminus and amino acid sequences are conserved throughout the region of the protein, although the first nearly 2500 amino acids of the conserved region in ALFY and Bchs (CRAB) exhibit a lesser degree of identity. This is in contrast to the last 1000 amino acids of the C-terminus where the protein domains (especially BEACH domain) show higher percentages of identity.

### 1.9.2 Functional studies of Bchs

Mutations in the *bchs* gene resulted in the development of characteristic neurological abnormalities similar to that exhibited in other *Drosophila* and human neurodegenerative disease models. This includes the progressive age-dependent accumulation of ubiquitinated inclusions throughout the adult CNS of *bchs* mutants which is not present in age-matched wild-type controls, subsequently leading to elevated neuronal apoptosis and general brain atrophy (Finley et al., 2003).

Two studies have been reported that implicated *bchs* in the regulation of synaptic morphogenesis. The first study showed that over-expression of Bchs in larval motor neurons led to morphological changes in the neuromuscular junction (NMJ) synapses (Kraut et al., 2001), while the second study established the genetic interactions between *bchs* and *rab11* (a known regulator of vesicle transport) in the control of synaptic bouton density (Khodosh et al., 2006), lending further support that Bchs may participate in the modulation of vesicular and protein trafficking pathways. Bchs is antagonistic to Rab11 which suppresses synapse development and it is possible that Bchs acts as a positive regulator of synaptogenesis via the autophagy pathway because the latter was shown to promote synapse development (Shen and Ganetzky, 2009).

Defects in the lysosomal trafficking pathway have been linked to altered ubiquitinated protein profiles, progressive age-related disorders and reduced viability (Cataldo et al., 1996; Cuervo, 2004; Hofmann and Falquet, 2001), suggesting that Bchs function may intersect with this pathway. In a genetic modifier screen conducted by Simonsen and co-workers, it was found that the Bchs gain-of-function rough eye phenotype was modified by mutations in selective endocytic and autophagic trafficking genes, cytoskeleton and motor proteins, ubiquitin and SUMO signaling pathways (Simonsen et al., 2007). The postulation that Bchs may be involved in lysosomal trafficking is augmented through another study where it was found that *bchs* mutations led to disruptions in the transport of endolysosomal compartments along motor neuron axons, causing a net reverse in direction of lysosomes from anterograde to retrograde transport and an overall reduction in endolysosomal vesicle mobility (Lim and Kraut, 2009).

*bchs* mutations also result in the reduced survival of motor neurons which are examined in third instar larvae using a GFP reporter expressed specifically in a subset of motor neurons (Lim and Kraut, 2009). It was recently discovered by Dr. Kathleen Osborne in Rachel Kraut's laboratory that three splice isoforms of *bchs* exist (manuscript submitted). These isoforms may be differentially affected by two *bchs* alleles, *bchs17(M)* and *bchs58(M)*, which are used in this study. *bchs17(M)* and *bchs58(M)* are derived from *bchs17(O)* and *bchs58(O)* respectively via mobilization of an intronic enhancer P (EP) element. A table listing the different types of *bchs* mutations, molecular lesions, genetic classification and phenotypes is shown on the following page **(Table 1)**.

| Allele Name | Molecular Lesion | Genetic Classification | Phenotypes |
|---|---|---|---|
| *EP2299* | EP element inserted into the first intron of *bchs* UTR | Over-expression in the presense of a driver; Neomorph | - Rough eye due to loss of photoreceptor cells (with GMR driver) in adult flies (Khodosh et al., 2006; Simonsen et al., 2007) |
| | | | - Accumulation of ubiquitinated inclusions in CNS, neuronal atrophy and shortened life-span in adult flies (Finley et al., 2003) |
| *bchs17(O)* | Derived from EMS screen in *EP2299*; non-sense mutation of G → A at nt. 10983 and stop codon at Trp2640 | Hypomorph due to disruption of the longest and intermediate *bchs* isoforms, leaving the smallest intact **(Figure 17)**; presence of a driver may OE dominant negative truncant(s) | - Reduced synaptogenesis at larval NMJs (Khodosh et al., 2006) |
| | | | - Reduced larval motor neuron survival (observed by Dr. Kathleen Osborne) |
| | | | - Endolysosomal trafficking in larval motor axons not examined |
| *bchs58(O)* | Derived from EMS screen in *EP2299*; 3 bases addition at nt.8552 and subsequent 17 bases deletion which causes a frame shift; change of 33 amino acids from aa.1831-1863 and stop codon at aa.1864 | Hypomorph due to disruption of the longest *bchs* isoform **(Figure 17)**; presence of a driver may OE a dominant negative truncant | - Reduced larval motor neuron survival (Lim and Kraut, 2009) |
| | | | - Accumulation of predominant ubiquitinated aggregates in larval NMJs (in this study) |
| | | | - Endolysosomal trafficking defect in larval motor axons (Lim and Kraut, 2009) |
| *bchs17(M)* | Derived from *bchs17(O)* via mobilization of EP element | Hypomorph due to disruption of the longest and intermediate *bchs* isoforms, leaving the smallest intact | - Reduced larval motor neuron survival (in this study) |
| | | | - Accumulation of predominant ubiquitinated aggregates in larval NMJs (in this study) |
| *bchs58(M)* | Derived from *bchs58(O)* via mobilization of EP element | Hypomorph due to disruption of the longest *bchs* isoform | - Reduced larval motor neuron survival (in this study) |
| | | | - Accumulation of predominant ubiquitinated aggregates in larval NMJs (in this study) |

**Table 1.** A description of the molecular lesions, genetic classification and observed phenotypes (both published in literature and reported in this study) of various *bchs* mutations which are used herein.

### 1.9.3 Functional studies of ALFY

Useful insights into the possible functions of Bchs can be provided by its human orthologue ALFY (autophagy-linked FYVE protein) **(Figure 5)**. Interestingly, the *ALFY* (also known as *WDFY3*; NCBI gene ID 23001) locus maps to a genomic region (on chromosome 4) associated with several cases of familial neurodegenerative disorders (Finley et al., 2003). ALFY is ubiquitously expressed in mouse tissue, with highest levels found in the brain (Simonsen et al., 2004). Upon amino acids starvation or treatment with a proteasome inhibitor on HeLa cells, ALFY relocalizes from the nuclear envelope to cytoplasmic structures containing ubiquitinated aggregates and autophagic membranes (Simonsen et al., 2004). This provided the first hint that ALFY may be involved in autophagic degradation of proteins. Subsequently, further evidence showed that ALFY and p62 interact to promote the clearance of p62-positive ubiquitinated aggresomes, and the formation of p62 bodies is dependent on ALFY in HeLa cells (but note that in the same paper, the authors reported the accumulation of Ref(2)P-positive, ubiquitin-positive structures in *bchs* mutant adult brains which perhaps could be due to residual Bchs function from alternatively spliced isoforms or due to different cell types) (Clausen et al., 2010). The turnover of p62 alone does not require ALFY, suggesting that the removal of p62 by itself may be via a different regulatory mechanism independent of ALFY (Clausen et al., 2010). In fact, p62 can bind to LC3 directly via the LC3 interacting region (LIR), unlike ubiquitinated substrates which require an autophagic adaptor.

Another line of evidence in *Drosophila* model demonstrated the accumulation of Ref(2)P, homologue of p62, which is colocalized with ubiquitinated inclusions in *bchs* mutant adult brains, further supporting the role of Bchs/ALFY in autophagic clearance of ubiquitinated aggregates (Clausen et al., 2010; Nezis et al., 2008). In addition, it was found that ALFY acts as an adaptor protein by interacting with Atg5-Atg12-Atg16L E3-like ligase complex through its WD40 domain, binds to p62 through its PH-BEACH domain (Clausen et al., 2010), and also recruits PI3P-containing autophagic membrane through its FYVE domain, thereby sequestering the autophagy machinery around aggregate-prone proteins to form the cargo-bound autophagosome (Filimonenko et al., 2010). However, both ALFY and Bchs do not seem to be essential for starvation-induced autophagy as knock-down of ALFY or mutations in Bchs do not

inhibit the formation of autolysosomal structures in response to nutrient starvation (Filimonenko et al., 2010).

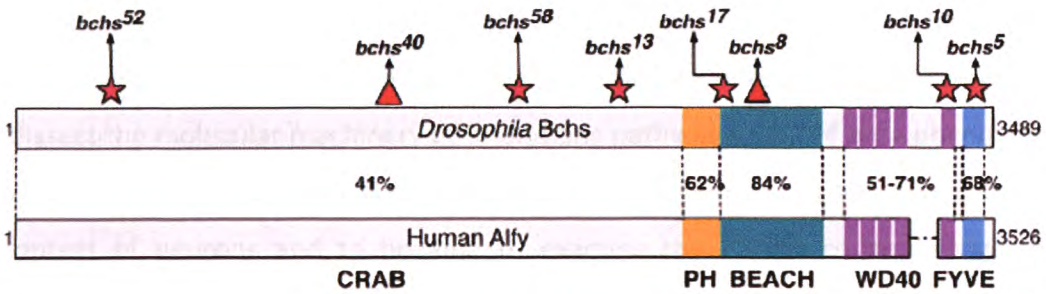


*Reproduced with permission from Development, 2006, Volume 133, Issue 23, Rita Khodosh, Adela Augsburger, Thomas Schwarz and Paul Garrity, Bchs, a BEACH domain protein, antagonizes Rab11 in synapse morphogenesis and other developmental events, Pages 4655 – 4665.*

**Figure 5.** Conservation of amino acid sequences between *Drosophila* Bchs and human ALFY. The PH, BEACH, five WD40 repeats and FYVE domains at the C-terminus exhibit a high level of amino acid identity in both *Drosophila* Bchs and human ALFY, as illustrated by the percentages between the relevant domains. The conserved region in ALFY and Bchs (CRAB) at the N-terminus also displayed a considerable level of amino acid identity, albeit to a lesser degree. Both proteins have a similar size of approximately 3500 amino acids. Different *bchs* mutant alleles affecting various domains in Bchs are generated from an EMS (ethyl methanesulfonate) screen in the *EP2299* line and are indicated at the top whereby stars represent non-sense mutations and triangles represent mis-sense mutations.

### 1.10 Objectives of study

The objectives of this study are to investigate the relationship between Bchs and autophagy pathway in the etiology of neurodegenerative diseases using a genetically tractable model organism, *Drosophila melanogaster*, in which exists a vast array of genetic and *in vivo* biology tools to dissect the molecular machinery or interacting pathways. First of all, a phenotypic assay was developed in order to examine the presence of genetic interactions between *bchs* and *atg7* in the context of neurons and to be able to examine the effects of modulation on *bchs* degenerative phenotype by pharmacological agents that affect the autophagy pathway. Secondly, it would be interesting to investigate where these ubiquitinated aggregates are localized subcellularly in primary neurons of *bchs* mutant and their distribution in *bchs* whole larval motor neurons. Thirdly, the relevance of Bchs in the recruitment of different compartmental vesicles, namely pre-autophagosome (Atg5 marker), autophagosome (Atg8 marker), recycling endosome (Rab11 marker) and late endolysosome (Spinster marker), will be investigated under two branches of autophagy stimulation, non-selective versus selective autophagy, as there may be a stimulus-dependent regulation to Bchs function. Conditions of nutrient starvation and TORC1 inhibition by rapamycin are examined under non-selective autophagy while expanded polyQ Htt expression is examined under selective autophagy. Fourthly, the potential involvement of motor proteins with Bchs in the regulation of cargo transport will be studied through co-immunoprecipitation assays and live imaging techniques will be employed to investigate the intracellular trafficking of GFP-Bchs with RFP-Atg5 or mCherry-Atg8 compartments in larval primary neurons.

# 2. Materials and Methods

## 2.1 Fly culture

The fly stocks were maintained on standard cornmeal food (recipe from Temasek Life Sciences Laboratory, Singapore) at 20°C, and experiments with flies were performed on semi-defined food (recipe from Bloomington Drosophila Stock Center, USA) at 25°C. The stocks used in this study are:

| Category | Genotype | Source |
|---|---|---|
| Control | *Canton S* | Bloomington Drosophila Stock Center, Indiana University, USA |
| | *yw* | BDSC, Indiana University, USA |
| Gal4 Drivers | *C155-elav* | BDSC, Indiana University, USA |
| | *RRaCD8GFP* | From Miki Fujioka, Thomas Jefferson University, USA |
| *bchs* Mutants | *yw; EP(2L)2299* | From Pernille Rorth, IMCB, Singapore |
| | *yw; bchs58(O)* | From Rita Khodosh, Harvard Medical School, USA |
| | *yw; bchs58(M)* | Isolated in Rachel Kraut's lab, NTU-SBS, Singapore |
| | *yw; bchs17(M)* | Isolated in Rachel Kraut's lab, NTU-SBS, Singapore |
| | *yw; Df(2L)clot7 / CyKrGFP* | BDSC, Indiana University, USA |
| *atg* Mutants | *yw; EPgy2 Atg7[EY10058]* | BDSC, Indiana University, USA |
| | *w; Atg7[d77] / CyO-GFP* | From Thomas Neufeld, University of Minnesota, USA |
| | *yw; UAS-Atg1[6A]* | From Thomas Neufeld, University of Minnesota, USA |
| Upstream Activation Site (UAS) Transgenes | *yw; +; UAS-mCherry-Atg8a* | From Thomas Neufeld, University of Minnesota, USA |
| | *yw; +; UAS-RFP-Atg5* | From Katja Köhler, ETH Zurich, Switzerland |
| | *w; +; UAS-Spinster-GFP* | From Sean Sweeney, University of York, UK |
| | *w; UAS-Rab11-GFP* | From Henry Chang, Purdue University, USA |
| | *w; UAS-Htt exon1-Q20* | From Larry Marsh, University of California, USA |
| | *w; UAS-Htt exon1-Q93* | From Larry Marsh, University of California, USA |
| | *w; UAS-dicer2* | Vienna Drosophila RNAi Center, Austria |
| | *w; UAS-bchsRNAi (45028)* | VDRC, Austria |
| | *w; UAS-bchsRNAi (110785)* | VDRC, Austria |
| | *w; UAS-GFP-Bchs* | Isolated in Rachel Kraut's lab, NTU-SBS, Singapore |

**Table 2.** A compendium of *Drosophila melanogaster* stocks categorized into allele functions that are used in this study and their respective sources are indicated.

### 2.2 Genetic crossing scheme for homologous recombination

In order to recombine *atg7[EY]* P-element insertion (*yw; EPgy2 Atg7[EY10058]*, Bloomington Drosophila Stock Center, Indiana University, USA) with *bchs58(M)* mutation on the second chromosome, virgin female flies of both genotypes were mated with the reciprocal males to generate trans-heterozygotes. Meiotic recombination events occur in the germline of only females and thus, virgin female flies from this progeny were mated to males of a balancer stock (*w; Sco/CyO; MKRS/TM6B*). Subsequently, potential male progeny candidates that successfully carry both *atg7[EY]* and *bchs58(M)* on the same chromosome were selected based on their eye color which should be the highest in orange-red intensity due to the presence of *mini-white* gene markers on P-element insertion. Every meiotic recombination event is unique and each single male fly which carries a potential recombination event was back-crossed individually to the balancer stock in order to generate a stable line **(Figure 6)**. Verification for positive recombinants was performed using primers-specific polymerase chain reaction (PCR) to detect for the presence of the two alleles in genomic DNA extracted from each single male recombinant candidate. The same process was repeated for sets of homologous recombinations between *bchs58(M)* and *atg7[d77]*, *bchs17(M)* and *atg7[EY]*, *bchs17(M)* and *atg7[d77]*, *UAS-bchsRNAi (45028)* and *UAS-dicer2*. Please refer to Appendix **(Table 3)** for specific primer pair sequences to detect each allele.

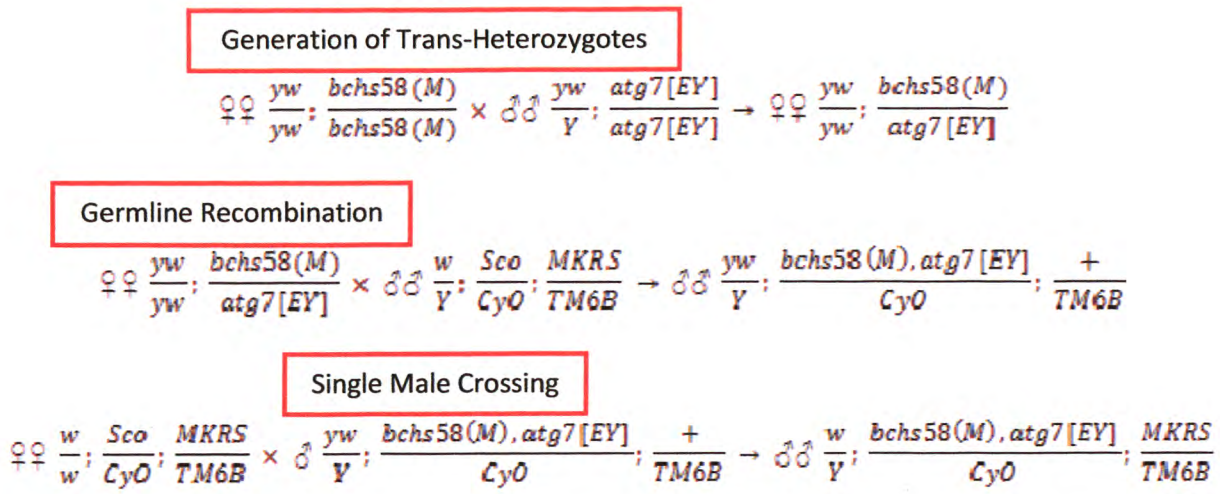


**Figure 6.** A genetic crossing scheme for homologous recombination using *bchs58(M)* and *atg7[EY]* alleles as an example. Positive recombinants were verified by primers-specific PCR. ♀♀ females, ♂♂ males.

### 2.3 Fly genomic DNA extraction and PCR

Each single male recombinant candidate was squished separately in 20 µL of extraction buffer (10 mM Tris-HCl pH 8.0, 25 mM NaCl, 1 mM EDTA and 200 µg/mL proteinase K) for about 20 seconds, followed by incubation at 37°C for 30 minutes to degrade proteins. Proteinase K (Promega, USA) was then heat inactivated at 95°C for 5 minutes. PCR was performed using 2 uL of the extracted genomic DNA template and the GoTaq® Hot Start Polymerase reaction kit (Promega, USA) in a total reaction volume of 20 µL according to manufacturer's instructions. The sets of primers used to verify the alleles in each recombination scheme are shown in **Table 3** of the Appendix. DNA gel electrophoresis or sequencing (1st BASE, Singapore) was subsequently applied to detect positive recombinants.

### 2.4 Reverse-transcription PCR of *atg7* alleles

80 adult fly heads were dissected from each genotype and 400 µL of TRIzol® reagent (Life Technologies, CA, USA) was added into each sample for homogenization. Phase separation was then performed using chloroform : TRIzol® of 1 : 5 ratio to extract total RNA from the aqueous phase. The RNA samples were purified using Direct-zol™ RNA MiniPrep (Zymo Research, CA, USA) as per the manufacturer's instructions and stored at -80°C until further application. First-strand cDNA synthesis was carried out on 3 µg of purified total RNA with the *atg7* gene-specific primer 5' GCGAATCTGTGAGCAGAAAG 3' or poly-dT primer by using GoScript™ Reverse Transcription System (Promega, WI, USA) following the manufacturer's instructions. A 25 µL PCR reaction volume was proceeded on each cDNA sample by using the GoTaq® polymerase (Promega, WI, USA) and respective primer sets for 35 cycles. For *atg7* cDNA: 5' TCCGCAGACGGATTGATCTC 3' and 5' TGAACATCGATGACAGCCTTG 3'. For *rp49* cDNA: 5' AGTCGGATCGATATGCTAAG 3' and 5' AGTAAACGCGGTTCTGCATG 3'.

### 2.5 Co-immunoprecipitation assay

400 µg of fresh (not frozen) protein lysates from adult heads of the respective genotypes were incubated in a final volume of 800 µL IP buffer (50 mM Tris-HCl, 100 mM NaCl, 0.5% Triton X-100 and 10 mM EDTA, pH 7.5) containing 20 µL of protein A/G Plus-agarose beads (according to manufacturer's instructions) (sc-2003, Santa Cruz Biotechnology, USA) for each sample with the following antibody dilutions separately – 1:2000 rabbit anti-Bchs (gift of Kia Zinn and Rachel Kraut), 1:1000 mouse anti-Flag (M2 clone, Sigma Aldrich, MO, USA), 1:1000 rabbit total IgG and 1:1000 mouse total IgG (Sigma Aldrich, MO, USA) – overnight at 4°C with gentle rocking. During this step, cOmplete protease inhibitors and PhosSTOP phosphatase inhibitors (Roche Diagnostics, Singapore) were added according to manufacturer's instructions. The immunoprecipitates were collected by centrifugation at 800x g for 5 minutes at 4°C and supernatant was discarded. The pellet was then washed with 1 mL of IP buffer and centrifuged as above. This step was repeated for a total of 4 times and the final pellet was resuspended in

20 µL of Laemmli buffer (50 mM Tris-HCl, 2% (w/v) SDS, 10% (v/v) glycerol, 5% (v/v) β-mercaptoethanol and 0.005% (w/v) bromophenol blue, pH 6.8).

### 2.6 SDS-PAGE and Western blotting

Heads from ten days old adult flies and third instar larval brains were lysed in cold buffer (50 mM Tris-HCl pH 7.5, 1% (v/v) Triton X-100, 150 mM NaCl, 0.1% (w/v) SDS and 5 mM EDTA) containing cOmplete protease inhibitors and PhosSTOP phosphatase inhibitors (Roche Diagnostics, Singapore) and then centrifuged at 15,000x g for 10 minutes at 4°C. The supernatant was transferred into a new tube and stored at -80°C for not more than three months or used subsequently for SDS-PAGE (polyacrylamide gel electrophoresis). Bradford assay (Bio-Rad Laboratories, Singapore) was used for protein quantification and 30 µg of protein was loaded for each well. The SDS-PAGE was run at 120 Volts, followed by "wet transfer" onto 0.2 µm (pore size) polyvinylidene fluoride (PVDF) membrane (Bio-Rad Laboratories, Singapore) at 100 Volts for one hour. The membrane was blocked with 5% (w/v) non-fat milk for one hour and then incubated with the respective primary antibodies, 1:2000 rabbit anti-Bchs (gift of Kia Zinn and Rachel Kraut) or 1:500 mouse anti-β-actin (sc-47778, Santa Cruz Biotechnology, USA) or 1:5000 mouse anti-dynein (P1H4, gift of Tom Hays) or 1:2000 rabbit anti-kinesin (AKIN01, Cytoskeleton, USA) overnight at 4°C. The secondary antibodies used are horseradish peroxidase (HRP)-conjugated goat anti-rabbit (Jackson ImmunoResearch Laboratories, USA) and HRP-conjugated goat anti-mouse (Jackson ImmunoResearch Laboratories, USA) antibodies, both in a dilution of 1:10,000 and incubated for one hour at room temperature. The membranes were washed with 0.05% (v/v) Tween-20 in Tris-buffered saline (TBS) and Immobilon Western Chemiluminescent HRP Substrate (Millipore, USA) was used for detection on Kodak X-ray film development station.

### 2.7 Three-dimensional (3D) larval brain volume measurements

Flies of respective genotypes were grown on semi-defined food with food dyes added in order to distinguish late third instar larvae through lightening of their mid-gut color due to a discontinuation in feeding and progressive digestion. Brains were dissected from the larvae, fixed with 4% (w/v) paraformaldehyde in 100 mM PBS for 20 minutes, stained with 1:2000 tetramethyl rhodamine iso-thiocyanate (TRITC)-conjugated phalloidin (Sigma Aldrich, MO, USA) in PBS containing 0.2% (v/v) Triton X-100 overnight at 4°C, washed and mounted in 90% glycerol (containing 100 mM propyl gallate) onto microscopy slides with spacers and cover-slips. Confocal image stacks of the specimens were acquired using the Carl Zeiss LSM710 microscope with set parameters of pinhole size: 3 AU; PMT gain: 450; laser (561 nm) power: 15%; z-interval: 12 µm; EC Plan-Neofluar 10x/0.3 NA objective lens.

Gebiss (Ground Truth Editing and Benchmarking for Image Stack Segmentation) was developed by Dr. Janos Kriston-Vizi (Bioinformatics Image Core, University College London, UK) as an ImageJ plugin (Abramoff et al., 2004) for semi-automated 3D image segmentation which can be used either as a ground truth (GT) in performance evaluation of image segmentation algorithms or in image analysis. Besides ImageJ installation, Gebiss requires a Java3D installation for spatial visualization. An alternative to the standard ImageJ is FIJI (Schindelin, 2008) which contains Java3D as part of a package. The Gebiss installation itself consists of downloading three .jar files (gebiss.jar, ij-plugins_toolkit_bii.jar and ImageJ_3D_ Viewer_bii.jar) into the "plugin" folder of ImageJ, after which a "Gebiss" submenu appears automatically in the plugin menu of ImageJ.

Gebiss is run after an 8-bit grayscale microscopy image stack is opened. The spatial voxel (3D pixel) dimensions can be imported automatically from the .LSM file or set manually in ImageJ. "Object-based GT Specification" tab is chosen and the whole brain image stack is segmented into foreground and background voxels by a seeded 3D region growing algorithm (Adams and Bischof, 2002) after the x-, y-, z-coordinates of the seed voxel (which has the brightest intensity) and a minimum threshold value of 23 (8-bit image, grayscale values of 0-255) have been specified **(Figure 7)**. The 3D object counter plugin in ImageJ is subsequently used for volume measurements of the segmented image stack in units of cubic micron ($\mu m^3$) dimension. For validation of the optimal minimum threshold value for segmentation, the ImageJ macro for GT

contour visualization is performed on two image stacks, the original RGB and the segmented binary stacks. Unpaired Student's t-test was used as the statistical tool to calculate *p* significance value in comparison between *bchs* (loss-of-function and over-expressing) brains and respective age-matched genetic background control brains.

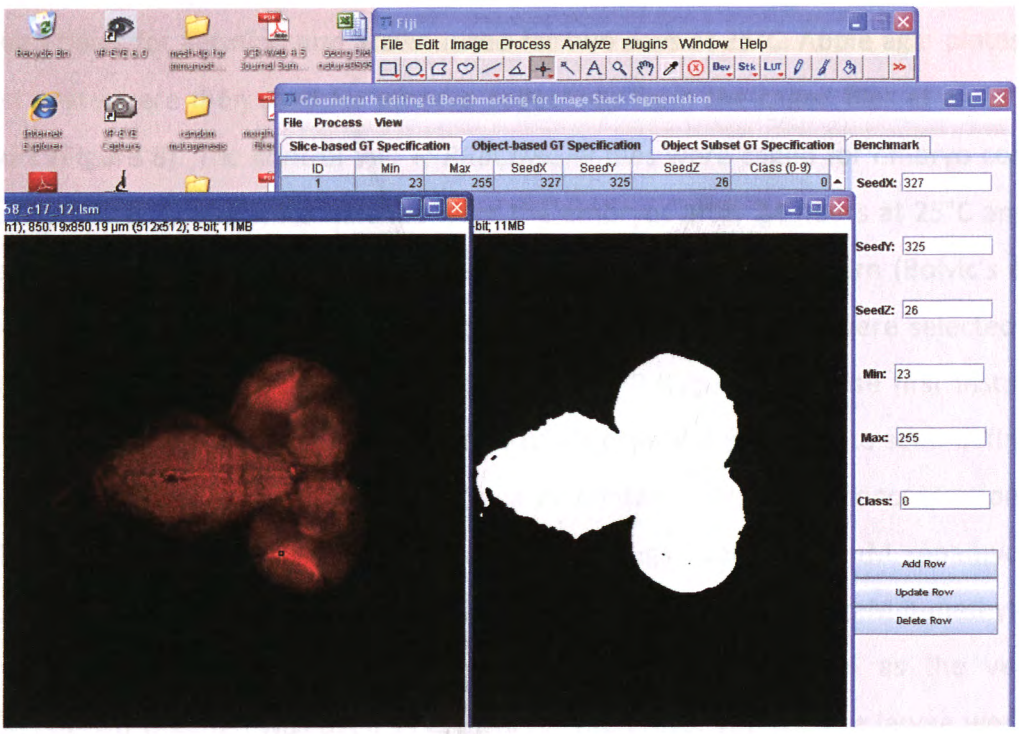


**Figure 7.** The user interface of Gebiss (ImageJ plugin) for 3D image segmentation of late third instar larvae brains. The tab for "Object-based Ground Truth (GT) Specification" is selected for 3D object segmentation of the original image stack (left window, larval brain labeled with TRITC-conjugated phalloidin in red) into a binary stack (right window) that is composed of foreground (white) and background (black) voxels (3D equivalent of pixels) after the x-, y- and z-coordinates of the seed voxel with the highest brightness intensity and the optimal minimum threshold value are specified in the options panel shown on the extreme right. The optimal minimum threshold is found to be 23 through reiterative validations of different threshold values and the default maximum threshold is 255 for an 8-bit image. After performing 3D image segmentation, the brain volume measurement can then be analyzed using the 3D object counter plugin.

### 2.8 Feeding of autophagy-modulating drugs by first to third instar larvae

Virgin female flies of the genotypes *yw; bchs58(O); RRaCD8GFP* (or *yw; bchs58(M); RRaCD8GFP* or *yw; bchs17(M); RRaCD8GFP*) and *yw; Df(2L)clot7/CyKrGFP; RRaCD8GFP* were crossed to the reciprocal males and flies from these two sets of crosses were caged separately in transparent holders with holes for aeration and acclimatized for two days at 25°C. Apple agar plates spread with yeast paste were then used for embryo collections from the caged flies at an interval of three hours **(Figure 8)**. The control *yw; +; RRaCD8GFP* flies were caged for embryo collections similarly. First instar larvae were hatched from the embryos after 24 hours at 25°C and larvae which do not express green fluorescent protein (GFP) in the tissue pattern (Bolvic's organ in first instar larvae) driven by the *Krüppel* promoter (Casso et al., 1999) were selected for the desired genotype *yw; bchs58(O)/Df(2L)clot7; RRaCD8GFP* **(Figure 9)**. These first instar larvae and those from the control were picked gently with forceps and placed onto semi-defined food in 2.0 mL eppendorf tubes that have been prepared containing different concentrations of the drugs. The concentrations of autophagy-modulating drugs used are 1 µM rapamycin (A.G. Scientific, USA), 0.2 µM and 2 µM wortmannin (A.G. Scientific, USA) and 5 mM 3-methyladenine (Calbiochem, USA). Semi-defined food containing 0.05% (v/v) ethanol as the vehicle of rapamycin and wortmannin was used as control for the drugs. The feeding larvae were grown into wandering third instar larvae, followed by dissection and immunohistochemistry of the nervous system.

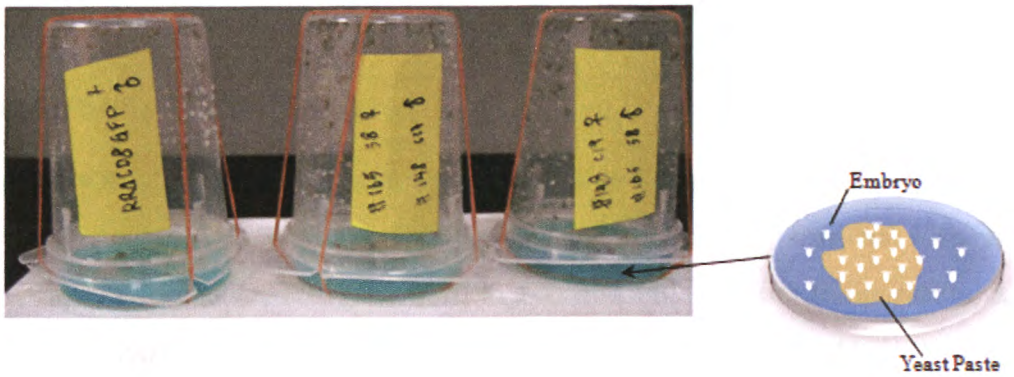


**Figure 8.** Caging of flies for embryos collection. Virgin female flies and males for the respective genetic crosses were contained in transparent holders with holes for aeration and acclimatized for two days at 25°C before the start of collections for laid embryos at every interval of three hours. Apple agar plates spread with yeast paste were used as the bottom vessels for collecting embryos oviposited by the female flies.

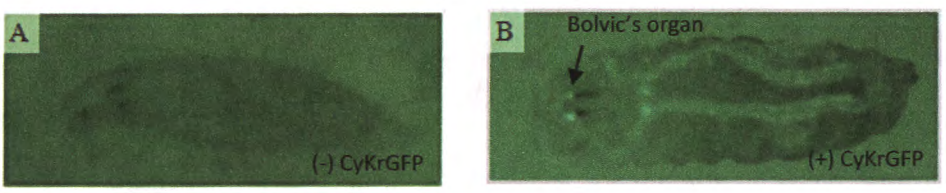


**Figure 9.** Differentiating the *CyKrGFP* (Curly of Oster, Krüppel-Gal4 driver, UAS-GFP) balancer chromosome marker in first instar larvae. **A)** Selection of a *bchs* null larva from the cross of *yw; bchs58(O); RRaCD8GFP* × *yw; Df(2L)clot7/CyKrGFP; RRaCD8GFP* based on the absence of GFP expression driven by the *Krüppel* promoter in Bolvic's organ. **B)** A *yw; bchs58(O)/CyKrGFP; RRaCD8GFP* larva is negatively selected due to the presence of GFP in Bolvic's organ.

### 2.9 RP2 motor neuron viability assay

Third instar larvae of desired genotypes (please refer to **Table 4** of Appendix) were dissected and immunohistochemistry was performed by 30 minutes of fixation with 4% (w/v) paraformaldehyde (Sigma Aldrich, MO, USA) in 100 mM PBS at room temperature, 1 hour of blocking with 5% (w/v) bovine serum albumin (BSA) (PAA Laboratories, MA, USA) in 0.1% (v/v) Triton X-100 PBS, overnight incubation at 4°C with primary antibodies of 1:500 rabbit anti-GFP (Clontech Laboratories, CA, USA), 1:10 mouse 1D4 anti-fasciclin II and 1:20 mouse 22C10 anti-futsch (Developmental Studies Hybridoma Bank, The University of Iowa, IA, USA). On the next day, washing was done with 0.1% (v/v) Triton X-100 PBS at an interval of 10 minutes (total 5 times). Secondary antibodies incubation was performed with 1:800 Cy2-conjugated goat anti-rabbit and 1:800 Cy3-conjugated goat anti-mouse (Jackson ImmunoResearch Laboratories, PA, USA) for 2 hours at room temperature. Washing was done with 0.1% Triton X-100 PBS at an interval of 10 minutes (total 4 times) and 15 minutes (total 3 times). The specimens were mounted in 90% glycerol (containing 100 mM propyl gallate) onto microscopy slides with 0.17 mm thickness glass cover-slips and viewed under 20x objective lens in a Nikon TE2000-S epifluorescence microscope. RP2 viability was scored by the presence of Cy2 fluorescence signal at muscle 2 where RP2 motor neuron innervates in each larval hemi-segment and the percentage of RP2 survival over total hemi-segments scored was calculated for each experimental set which was repeated for triplicates. Chi-square statistical test was performed for the *p* value.

### 2.10 Quantitative size analysis of ubiquitinated aggregates in larval NMJs

Wild-type control and *bchs* mutant third instar larvae were dissected **(Figure 10)**, fixed with 4% (w/v) paraformaldehyde (Sigma Aldrich, MO, USA) in 100 mM PBS for 30 minutes at room temperature and blocked with 5% (v/v) normal goat serum (Life Technologies, CA, USA) in 0.1% (v/v) Triton X-100 PBS for 1 hour. Primary antibody incubation was performed overnight at 4°C with 1:1000 mouse anti-ubiquitinated conjugates (clone FK2, Enzo Life Sciences, NY, USA) antibody. On the next day, washing was done with 0.1% Triton X-100 PBS at an interval of 10 minutes (total 5 times). Secondary antibodies incubation was performed with 1:800 Cy5-conjugated goat anti-mouse and 1:500 Cy2-conjugated goat anti-HRP (Jackson ImmunoResearch Laboratories, PA, USA) for 2 hours at room temperature. Washing was done with 0.1% Triton X-100 PBS at an interval of 10 minutes (total 4 times) and 15 minutes (total 3 times). The specimens were mounted in 90% glycerol (containing 100 mM propyl gallate) onto microscopy slides with cover-slips and image stacks of larval NMJ at muscle 2 were acquired under 40x objective lens (N.A. = 1.35) using the DeltaVision OMX® microscope (Applied Precision, WA, USA) with softWoRx® 5.0 for image deconvolution. To measure the area of ubiquitinated aggregates, particle analysis from ImageJ was used (Schneider et al., 2012). The measurement scale (in micrometers) was defined for the 8-bit image projection from Cy5 channel and the image segmentation was adjusted to a threshold of grayscale value 70, followed by conversion to a binary image. The region of interest (ROI) was marked using the rectangular selection tool and the function of 'Analyze Particles' was performed to measure the area of particles within ROI. Particle size was categorized into three groups: 0 – 1 $\mu m^2$, 1.1 – 10 $\mu m^2$ and 10.1 – 50 $\mu m^2$. The percentages of NMJs with ubiquitinated aggregates in each of the three groups were calculated for each experimental set which was repeated for triplicates. Chi-square statistical test was performed for the *p* value.

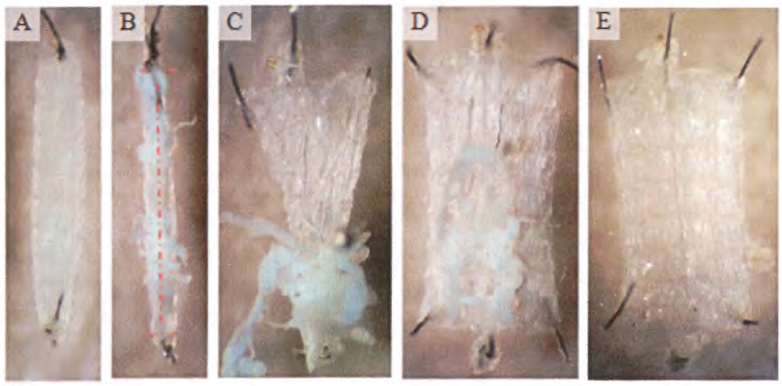


**Figure 10.** Sequential order of open-book dissection to obtain the larval peripheral nervous and muscular systems. **A)** A third instar larva is pinned down on both ends with the ventral side facing upwards on a Sylgard® silicone support. **B)** Incisions are made along the ventral midline of the larva and at both ends. **C)** The cut ends are opened up and corners are pinned down for anchorage. **D)** The larval cuticle wall is stretched out fully. **E)** The internal organs (mid-gut, fat bodies, salivary glands etc.) are discarded, while leaving the muscular and peripheral nervous tissues intact.

### 2.11 Primary neuron culture from third instar larval brains

This protocol is modified from the previous study of Kraft and co-workers (Kraft et al., 2006). 22 mm x 22 mm acid-washed glass cover-slip was coated with 30 µg/mL of mouse laminin (BD Biosciences, NJ, USA) and 167 µg/mL of concanavalin A (Sigma Aldrich, MO, USA) dissolved in sterile water onto a 35 mm diameter culture dish (Corning, MA, USA). The selected larvae (please refer to **Table 4** of Appendix for genotypes) were washed with 90% (v/v) ethanol for three times and sterile water for two times to remove food debris and microbial contaminants. To isolate primary neurons for each culture dish, four third instar larval brains were extracted in Shields and Sang, bacto-peptone and yeast extract (Sigma Aldrich, MO, USA) culture medium containing penicillin-streptomycin and antibiotics-antimycotics (PAA Laboratories, MA, USA) on a dissection plate. The brains were washed and decanted with sterile hemolymph-like 3 (HL3) saline (70 mM NaCl, 115 mM sucrose, 5 mM trehalose, 5 mM KCl, 20 mM $MgCl_2$, 1 mM $CaCl_2$, 10 mM $NaHCO_3$, 5 mM HEPES, pH 7.4) for three times and then incubated with 0.5 mg/mL of

collagenase type 1 (Sigma Aldrich, MO, USA) in HL3 for one hour at room temperature. Subsequently, the enzymatically digested brain tissues was washed and decanted three times with complete culture medium including 10% (v/v) heat-inactivated foetal bovine serum (HyClone, Thermo Fisher Scientific, MA, USA), 20 µg/mL of bovine pancreas insulin (Sigma Aldrich, MO, USA), 2% (v/v) fly extracts, penicillin-streptomycin and antibiotics-antimycotics. The brain tissues was dissociated into a final volume of 150 µL single cells suspension by trituration with complete medium for three rounds and then aliquoted onto the coated cover-slip in culture dish. On the next day, 900 µL of complete medium was added to the culture dish and primary neurons were incubated at room temperature (25°C) for 3 – 4 days to allow for attachment and the growth of neurite processes **(Figure 11)**.

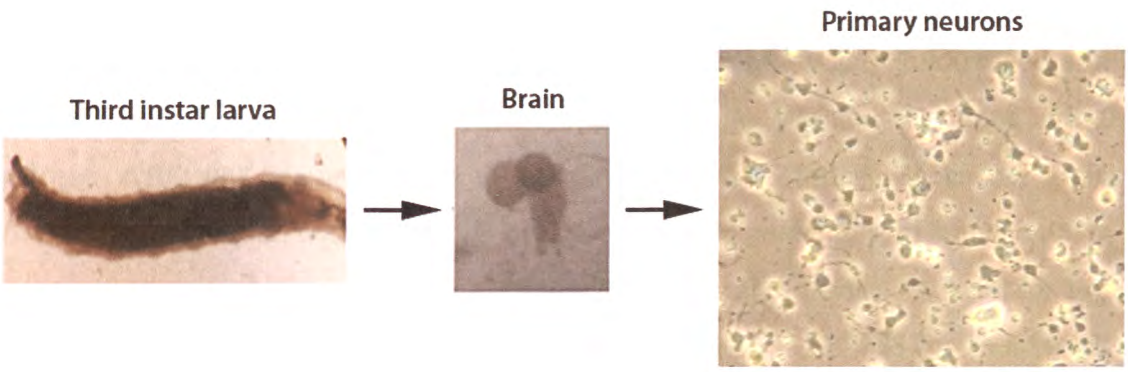


**Figure 11.** Work-flow of the primary culture of neurons from third instar larval brains. The third instar larvae were washed off food debris and other dirt thoroughly before extracting the brains in basal medium containing antibiotics and antimycotics. After digesting the extracellular matrix with collagenase, the brain tissue was dissociated into cells and plated onto coated glass cover-slips in culture dish. On the third day of culture, neurites can be seen extending from attached cells, most of which are bipolar interneurons.

### 2.12 Quantitative colocalization analysis of Bchs with different compartmental markers

The primary neurons were induced for autophagy in each of the three different conditions separately: five hours of nutrient starvation with HL3, five hours of 50 nM rapamycin in complete medium or Htt Q93 formation through genotype expression. The control for basal autophagy was incubation of primary neurons in complete medium alone or Htt Q20 formation. Immunocytochemistry was performed by fixing with 4% (w/v) paraformaldehyde (Sigma Aldrich, MO, USA) in 100 mM PBS for 15 minutes at room temperature and blocking with 5% (v/v) normal goat serum (Life Technologies, CA, USA) in 0.05% (v/v) Triton X-100 PBS for 1 hour. For the study with mCherry-Atg8a or RFP-Atg5, primary antibodies incubation was performed overnight at 4°C with 1:500 rabbit anti-Bchs (kindly provided by Kia Zinn and Rachel Kraut) and 1:100 mouse anti-DsRed (BD Pharmingen™, NJ, USA). For the study with Spinster-GFP or Rab11-GFP, primary antibodies incubation was performed overnight at 4°C with 1:500 rabbit anti-Bchs and 1:1000 mouse anti-GFP (Clontech Laboratories, CA, USA). Washing was done with 0.05% (v/v) Triton X-100 PBS for an interval of 10 minutes (total 3 times). Secondary antibodies incubation was performed with 1:400 Cy2- or Cy5-conjugated goat anti-rabbit and 1:400 Cy5- or Cy2-conjugated goat anti-mouse (Jackson ImmunoResearch Laboratories, PA, USA) for 1 hour at room temperature. Washing was done with 0.05% (v/v) Triton X-100 PBS for an interval of 10 minutes (total 4 times) and then incubated with 1 µg/mL of 4',6-diamidino-2-phenylindole (DAPI), dihydrochloride (Life Technologies, CA, USA) in PBS for 3 minutes. Washing was done briefly with PBS for a few times, with the last wash in Milli-Q water and the cover-slip was mounted onto microscopy slide to be viewed under 100x magnification using the DeltaVision OMX® microscope (Applied Precision, WA, USA) with softWoRx® 5.0 for image deconvolution. For the quantitative colocalization analysis of Bchs with the different compartmental markers, the plugin of 'Intensity Correlation Analysis' from ImageJ was used after channel splitting and background subtraction (Li et al., 2004). The results for Rr (Pearson's correlation coefficient), Ch1 : Ch2 ratios, M1 (Mander's colocalization coefficient for Channel 1) and M2 (Mander's colocalization coefficient for Channel 2) were tabulated from each image (n≈15 for each experimental set). Unpaired Student's t-test was used as the statistical tool to calculate *p*

significance value in comparison between treated (induced autophagy) and control (basal autophagy) groups.

### 2.13 Immunocytochemistry for endogenous Atg5 or Atg8 compartments in primary neurons

*bchs17(M)/Df(2L)clot7* and wild-type control primary neurons were fixed with 4% (w/v) paraformaldehyde (Sigma Aldrich, MO, USA) in 100 mM PBS for 15 minutes at room temperature and blocked with 5% (v/v) normal goat serum (Life Technologies, CA, USA) in 0.05% (v/v) Triton X-100 PBS for 1 hour. Primary antibodies incubation was performed with 1:1000 mouse anti-ubiquitinated conjugates (clone FK2, Enzo Life Sciences, NY, USA) and 1:500 rabbit anti-drAtg5 (Novus Biologicals, CO, USA) or 1:500 rabbit anti-drAtg8 (kind gift of Katja Köhler) overnight at 4°C. On the next day, washing was done with 0.05% (v/v) Triton X-100 PBS for an interval of 10 minutes (total 3 times). Secondary antibodies incubation was performed with 1:1000 Cy2-conjugated goat anti-mouse and 1:500 Cy5-conjugated goat anti-rabbit (Jackson ImmunoResearch Laboratories, PA, USA) for 1 hour at room temperature. Washing was done with 0.05% (v/v) Triton X-100 PBS for an interval of 10 minutes (total 4 times) and then incubated with 1 µg/mL of 4',6-diamidino-2-phenylindole (DAPI), dihydrochloride (Life Technologies, CA, USA) in PBS for 3 minutes. Washing was done briefly with PBS for a few times, with the last wash in Milli-Q water and the cover-slip was mounted onto microscopy slide to be viewed under 100x magnification using the DeltaVision OMX® microscope (Applied Precision, WA, USA) with softWoRx® 5.0 for image deconvolution.

### 2.14 Time-lapse imaging of GFP-Bchs with RFP-Atg5 or mCherry-Atg8a in primary neurons

Primary neurons isolated from the genotypes expressing one copy of *UAS-GFP-Bchs* and *UAS-RFP-Atg5* or *UAS-mCherry-Atg8a* transgenes through the *C155-elav* Gal4 transcriptional activator were cultured on 35 mm (diameter) Fluorodish with 0.17 mm (thickness) optical quality glass bottom (World Precision Instruments, FL, USA) that had been coated with 30 µg/mL of mouse laminin (BD Biosciences, NJ, USA) and 167 µg/mL of concanavalin A (Sigma Aldrich, MO, USA) as described previously. For live imaging of primary neurons under basal autophagy (control) condition, the cells were incubated in complete culture medium at room temperature and single focal-plane images were acquired at 100x magnification using the DeltaVision OMX® microscope (Applied Precision, WA, USA) with softWoRx® 5.0 for image deconvolution. The respective channels were acquired sequentially at every interval of 10 minutes for a total duration of 4 hours for each of the tagged proteins (GFP-Bchs: fluorescein isothiocyanate (FITC) channel = 50% transmission, 800 ms; RFP-Atg5: tetramethylrhodamine isothiocyanate (TRITC) channel = 50% transmission, 800 ms; mCherry-Atg8a: TRITC channel = 32% transmission, 600 ms). For live imaging of primary neurons under nutrient starvation, the cells were incubated in hemolymph-like 3 (HL3) saline at room temperature and immediately imaged as described. For live imaging of primary neurons transfected with Huntingtin N-terminus containing 15Q (normal poly-glutamine) or 128Q (expanded poly-glutamine), 3 µL of FuGENE® HD transfection reagent (Promega, WI, USA) was used to couple 1 µg of pCINeoHtt1955.15Q.wt or pCINeoHtt1955.128Q.wt plasmid DNA (kind gift of Anat Yanai and Mahmoud Pouladi) respectively in a 3 : 1 ratio in a final volume of 50 µL complete culture medium without penicillin/streptomycin and antibiotics/antimycotics. The mixture was incubated for 10 minutes at room temperature to allow the formation of transfection reagent : DNA complex. Subsequently, this mixture was added onto the cells with 1 mL of complete culture medium (without penicillin/streptomycin and antibiotics/antimycotics) and incubated at room temperature for 48 hours (without medium change) to enable protein expression prior to time-lapse imaging as described.

# 3. Results

## A. Pathological effects in the absence of Bchs

Before we proceed to investigate the modulation of *bchs* neurodegenerative phenotype by pharmacological agents and genes which have been generally accepted in scientific literature to act upon the autophagy pathway, we first need to have a quantitative phenotypic assay for the measurement of degeneration. Dr. Rachel Kraut has developed a novel and intuitive method of counting visually the percentages of a specific subset of motor neurons that expresses GFP in third instar larvae, thereby enabling a quantitative measurement of viability (Lim and Kraut, 2009). Third instar larvae provide an anatomically accessible platform for probing *in vivo* tissue functions, particularly the neuromuscular system which innervates the larval body wall. Characteristics of neurodegenerative disorders have been recapitulated, such as poly-glutamine length-dependent pathology that occurs progressively of a later onset, in third instar larvae and pupae stages (Marsh and Thompson, 2004). As we will like to develop a new assay that can represent better the overall neuronal atrophy, we decided initially to measure the brain volume of late third instar larvae, which has never been performed previously.

### 3.1 Optimization and validation of threshold for image stack segmentation

Prior to the 3D volumetric measurements of brains from third instar larvae of different genotypes in order to quantify the degree of neurodegeneration, it is important to have a reliable tool for the post-acquisition processing of image stacks and accurate extraction of data values. Gebiss (Ground Truth Editing and Benchmarking for Image Stack Segmentation) was developed by Dr. Janos Kriston-Vizi and Dr. Martin Wasser (Bioinformatics Image Core, University College London, UK; Bioinformatics Institute, A-Star, Singapore) as a freely available plugin in ImageJ for a user-interactive image segmentation and visualization of 3D objects (Kriston-Vizi et al., 2011). Segmentation refers to the separation of foreground pixels from background pixels through parameters defined by the user. This is an important step to distinguish between "real signal" and "noise" before the quantitative analysis of images. The ground truth (GT) is a reference data set that lies as close as possible to the real scenario

achieved through manual image segmentations performed by a human expert. During image segmentation, pixels with grayscale values ≥ defined threshold are classified as the foreground while pixels with grayscale values < defined threshold are classified as the background.

In order to determine the optimal minimum threshold, values between 15 and 35 (an 8-bit image has 0-255 grayscale values) were empirically tested. **Figures 12A, 12B and 12C** illustrate three different segmentations, as outlined by the green contour line, using different threshold values of 15, 23 and 35 on the same brain image z-stack of a homozygous *bchs58(O)* mutant. *bchs58(O)* allele (originally from Khodosh et al., 2006) had been sequenced in our laboratory and found to have an addition of 3 bases at nucleotide position 8552 followed by a deletion of 17 bases which results in a frame shift mutation and change of 33 amino acids from position 1831 to 1863 and a stop codon at 1864 (Dr. Kathleen Osborne, unpublished). This truncation removes the PH, BEACH, WD40 and FYVE domains and has a negligible level of Bchs protein in mutants. With increasing minimum threshold values, the segmentation boundary adheres more closely to the third instar larval brain surface **(Figures 12A, 12B and 12C)**. The minimum threshold value of 23 was subsequently chosen for performing segmentations on every brain image z-stack acquired because at higher threshold values, it was observed that some pixels of the brain were cut off. **Figure 12D** shows a 3D volume rendering of a *bchs58(O)* larval brain with the segmented isosurface illustrated as a green mesh overlaying the original voxels (3D equivalent of pixels) labeled in red.

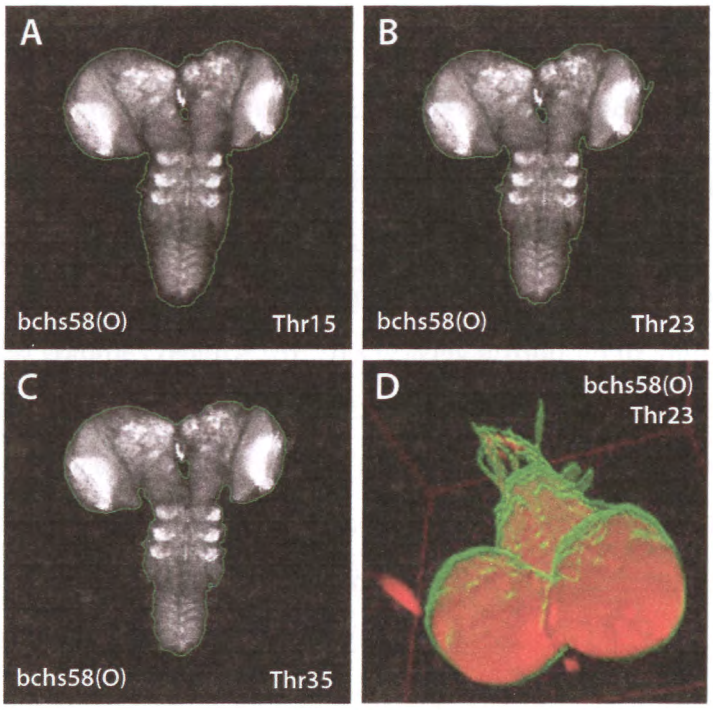


**Figure 12.** Image stack segmentations and 3D rendered volume of a third instar larval brain. **(A, B and C)** Confocal images (z-interval = 12 µm) were acquired from a homozygous *bchs58(O)* brain labeled with TRITC-phalloidin. Segmentations were performed by the Gebiss plugin in ImageJ using minimum threshold values of 15, 23 and 35. The green contour line illustrates the boundary between foreground and background as segmented by the indicated threshold value, thereby enabling the validation of image stack segmentation. **(D)** The image stack can be visualized as a 3D rendered volume (original stained voxels shown in red) with an overlaying isosurface (shown as a green mesh) outlining the segmented boundary.

### 3.2 *bchs* LOF has reduced brain volume while *bchs* GOF has enlarged brain volume

Within the group of control genotypes consisting of wild-type *Canton S*, genetic background *yellow white* (*yw*) and *C155-elav* Gal4 driver for expression throughout the nervous system via the *elav* (embryonic lethal abnormal vision) promoter, there exist significant differences in late third instar larval brain volumes **(Figure 13)**. This is likely attributed to inherent variation in the genetic background of these control genotypes. However, comparison between homozygous *bchs58(O)* with the respective control for its genetic background *yw* revealed a significant reduction of 17% brain volume in the loss-of-function (LOF) mutant **(Figure 13)**. *bchs58(O)* allele in combination with a single chromosomal deficiency (deletion) encompassing the entire *bchs* locus and more than 80 genes, *Df(2L)clot7* (abbreviated as *cl7*), also showed a similarly significant reduction of 15% brain volume when compared to *yw* **(Figure 13)**, suggesting that *bchs58(O)* allele behaves like a null allele. This quantification of *Drosophila melanogaster* brain volume has not been performed previously, although it was postulated indirectly that there is an approximately 40% reduction of adult brain volume in two weeks old *bchs* mutant due to an observation of about one-sixth decrease in linear dimension (Finley et al., 2003).

In comparison to adult brain, the smaller reduction of larval brain volume in *bchs* mutant may be attributed to a shorter duration of the larval stage (5-6 days), while there is time for progressive neurodegeneration to occur in the aged adults. In contrast, when Bchs was over-expressed in the nervous system using *C155* and *yw; EP2299* (Rorth, 1996) that consists of an enhancer *P*-element (EP; multiple upstream activation sequences) inserted in the first intron of *bchs* gene, there was a significant increase of 15% larval brain volume compared to its genetic background control **(Figure 13)**. The enlarged brain volume could be caused by a change in the homeostatic balance between cell growth, proliferation and death through a combination of factors, including decreased senescence-promoting signals and increased growth stimuli. However, as this is not a main focus of our study, further investigation was not pursued.

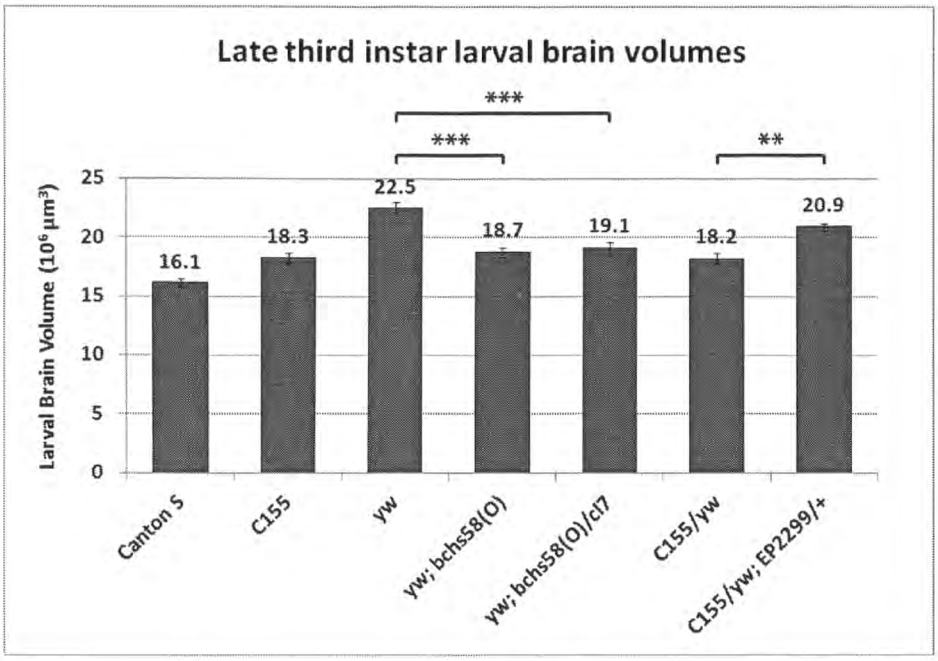


**Figure 13.** Comparison of late third instar larval brain volumes between different genotypes. *bchs* mutant larvae exhibited a significant reduction in brain volume compared to its genetic background control *yw*. On the contrary, Bchs over-expression resulted in an increased brain volume compared to its respective control *C155/yw*. It was observed that genetic background plays a significant contribution towards the brain volume, as shown by *Canton S*, *C155* and *yw*. Thirty brains were dissected from each genotype for volume measurements and unpaired Student's t-test was used for statistical analysis. Error bars represent standard deviation. ** ($p < 0.01$), *** ($p < 0.001$).

### 3.3 Motor neuron viability as an alternative assay to measure degeneration

Due to the effects of genetic background variation on brain volume, we decided that an alternative assay, wherein labeled motor neurons are counted in the degenerative state gives a more reliable readout of the modulation on *bchs* degenerative phenotype by genetic or pharmacological interventions. Using a method to score for the percentage of motor neuron survival through a GFP reporter specifically expressed in two identified and stereotypic motor neurons, aCC and RP2, it is possible to quantify the extent of degeneration and effects of any modulation, albeit based on the level of detectable GFP in this subset of motor neurons **(Figure 14)** (Lim and Kraut, 2009). The GFP reporter is tagged to CD8, which localizes it to the plasma membrane, and is under transcriptional control of an upstream activation sequence (UAS), the target enhancer of the yeast Gal4 transcriptional activator. A promoter element isolated from the *even-skipped* upstream region (designated RRa) drives expression of Gal4 in aCC and RP2 neurons, thus when genetically combined with UAS-CD8GFP, these two motor neurons can be specifically labeled (Fujioka et al., 2003). This driver-reporter chromosome is referred to as RRaCD8GFP. The aCC and RP2 motor neurons originate from the intersegmental nerve (ISN) bundle (shown in yellow in **Figure 14**) and innervate muscle 1 and 2 respectively (Schmid et al., 1999).

The consistent appearance of a number of apparently unaffected neurons that are labeled with anti-futsch and anti-fasciclin II would seem to indicate that not all motor neurons are affected by the *bchs* mutation; however, it is important to note that adventitious or compensatory growth of neighboring neurons had been described in other motor neuron degenerative phenotypes in mouse (Schaefer et al., 2005) and was suggested to occur in *bchs* mutants (Lim and Kraut, 2009).

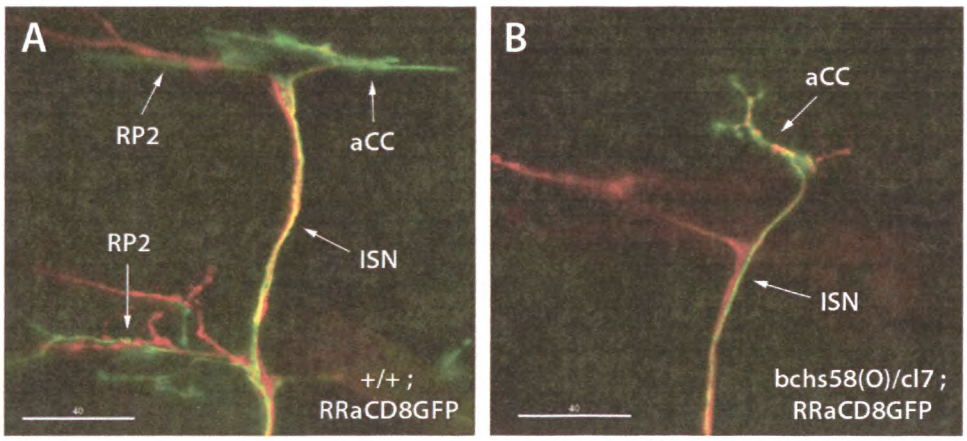


**Figure 14.** Expression of a GFP reporter in aCC and RP2 motor neurons of dissected open-book preparations of third instar larval specimens. **(A)** *+/+; RRaCD8GFP* is used as the control genotype in which both aCC and RP2 motor neurons remain intact in each hemi-segment. aCC and RP2 are labeled with anti-GFP antibody (green) while anti-futsch and anti-fasciclin II (fasII) antibodies label all neurons (red), as a reference marker to show that the dissection was intact and to show the location of nerve bundle. aCC and RP2 motor neurons originate from the ISN bundle as shown in yellow. **(B)** The *bchs* LOF mutant with GFP reporter demonstrates a loss of RP2 and aCC appears shrivelled. Wide-field image projections were captured at 20x magnification using DeltaVision OMX® microscope and scale bar represents 40 µm.

### 3.4 *bchs* mutants have lower RP2 motor neuron survival than wild-type controls

A comparison of the different *bchs* non-sense and knock-down mutants revealed that there is a significantly reduced percentage of RP2 motor neuron survival than in wild-type controls **(Figure 15)**, supporting the hypothesis that loss of Bchs function leads to progressive neurodegeneration. The gradation in penetrance of the motor neuron loss phenotype is an indication that the degeneration is progressive, because reduction to a very low (almost undetectable) level of Bchs expression **(Figure 16)** is evidently not sufficient to cause complete loss of RP2 motor neurons by the stage at which the animals were examined (late third instar). As shown in **Figure 15**, *bchs17(M)/cl7* had a more severe degenerative phenotype than *bchs58(M)/cl7* with about 32% RP2 death versus 15% RP2 death, consistent with the removal of two Bchs isoforms in *bchs17(M)* versus only one Bchs isoform in *bchs58(M)* **(Figure 17)**.

In light of the molecular lesions, it was surprising that *bchs58(O)/cl7* had the most severe degenerative phenotype with about 64% RP2 death, and we speculate that this is possibly due to the expression of a truncated Bchs that acts as a dominant negative protein. Two other deficiency alleles *bchs1Cy* and *bchs[exel7024]*, in heterozygosity with *cl7*, only resulted in approximately 50% RP2 death (Lim and Kraut, 2009). However, *bchs1Cy* is located on the *Curly of Öster* (*CyO*) balancer chromosome. Sequencing and Western blot analysis of *bchs[exel7024]* in our laboratory found that this apparent deletion does not encompass the entire *bchs* locus (data not shown). We had attempted to generate a smaller deficiency of *bchs* via FLP recombinase and FRT (FLP recombinase target) site but were unsuccessful, therefore *bchs17(M)* and *bchs58(M)* alleles were mostly used throughout this study.

Knock-down of Bchs protein using a single copy of *UAS-bchsRNAi, dicer2* (VDRC 45028) leads to 7% RP2 death compared to *UAS-dicer2* alone whose percentage of RP2 survival is close to 100% **(Figure 15)**. Bchs knock-down in combination with the deficiency *cl7* further increases RP2 death to 17% similarly to *bchs58(M)/cl7*, providing support that the latter is a hypomorph. These results suggest that the over-expression of Dicer 2 on its own has minimal effect on RP2 survival, and that the amount of Bchs protein reduction approximately correlates with the percentage of RP2 death. In addition, the *bchs* gene is not an essential gene for development (or viability *per se*) as the loss of Bchs does not cause overt phenotypic abnormalities other

than neurodegeneration and shortened life-span (Finley et al., 2003), which are typical characteristics of human neurodegenerative diseases.

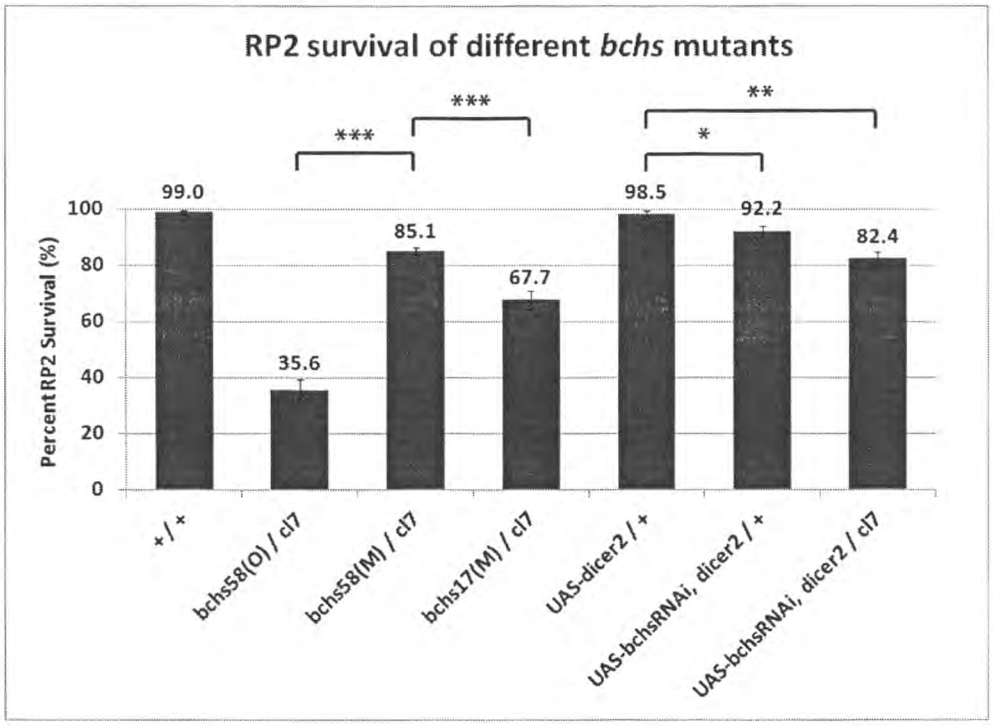


**Figure 15.** Comparison of the percentage of RP2 motor neuron survival between *bchs* mutants and wild-type controls. The *bchs* non-sense and knock-down mutants resulted in a decreased percentage of RP2 survival than their respective controls (wild-type and a single copy of *UAS-dicer2*) significantly. *bchs17(M)/cl7* has a more severe degenerative phenotype than *bchs58(M)/cl7* while the latter has a similar penetrance of RP2 death as *UAS-bchsRNAi, dicer2/cl7* (of VDRC 45028). Error bars represent standard deviation of three independent experimental replicates with an average total n of 300 hemi-segments for each genotype. Chi-square test is used for statistical analysis. * $p < 0.05$, ** $p < 0.01$ and *** $p < 0.001$.

### 3.5 Characterization of Bchs expression level in wild-type controls and *bchs* mutants

It was discovered in our laboratory by Dr. Kathleen Osborne that there are likely three alternatively spliced transcripts of *bchs* which are affected differentially by the position of mutation from *bchs58(M)* and *bchs17(M)* (manuscript submitted) **(Figure 17)**. It is hypothesized that the molecular lesion caused by *bchs58(M)* removes one Bchs isoform while *bchs17(M)* removes two Bchs isoforms due to the expression of truncated proteins. Western blot analysis with a polyclonal antibody raised against the C-terminal 1008 amino acids of Bchs protein confirmed the expression of three Bchs isoforms (approximately 390 kDa, 290 kDa and 250 kDa) both in third instar larval brains and 10-day old adult heads in the control genotypes of *Canton S*, *yw* and *C155* **(Figure 16)**. The over-expression (OE) of Bchs using *C155/yw; EP2299/+* also dramatically increased the levels of all Bchs isoforms, providing support for the notion that there are three endogenous isoforms of Bchs protein. On the other hand, the knock-down of Bchs using two different Vienna *Drosophila* RNAi Center (VDRC) lines (id 45028 and id 110785) and recombined with *UAS-dicer2* led to an almost complete reduction of all Bchs isoforms; this loss is even more evident in aged adult heads (based on observation of the Western), presumably due to sufficient time for protein turnover to occur, depending on its half-life and a steady-state equilibrium of protein level. When the *UAS-bchsRNAi* lines are not recombined with *UAS-dicer2* as a control, the levels of Bchs protein remain the same as wild-type strains (data not shown). Both *bchs58(M)/cl7* and *bchs17(M)/cl7* also showed negligible expression levels of Bchs; two very faint bands were detectable in *bchs58(M)/cl7* and similarly, a single faint band was seen in *bchs17(M)/cl7* **(Figure 16)**.

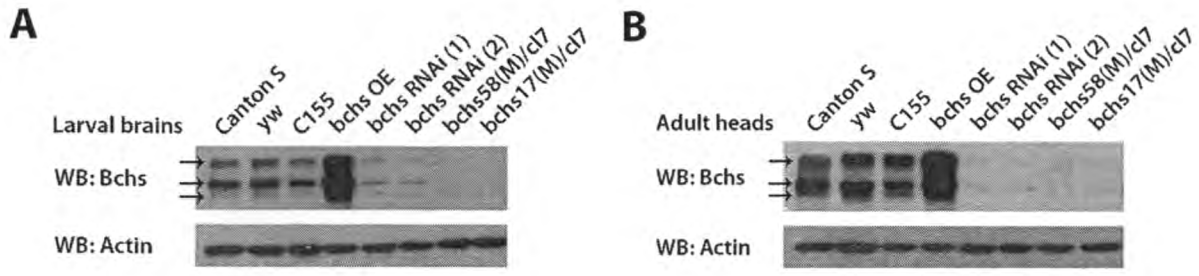


**Figure 16.** Characterization of Bchs expression level in controls and *bchs* mutants. The control genotypes *Canton S*, *yw* and *C155* show three isoforms of Bchs protein in both **(A)** third instar larval brains and **(B)** 10-days old adult heads. The over-expression (OE) of Bchs using *C155/yw; EP2299/+* leads to a significant increase in all three Bchs isoforms while the knock-down of Bchs using both VDRC id 45028 (*bchs RNAi (1)*) and VDRC id 110785 (*bchs RNAi (2)*) recombined with *UAS-dicer2* results in a significant reduction of all Bchs isoforms especially in aged adult heads. *bchs58(M)/cl7* and *bchs17(M)/cl7* also showed negligible levels of Bchs protein. Actin is used as a loading control.

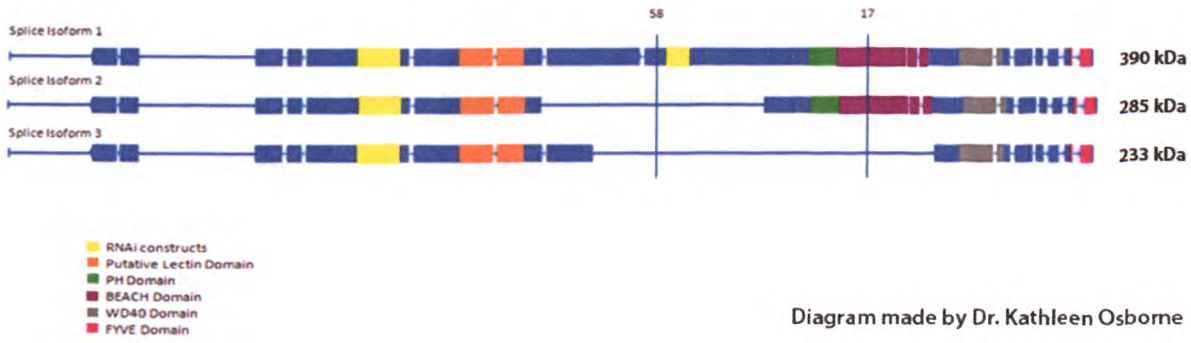


**Figure 17.** There are three alternatively spliced isoforms of the large adaptor Bchs protein. Based on reverse transcription PCR results (unpublished data by Dr. Kathleen Osborne), the *bchs* gene has three alternatively spliced transcripts as shown by the exons in blocks and the introns in lines. The identifiable domains and respective protein sizes for the different isoforms are indicated. The *bchs58* mutation affects the largest isoform while *bchs17* mutation affects the largest and intermediate isoforms. RNAi construct (highlighted in yellow) from VDRC id 45028 targets against exon 9 of the largest isoform and that from VDRC id 110785 targets against exon 5 on all three Bchs isoforms. It is noted that the smallest Bchs isoform, the only one remaining intact in *bchs17*, lacks the PH-BEACH domain.

### 3.6 Pharmacological induction of autophagy ameliorates *bchs* RP2 motoneuronal death

Rapamycin is a well-known inducer of autophagy via inhibition of the target of rapamycin (TOR) serine/threonine kinase activity (Noda and Ohsumi, 1998; Sarkar et al., 2009). Its mode of action involves binding to the immunophilin FK506-binding protein 12 (FKBP12) which together stabilizes the interaction between TOR and regulatory associated protein of TOR (Raptor), consequently inhibiting TOR kinase activity and relieving the suppression on autophagy (Chiu et al., 1994; Hara et al., 2002; Kim et al., 2002). Based on the homology between Bchs and ALFY, the latter of which participates in selective autophagic degradation, and the conserved role of BEACH family proteins in the lysosomal trafficking pathway, we proceeded to investigate whether rapamycin feeding from first instar to third instar larvae is able to modulate the RP2 degenerative phenotype in three different allelic mutations of *bchs*.

*bchs58(M)* and *bchs17(M)* are isolated in our laboratory by Dr. Kathleen Osborne and have the EP element mobilized precisely from the first intron of the original strains *bchs58(O)* and *bchs17(O)* respectively. Excision of the EP element insertion from these alleles was desirable because *bchs58(O)* and *bchs17(O)* were derived from the UAS-containing *EP2299* line using ethyl methanesulfonate (EMS) (Khodosh et al., 2006) and the presence of this EP element can drive the expression of a truncated Bchs form, which may have an unknown neomorphic effect and confound results. *bchs17(O)* is also a non-sense mutation with a single base change G → A at nucleotide position 10983, consequently substituting tryptophan at position 2640 for a stop codon.

As previously reported (Lim and Kraut, 2009), *bchs* mutants have a significantly reduced RP2 motor neuron survival compared to wild-type control **(Figure 18)**. The supplementation of 1 µM rapamycin in food resulted in an increased percentage of RP2 motor neuron survival for all *bchs* mutants, the effect of which was most significant for *bchs58(O)/cl7* and *bchs58(M)/cl7*, and milder for *bchs17(M)/cl7* **(Figure 18)**. This suggests that autophagy is deficient in *bchs* mutants which can be compensated through rapamycin feeding. Unlike *bchs58(O)/cl7* and *bchs58(M)/cl7*, there may be an impairment in a rate-limiting step of the autophagy pathway in *bchs17(M)/cl7* which interferes with the downstream effects of rapamycin.

In order to ascertain the autophagic activity of rapamycin treatment, which has been demonstrated to induce autophagosomal formation and autophagic flux in cell lines and primary mouse neurons, in our larval system, mCherry-Atg8a autophagosomal marker was expressed in muscles using the *24B-mef2* Gal4 tissue driver to examine the approximate number of autophagosomal punctae. We had thought initially to investigate via Atg8/LC3 turnover assay using bafilomycin A1, a vacuolar type $H^+$ ATPase inhibitor that prevents lysosomal acidification and thus degradation. However, as Filimonenko and co-workers found that ALFY siRNA knock-down in HeLa cells did not alter the LC3-I/LC3-II ratio compared to control siRNA in the presence of bafilomycin A1 (Filimonenko et al., 2010), possibly due to the non-detectable small proportion of lysosomal degradation by ALFY-mediated aggrephagy in comparison with total basal macroautophagy, this assay was not performed in our study. We fed wild-type larvae expressing mCherry-Atg8a in muscles from first instar till third instar with 1 μM rapamycin and observed in general, an increased formation of punctate autophagosomal structures **(Figure 19)**, providing support for autophagy induction by rapamycin treatment.

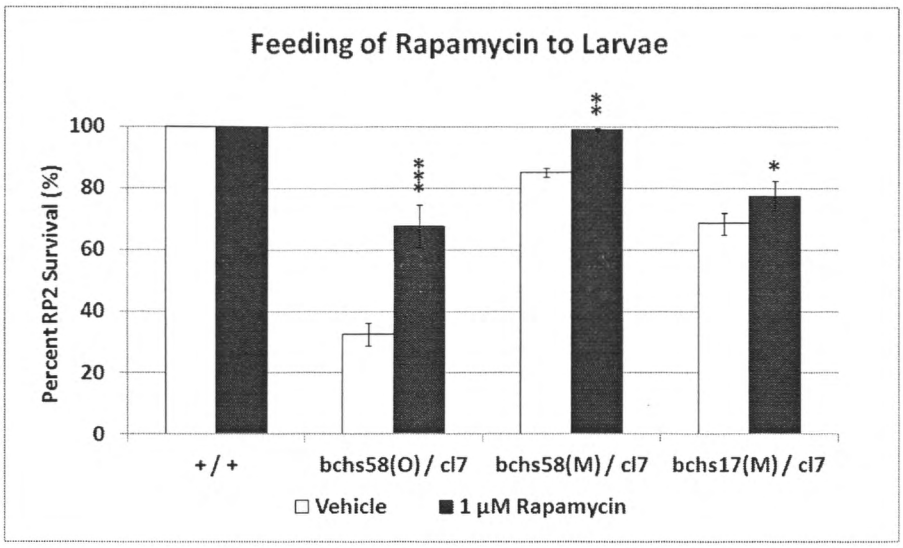


**Figure 18.** Rapamycin feeding ameliorates neuronal death in *bchs* mutant larvae. Larvae were grown in food containing 0.05% ethanol (vehicle) or 1 µM rapamycin from first to third instar stage. All the *bchs* mutants (*bchs58(O)/cl7*, *bchs58(M)/cl7* and *bchs17(M)/cl7*) showed a significant increase in the percentage of RP2 motor neuron survival to varying degrees when fed with rapamycin-supplemented food. Error bars represent standard deviation of three experimental replicates for each condition which has an average total n of 300 hemi-segments. Chi-square test was used for statistical analysis. * $p < 0.05$, ** $p < 0.01$ and *** $p < 0.001$.

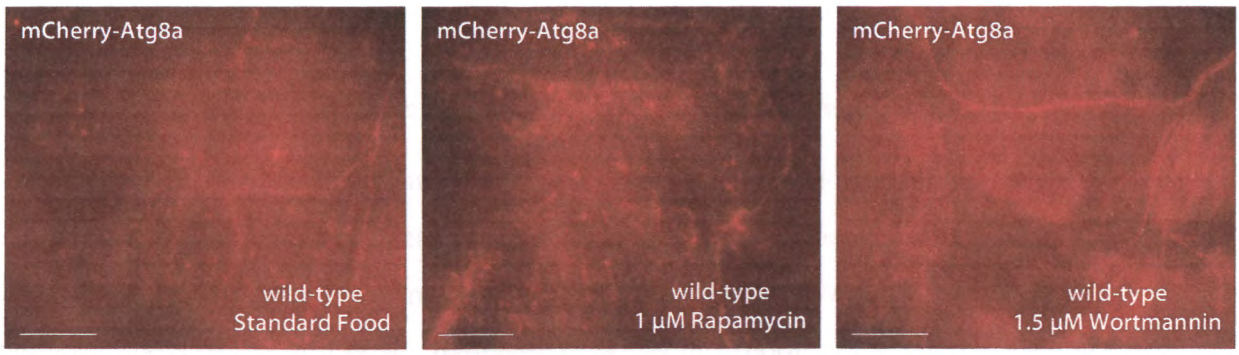


**Figure 19.** Rapamycin feeding enhances autophagosome formation in wild-type larvae while wortmannin feeding suppresses it. Representative image projections of wild-type larvae over-expressing mCherry-Atg8a in muscles via *24B-mef2-Gal4* and fed from first instar till third instar stage in standard food or food containing autophagy-modulating drugs are shown. 40x magnification, scale-bar represents 20 μm.

### 3.7 Pharmacological inhibition of autophagy causes RP2 motoneuronal death

Wortmannin, LY294002 and 3-methyladenine (3-MA) are broad-spectrum phosphatidylinositol 3-kinase (PI3K) inhibitors that can suppress the activity of three classes of PI3K (Powis et al., 1994; Vlahos et al., 1994). The inhibition of different classes of PI3K will have varying effects on different steps of the autophagy pathway (Petiot et al., 2000); however, these three drugs are widely used as autophagy inhibitors at low $IC_{50}$ (50% inhibitory concentration) via the suppression of PI3K class III which is important for the nucleation of phagophore through PI3P production (Blommaart et al., 1997; Seglen and Gordon, 1982).

At a lower concentration of 0.2 μM wortmannin, wild-type control, *bchs58(O)/cl7* and *bchs58(M)/cl7* showed a significant reduction of RP2 survival that is further exacerbated with a ten-fold increase of wortmannin concentration in *bchs* mutants but not in wild-type **(Figure 20)**. This indicates that autophagy function in wild-type is sufficiently robust to compensate for increased perturbations of Vps34 (PI3K class III) activity; however, autophagy in *bchs* mutant has evidently been compromised to the extent that it is sensitized to drug-induced decrements in autophagic capacity. At 0.2 μM or 2 μM wortmannin feeding, *bchs17(M)/cl7* did not exhibit an exacerbation of RP2 death **(Figure 20)**. One possible explanation is that the localized recruitment and downstream effects of PI3P-enriched sites which act as a rate-limiting initiation step in the autophagy pathway has been disrupted in *bchs17(M)/cl7* due to the more extensive loss of Bchs isoforms which results in a more severe failure to bind and recruit PI3P through the FYVE domain. If this was the case, then further inhibition of PI3P production by wortmannin would have no effect. It was shown that wortmannin feeding suppressed the formation of mCherry-Atg8a punctae in muscles of wild-type larvae, providing support for autophagy inhibition by wortmannin **(Figure 19)**.

Similarly, the feeding of 5 mM 3-MA caused RP2 death in wild-type, and increased death in *bchs58(O)/cl7* and *bchs58(M)/cl7*, but not *bchs17(M)/cl7* **(Figure 21)**. This provides support that autophagy inhibition by wortmannin and 3-MA at the concentrations used leads to neuronal death even in wild-type, and moreover that the localized effects of PI3P may be more impaired in *bchs17(M)/cl7*, thus resulting in its failure to show a response towards wortmannin or 3-MA feeding and only a small elevation in RP2 survival when fed with rapamycin. Both wild-type

control and *bchs* mutant larvae were not able to survive beyond the second instar stage at 10 mM of 3-MA supplemented food, indicating that autophagy function is important for maintaining metabolic homeostasis at the whole organism level.

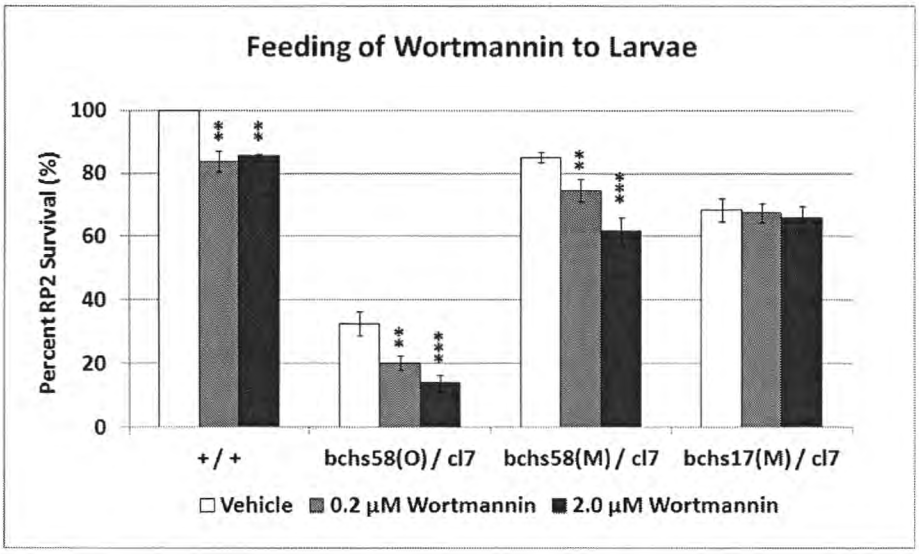


**Figure 20.** Wortmannin feeding causes neuronal death in wild-type control and *bchs* mutant larvae. Larvae were grown in food containing 0.05% ethanol (vehicle), 0.2 µM and 2.0 µM wortmannin from first to third instar stage. The *bchs58(O)/cl7* and *bchs58(M)/cl7* mutants showed a dose-dependent exacerbation of RP2 motor neuron death while the wild-type control did not. *bchs17(M)/cl7* did not show a response towards wortmannin feeding. Error bars represent standard deviation of three experimental replicates for each condition which has an average total n of 300 hemi-segments. Chi-square test was used for statistical analysis. ** $p < 0.01$ and *** $p < 0.001$.

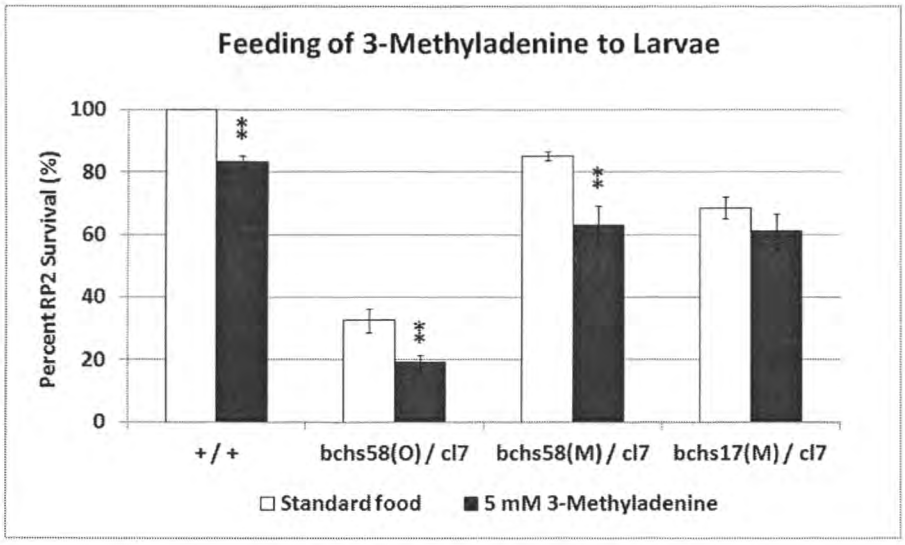


**Figure 21.** 3-Methyladenine feeding causes neuronal death in wild-type control and *bchs* mutant larvae. Larvae were grown in standard food or supplemented food with 5 mM 3-MA from first to third instar stage. Wild-type, *bchs58(O)/cl7* and *bchs58(M)/cl7* showed a significant decrease in the percentage of RP2 motor neuron survival after 3-MA feeding, except *bchs17(M)/cl7*. Error bars represent standard deviation of three experimental replicates for each condition which has an average total n of 300 hemi-segments. Chi-square test was used for statistical analysis. ** $p < 0.01$.

### 3.8 Homologous recombination between different *bchs* and *atg* alleles

In order to knock down Bchs expression in the brain using *UAS-bchsRNAi*, it was necessary to recombine this allele with *UAS-dicer2* together on the second chromosome. Dicer belongs to the class of RNase III enzyme that cleaves dsRNA molecules into shorter RNA duplexes which then exert a silencing effect on gene expression at the transcriptional level (Bernstein et al., 2001). Dicer 2, but not Dicer 1, has been demonstrated to enhance the knock-down efficiency of transgenic siRNA in *Drosophila melanogaster* (Dietzl et al., 2007) and Dicer 2 is required to cleave siRNA precursors, unlike Dicer 1 which exhibits greater selectivity towards pre-miRNA processing (Lee et al., 2004). In order to verify the presence of the two P element insertions

*UAS-bchsRNAi* and *UAS-dicer2* on a single chromosome for each recombination event, primer-specific PCR was performed to detect the insertions.

As shown in **Figure 22**, the respective bands for different alleles were detected by gel electrophoresis after PCR. **Table 3** in the Appendix lists the specific primer pairs and their corresponding product size used for detecting each allele. Other sets of homologous recombination occur for the pairs of alleles including *bchs17(M)* and *EPgy2 atg7[EY10058]* (abbreviated as *atg7[EY]*), *bchs17(M)* and *atg7[d77]*, *bchs17(M)* and *UAS-atg1[6A]*, *bchs58(M)* and *atg7[EY]*, *bchs58(M)* and *atg7[d77]*, *bchs58(M)* and *UAS-atg1[6A]*. This is required because the different *atg* alleles to be used in the genetic interaction studies are located on the second chromosome similarly to *bchs17(M)* and *bchs58(M)* which needs to be in heterozygosity with the *bchs* deficiency *Df(2L)clot7*. **Figure 23** shows the sequence verification for *bchs17(M)* and *bchs58(M)* mutations. As mentioned previously, *bchs17(M)* has a single base change from TGG to TGA (highlighted in yellow box) which results in a stop codon within the BEACH domain of Bchs while *bchs58(M)* has an addition of 3 bases TTA (highlighted in yellow box) and a subsequent deletion of 17 bases TCCAGCTCCTGTTTAGC (not shown; wild-type sequence can be obtained from FlyBase) which results in amino acids change and a stop codon at mid-length of the Bchs protein.

We wanted to test potential interactions of *bchs* alleles with gain- and loss-of-function alleles of autophagy genes, to examine whether these would modify the phenotype, and thus give further support to the idea that neuronal death in *bchs* mutant is truly due to loss of autophagic function. For this purpose, we obtained several mutant or over-expressing alleles in autophagy genes. *atg7[EY]* has an EP element inserted 73 bases upstream of *atg7* transcriptional start site; *atg7[d77]* is an a*tg7* deletion that removes most of exon 4 and whole of exons 5 and 6; *UAS-atg1[6A]* transgene over-expresses *atg1* (Juhasz et al., 2007; Scott et al., 2007). *atg7[d14]* is another *atg7* deletion that extends longer than *atg7[d77]* into the first five exons of *atg7* and the first two exons of neighboring *sec6* gene. Unfortunately, attempts to recombine *atg7[d14]* (on right arm of second chromosome) with *Df(2L)clot7* (on left arm of second chromosome) in order to bring into heterozygosity with *atg7[d77]* were unsuccessful, in spite of the large cytological distance between the two loci (led to lethality; data not shown). The fact that a

recombination between the *atg7* deficiency and the *bchs* deficiency was not viable may indicate synthetic lethality, and a strong interaction between the two genes.

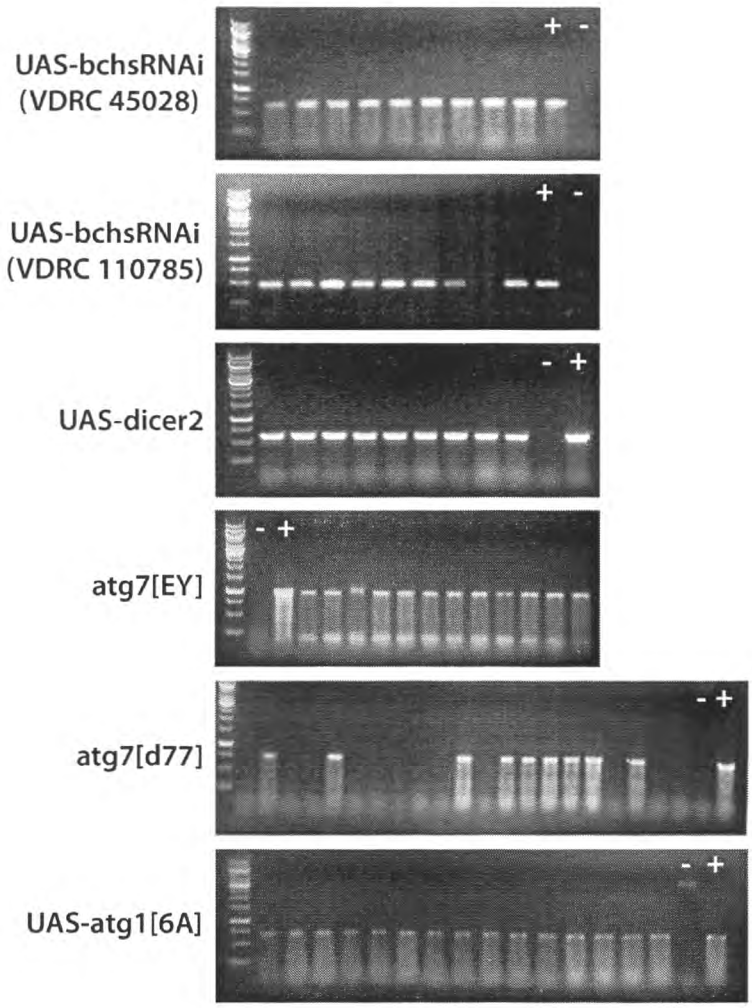


**Figure 22.** DNA gel electrophoresis of PCR products for specific detection of the different alleles used in recombination. Each single putative recombinant male fly was extracted for its genomic DNA and primers-specific PCR was performed to verify the presence of the allele. Each lane represents individual PCR reaction from the different putative recombinants. "+" indicates positive control obtained from the original fly line containing the corresponding allele, while "-" indicates negative control obtained from the partnering fly line used in each recombination set.

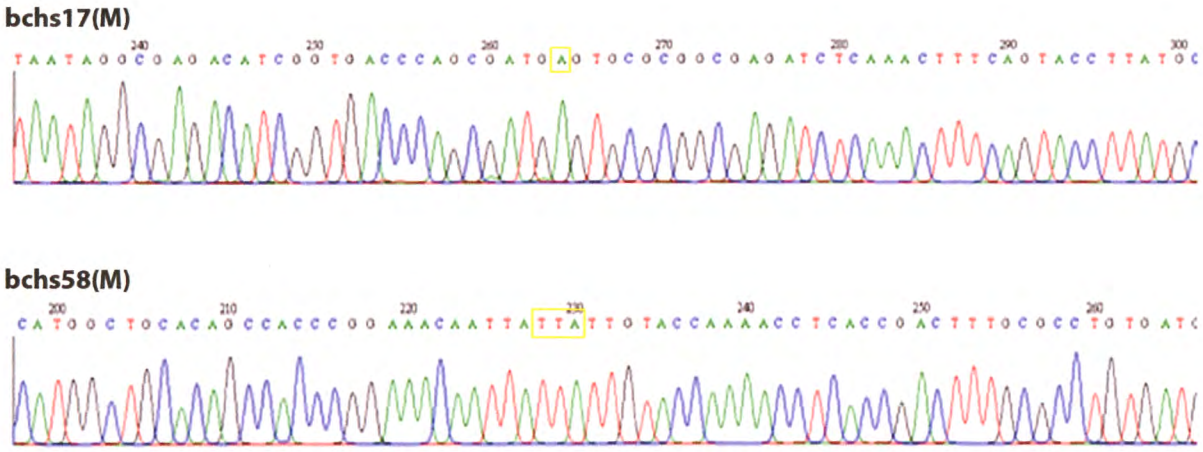


**Figure 23.** Verification of sequences from *bchs17(M)* and *bchs58(M)* alleles. Homozygous *bchs17(M)* and *bchs58(M)* mutations at different regions of the *bchs* gene were amplified by PCR and the gel-purified DNA products were sequenced. The yellow box highlights the mutation caused by a single base change from G → A in *bchs17(M)* which results in a stop codon, while there is an addition of 3 bases followed by a deletion of 17 bases (not shown) in *bchs58(M)* which results in a frame-shift mutation and subsequent stop codon.

### 3.9 *atg7* mRNA expression increases in *atg7[EY]*

In order to verify that *atg7[EY]*, when driven with the Gal4 transcriptional activator, over-expresses *atg7* mRNA, reverse-transcription PCR was performed using gene-specific primers. This was necessary because in published work, it was not demonstrated that the EY insertion in fact gives increased expression of Atg7 in this line. There are two alternatively spliced transcripts of *atg7* as shown in **Figure 24**. FlyBase has also annotated two *atg7* transcripts and polypeptides. Adult heads obtained from the genotype *C155/yw; atg7[EY]/+* have significantly elevated levels of both *atg7* transcripts compared to wild-type *Canton S*. As expected, it was observed that heterozygous *atg7[d77]/+* adult heads have slightly lower levels of both *atg7* transcripts than *Canton S*. As for the *atg7* loss-of-function alleles, it has been shown by Juhász and co-workers (Juhasz et al., 2007) that *atg7[d77]/atg7[d14]* (trans-heterozygous mutant for *atg7*) has strongly reduced *atg7* expression.

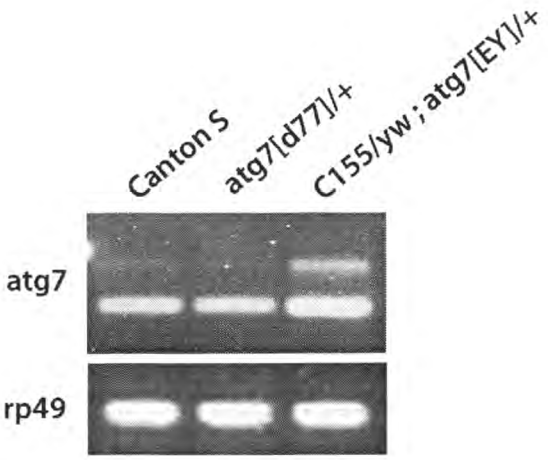


**Figure 24.** Reverse-transcription PCR on total RNA isolated from adult heads of wild-type and *atg7* mutants. *C155/yw; atg7[EY]/+* has elevated expression levels of two alternatively spliced *atg7* transcripts than wild-type *Canton S* significantly, while *atg7[d77]/+* is observed to have slightly reduced *atg7* expression than *Canton S*. RT-PCR was also performed on *rp49* ribosomal RNA as a loading control.

### 3.10 *atg7* over-expression rescues the *bchs* degenerative phenotype

Atg7 is an E1-like ubiquitin activating enzyme which is involved in the conjugation process of phosphatidyl-ethanolamine (PE) to Atg8 (Ichimura et al., 2000). Atg7 acts at the first step of the two conjugation pathways for ubiquitin-like proteins Atg8 and Atg12 that aids in the expansion of the phagophore, while Atg1 kinase is positioned upstream in a hierarchical functional order of core Atg proteins machinery with an important role in the early steps of signaling initiation and isolation membrane nucleation (Geng and Klionsky, 2008; Suzuki et al., 2007). Thus, *atg1* and *atg7* alleles were chosen to be recombined with *bchs17(M)* and *bchs58(M)* alleles. However, the over-expression of Atg1 using *UAS-atg1[6A]* resulted in death of all aCC and RP2 motor neurons **(Figure 25)** which support previous findings that excessive autophagy induction through Atg1 leads to apoptosis (Scott et al., 2007). On the other hand, a basal level of Atg7 was demonstrated to promote neuronal health by suppressing the accumulation of ubiquitinated inclusions, thereby contributing towards *Drosophila* adult longevity (Juhasz et al., 2007).

In this study, it is shown for the first time that there is a genetic interaction between *bchs* and *atg* genes, in the strictest sense of the term, where the loss-of-function phenotype is either exacerbated or rescued, by a quantifiable assay. The over-expression of Atg7 rescues neurodegeneration substantially, increasing the percentage of RP2 survival to almost 100% in both *bchs17(M)/cl7* and *bchs58(M)/cl7* **(Figure 26)**. Notably, genetic augmentation of autophagy function has a greater efficacy than rapamycin feeding, which is only able to partially rescue *bchs17(M)/cl7* **(Figure 18)**. *bchs58(M)/cl7* has a similar percentage of RP2 death as *atg7[d77]/+* and their combination resulted in a further reduction of RP2 survival. This is not the case for *bchs17(M)/cl7*, where combination with a single copy deletion of *atg7* does not exacerbate RP2 death **(Figure 26)** similar to what was observed after wortmannin and 3-MA feeding **(Figures 20 and 21)**. This provides additional evidence that *bchs58(M)* behaves like a hypomorph and *bchs17(M)* behaves like an amorph with near or complete loss of gene function. The epistatic relationships revealed by these experiments suggest that Bchs is likely to play a role in autophagy upstream of Atg7 because over-expression of Atg7 compensates for

Bchs deficiency, while a decrease of Atg7 function further exacerbates the neurodegeneration mediated by a hypomorphic (partial) loss in Bchs.

In order to ascertain the autophagic activity of Atg7 over-expression, an increased formation of mCherry-Atg8a punctate structures was observed in wild-type muscles after Atg7 over-expression **(Figure 27)**. Conversely, one chromosomal copy deletion of Atg7 appears to lower slightly the approximate number of mCherry-Atg8a punctae in general.

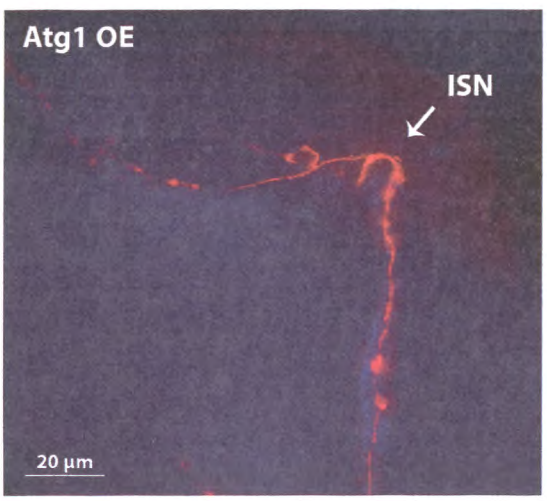


**Figure 25.** Over-expression of *atg1* specifically in aCC and RP2 motor neurons via the *RRa-eve* driver leads to their atrophy. Dissected third instar larvae were immunostained with phalloidin (F-actin in muscles, blue), anti-futsch, anti-fasciclin (marker for neuronal cytoplasm and membrane respectively, red) and anti-GFP (reporter for aCC and RP2, green). A representative deconvolved image projection acquired at 40x magnification is shown whereby the inter-segmental nerve (ISN) bundle is present but both aCC and RP2 motor neurons are absent. Scale-bar represents 20 µm.

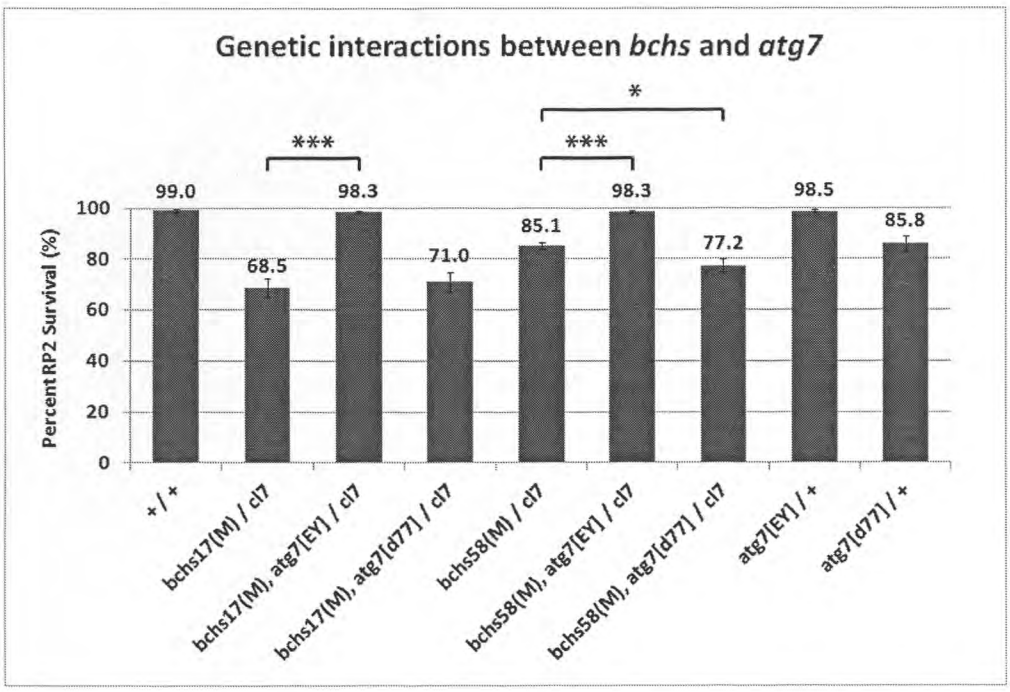


**Figure 26.** The over-expression of *atg7* rescues RP2 death in *bchs* mutants. *bchs17(M)/cl7* and *bchs58(M)/cl7* in combination with *atg7[EY]* rescues RP2 motor neuron survival to almost 100% while the combination with *atg7[d77]* only exacerbates RP2 death in *bchs58(M)/cl7*. Error bars represent standard deviation of three independent experimental replicates with an average total n of 300 hemi-segments for each genotype. Chi-square test is used for statistical analysis. * $p < 0.05$ and *** $p < 0.001$.

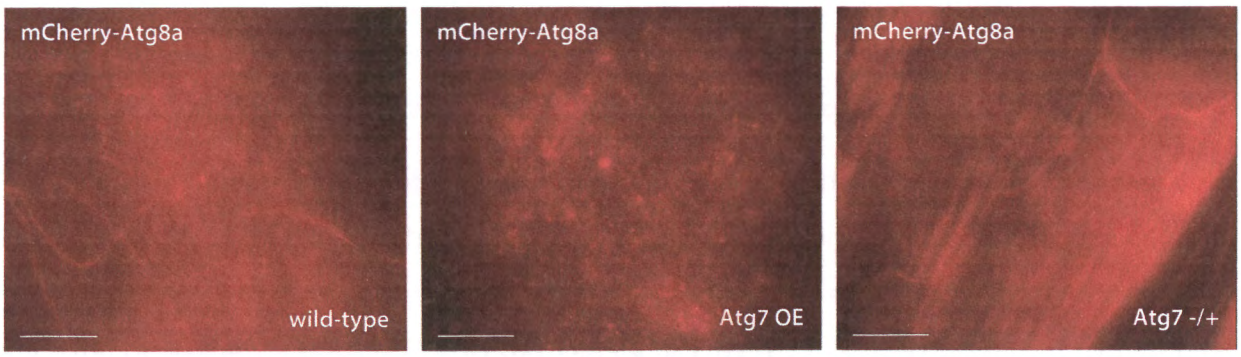


**Figure 27.** The over-expression of Atg7 enhances autophagosome formation in wild-type larvae while a single copy deletion of Atg7 suppresses it. Wild-type third instar larvae expressed mCherry-Atg8a in muscles via *24B-mef2-Gal4* and were combined with *atg7[EY]* or *atg7[d77]*. Representative image projections acquired at 40x magnification are shown and the scale-bar represents 20 μm.

### 3.11 Ubiquitinated aggregates accumulate in neuronal termini of *bchs* NMJs

The abnormal accumulation of ubiquitinated aggregates in the adult brains of aged *bchs* mutants (Finley et al., 2003) is the main pathological hallmark for mutation in this gene and was the inspiration for its name, *blue cheese*, because of a similarity in the morphological appearance of the afflicted brains to this variety of cheese. This is accompanied by neuronal death and overall brain atrophy (Finley et al., 2003), similar to what we have observed with a reduction in larval brain volume **(Figure 13)** and the loss of RP2 motor neurons in *bchs* mutants **(Figure 15)**. Therefore, we decided to investigate the subcellular distribution of ubiquitinated aggregates present within remaining intact neurons of *bchs* mutants through immunohistochemistry at the third instar larval stage which allows more amenable visualization of peripheral neurons. Observations of the motor neuron axons and cell bodies in *bchs* mutants did not reveal a noticeable accumulation of ubiquitinated conjugates **(Figure 28)**. However, it was observed that deposition of ubiquitinated conjugates were localized in neuronal termini of *bchs* NMJs **(Figure 29)**. It seems that the size of ubiquitinated aggregates correlates with the severity of RP2 degeneration in different *bchs* mutants **(Figure 15)**. In order to analyze the accumulation of ubiquitinated aggregates quantitatively, their area sizes are categorized into three groups: 0 – 1 $\mu m^2$ (small), 1.1 – 10 $\mu m^2$ (medium) and 10.1 – 50 $\mu m^2$ (large). The third instar larval NMJ of muscle 2, which is innervated by the RP2 motor neuron, was chosen for investigation (Schmid et al., 1999).

*bchs58(M)/cl7* and *bchs17(M)/cl7* exhibit a significant decrease in the deposition of small ubiquitinated aggregates and a concomitant increase in the accumulation of medium and large ubiquitinated aggregates compared to the wild-type control **(Figure 30)**. There is also a shift towards the formation of larger ubiquitinated aggregates in *bchs58(O)/cl7*, albeit to a lesser extent than the other two allelic combinations. Although *bchs58(O)/cl7* has a more severe RP2 degenerative phenotype than *bchs58(M)/cl7* and *bchs17(M)/cl7*, the percentage of NMJs with medium or large ubiquitinated aggregates is comparatively smaller. This could be due to the detectable level in *bchs58(O)/cl7* whereby most of the RP2 motor neurons with large ubiquitinated aggregates may have undergone atrophy. It is interesting to note that these large

ubiquitinated aggregates were never observed along motor neuron axons of wild-type and *bchs* mutants, but only at termini.

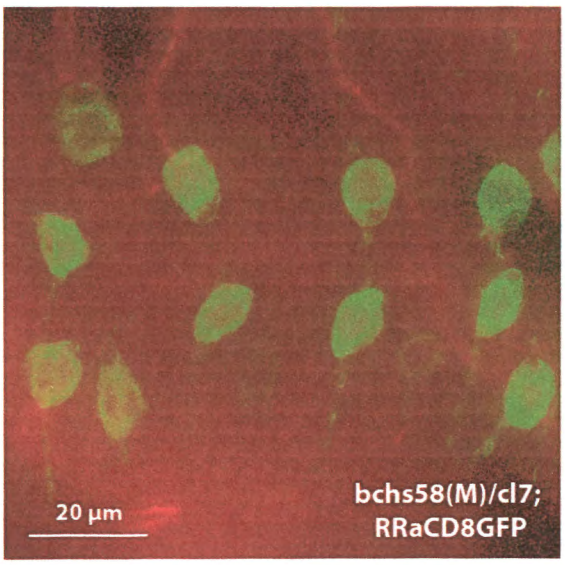


**Figure 28.** Ubiquitinated aggregates were not observed in cell bodies of aCC and RP2 labeled with GFP in third instar *bchs* larval brain. Immunostaining was performed with anti-GFP (green) and anti-ubiquitinated conjugates (mono- and poly-ubiquitin modifications) (red). A deconvolved image projection acquired at 40x magnification is shown and the scale-bar represents 20 µm.

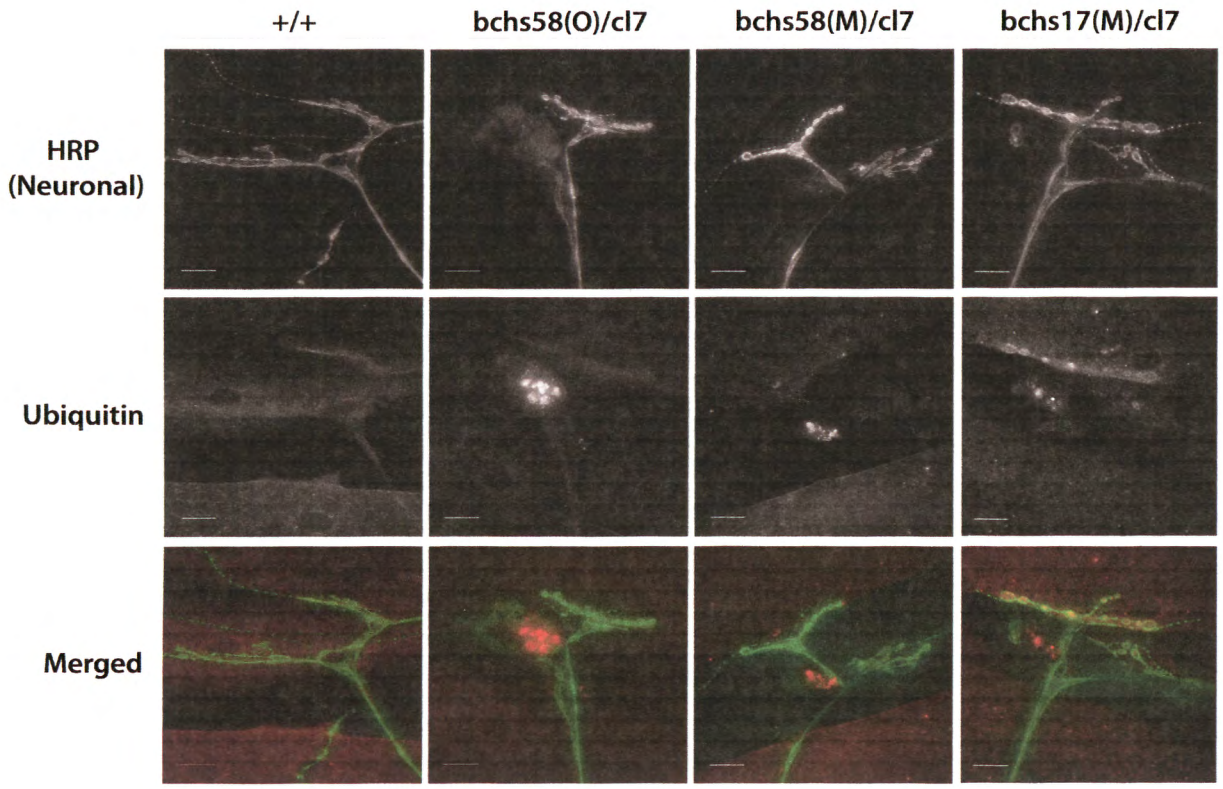


**Figure 29.** Ubiquitinated aggregates were observed in neuronal termini of *bchs* NMJs. Anti-HRP, which has immuno-reactivity against specific carbohydrate moieties present on *Drosophila* neuronal membrane, and anti-ubiquitinated conjugates (mono- and poly-ubiquitin modifications) were used for immuno-histochemistry on dissected third instar larval specimens. Ubiquitinated aggregates of a similar magnitude as that illustrated in the *bchs* mutants, which also demonstrate atrophying RP2 motor neuron at muscle 2, were never observed in the synaptic termini of wild-type NMJs. Wide-field deconvolved image projections were acquired at 40x magnification and scale-bar represents 20 µm.

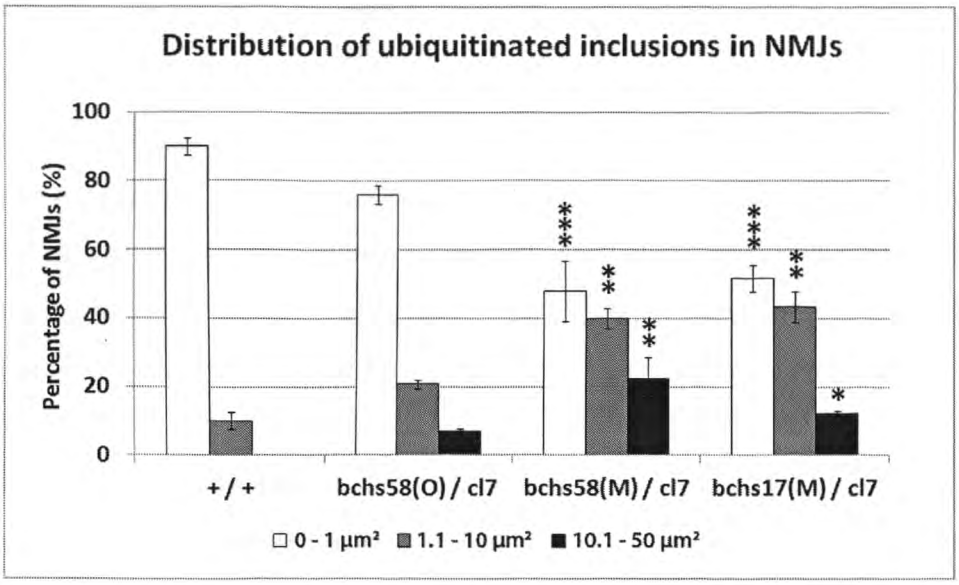


**Figure 30.** The size of ubiquitinated aggregates increases in neuronal termini of *bchs* NMJs. Ubiquitinated aggregates are categorized according to area size into three groups: 0 – 1 $\mu m^2$ (small), 1.1 – 10 $\mu m^2$ (medium) and 10.1 – 50 $\mu m^2$ (large). The NMJ at muscle 2 is chosen for investigation. There is a shift towards the accumulation of medium and large ubiquitinated aggregates in *bchs* mutants, with a concomitant reduction in the deposition of small ubiquitinated conjugates. Error bars represent standard error of the mean (SEM) for two independent experimental replicates with an average total n of 30 hemi-segments for each genotype. Chi-square test is used for statistical comparison between the *bchs* mutants and wild-type control. * $p < 0.05$, ** $p < 0.01$ and *** $p < 0.001$.

### 3.12 Rapamycin promotes the clearance of ubiquitinated aggregates in *bchs* NMJs

As *bchs58(M)/cl7* and *bchs17(M)/cl7* have a greater observable accumulation of medium and large ubiquitinated aggregates than *bchs58(O)/cl7*, investigation was carried out on the former *bchs* mutants to examine whether the feeding of autophagy-modulating drugs to larval stage has an effect on the distribution pattern of ubiquitinated aggregates in RP2 NMJs and whether this correlates with motor neuron viability. After *bchs58(M)/cl7* and *bchs17(M)/cl7* larvae were fed with 1 μM rapamycin from first instar to third instar stage as described previously, the percentages of NMJs containing medium and large ubiquitinated aggregates decreased significantly, while the percentage of NMJs containing small ubiquitinated aggregates increased significantly **(Figure 31A)** compared to corresponding *bchs* larvae that were fed on standard food in the absence of rapamycin **(Figure 31B)**. This provides supporting evidence that the administration of rapamycin, which has been found to enhance autophagosomal formation and autophagy flux in different cellular systems and animal models (Bove et al., 2011; Rubinsztein and Nixon, 2010), promotes the degradative removal of ubiquitinated aggregates and prevents its accumulation in synaptic termini, thereby contributing towards increased RP2 motor neuron survival in *bchs* mutants **(Figure 18)**.

On the other hand, the feeding of 2 μM wortmannin or 5 mM 3-MA did not have an effect on the distribution pattern of ubiquitinated aggregates in *bchs58(M)/cl7* and *bchs17(M)/cl7* **(Figures 32A and 33A)**. However, 3-MA feeding caused a significant shift towards the formation of medium (but absence of large) ubiquitinated aggregates in wild-type larvae compared to corresponding controls that were not fed with 3-MA **(Figure 33B)**. This suggests that there is an upper detection limit for the accumulation of ubiquitinated aggregates in NMJs depending on the severity of degeneration, as wortmannin and 3-MA led to RP2 death in both wild-type and *bchs58(M)/cl7* **(Figures 20 and 21)**. 3-MA may be a more potent autophagy inhibitor than wortmannin, because it results in the observable accumulation of ubiquitinated aggregates in wild-type larvae **(Figure 33A)**. Taken together, this indicates that the accrual of ubiquitinated aggregates in the synaptic termini of *bchs* NMJs impedes neuronal homeostasis and can lead to atrophy, since rescue of the degenerative phenotype is also accompanied by reduction of aggregates.

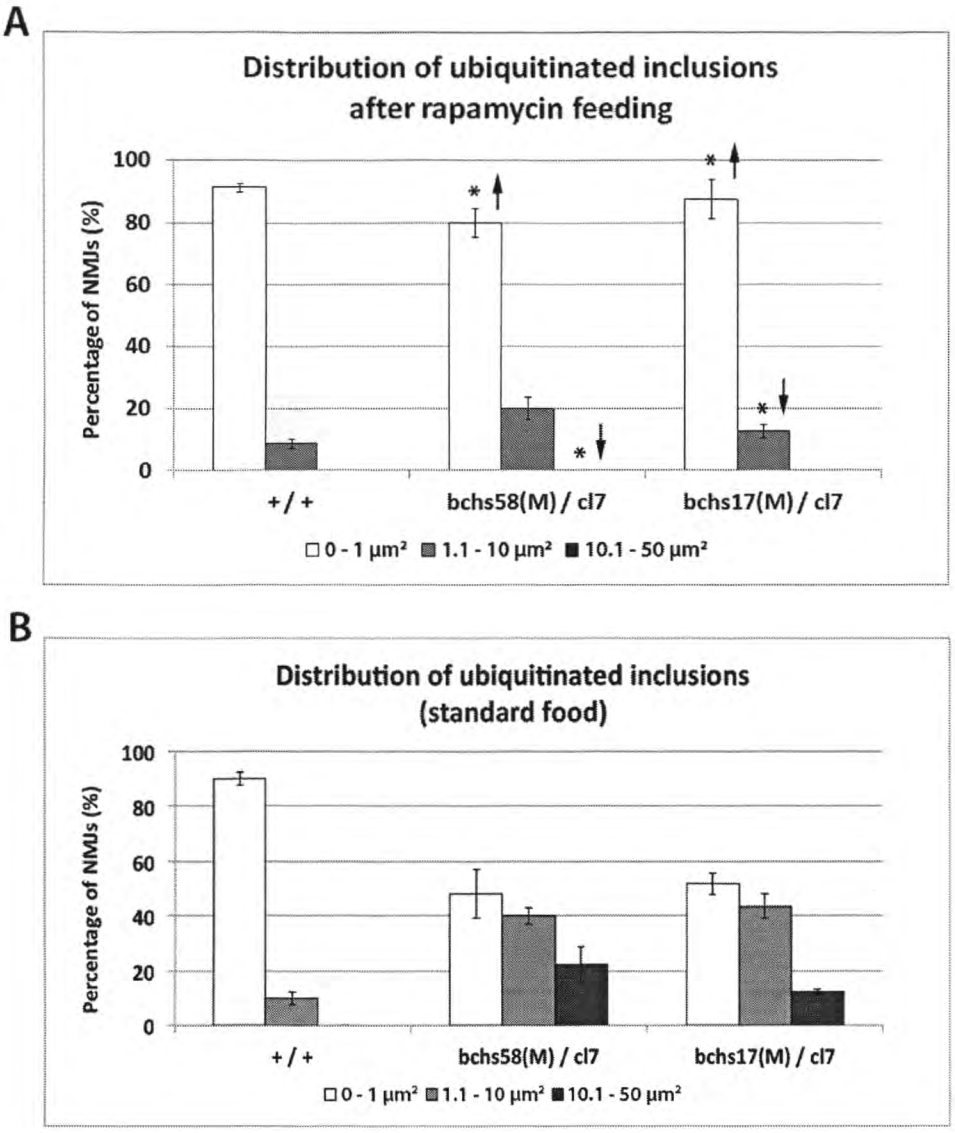


**Figure 31.** Rapamycin feeding suppresses the accumulation of ubiquitinated aggregates in *bchs* NMJs. There is an increased percentage of NMJs with small ubiquitinated conjugates and a concomitant reduction in the deposition of medium and large ubiquitinated aggregates in *bchs* mutants after **(A)** 1 µM rapamycin feeding compared to corresponding *bchs* mutants that were fed in **(B)** standard food. Error bars represent standard error of the mean (SEM) for two independent experimental replicates with an average total n of 30 hemi-segments for each genotype. Chi-square test is used for statistical analysis between feeding in the presence and absence of rapamycin. * $p < 0.05$.

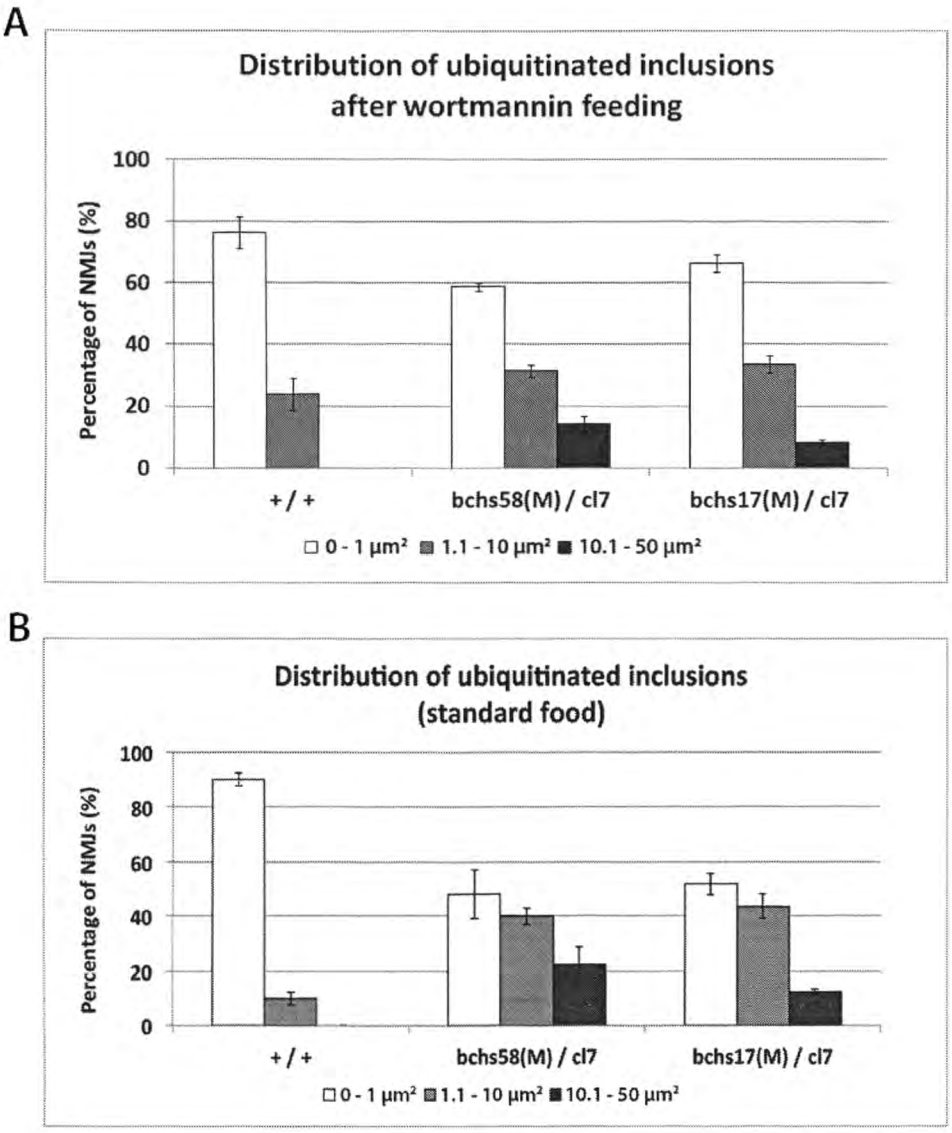


**Figure 32.** Wortmannin feeding did not alter the distribution pattern of ubiquitinated aggregates in wild-type and *bchs* NMJs. There is no significant difference in the deposition of small, medium and large ubiquitinated aggregates after **(A)** 2 µM wortmannin feeding compared to the corresponding genotypes that were fed in **(B)** standard food. Error bars represent standard error of the mean (SEM) for two independent experimental replicates with an average total n of 30 hemi-segments for each genotype. Chi-square test is used for statistical analysis between feeding in the presence and absence of wortmannin.

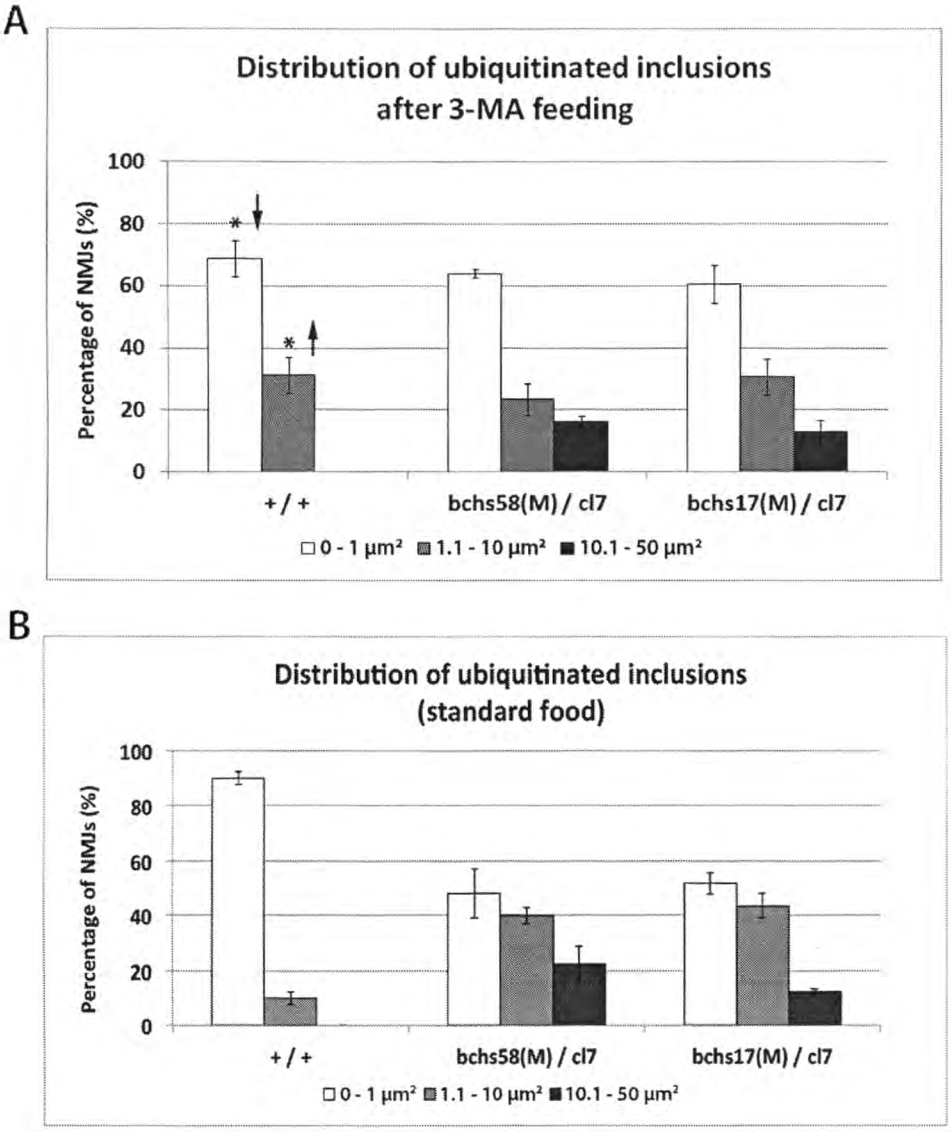


**Figure 33.** 3-MA feeding leads to a greater deposition of ubiquitinated aggregates in wild-type NMJs. There is a decreased percentage of NMJs with small ubiquitinated conjugates and a concomitant increase in the accumulation of medium ubiquitinated aggregates in wild-type after **(A)** 5 mM 3-MA feeding compared to the corresponding control that was fed in **(B)** standard food. Error bars represent standard error of the mean (SEM) for two independent experimental replicates with an average total n of 30 hemi-segments for each genotype. Chi-square test is used for statistical analysis between feeding in the presence and absence of 3-MA. * $p < 0.05$.

### 3.13 Autophagic vacuoles accumulate in *bchs* primary neurons and do not over-lap with ubiquitinated aggregates

As there is an accumulation of ubiquitinated aggregates in neuronal termini of *bchs* NMJs **(Figure 29)**, it is of interest to investigate whether there is an aberrant blockage in any steps of the autophagy pathway. Therefore, the subcellular localization of Atg5 which marks the pre-autophagosome (but not completed autophagosome) and Atg8 which marks the autophagosome and autolysosome were chosen for study in the neuromuscular system of *bchs* third instar larvae. However, there was no detectable difference in the deposition of Atg5 or Atg8 punctae along motor neuron axons and synaptic termini between wild-type control and *bchs* mutant that could be caused by a problem in immuno-histochemistry **(Figure 34)**. Due to the difficulty of observing sufficient numbers of autophagic vacuoles in motor neurons to reach significance (as these represent a small subset of the neuronal population), primary neurons cultured from third instar larval brains was utilized as a tool to study the intracellular distribution of Atg5- and Atg8-positive compartments together with ubiquitinated conjugates.

Atg5-positive compartments accumulate throughout the cell while Atg8-positive compartments accumulate preferentially in the neurites of *bchs17(M)/cl7* but not in wild-type **(Figures 35 and 36)**. In addition, ubiquitinated aggregates are observed in the perikarya and axons of *bchs* mutant but not in wild-type which correlates with the earlier finding that ubiquitinated aggregates accumulate in synaptic termini of *bchs* larval NMJs **(Figure 29)**. These ubiquitinated aggregates found in *bchs* mutant do not over-lap with either the neighboring Atg5 or Atg8 autophagic vacuoles compared to the control induced to form aggregates by Htt exon one Q93 expression (as shown by the enlarged image insets in **Figures 35 and 36**), suggesting that the loss of Bchs protein prevents the recruitment of autophagy machinery components around target substrates. Therefore, non-degraded substrates accumulate in various parts of *bchs* neuron due to impairment in the early recognition step of the selective autophagy process.

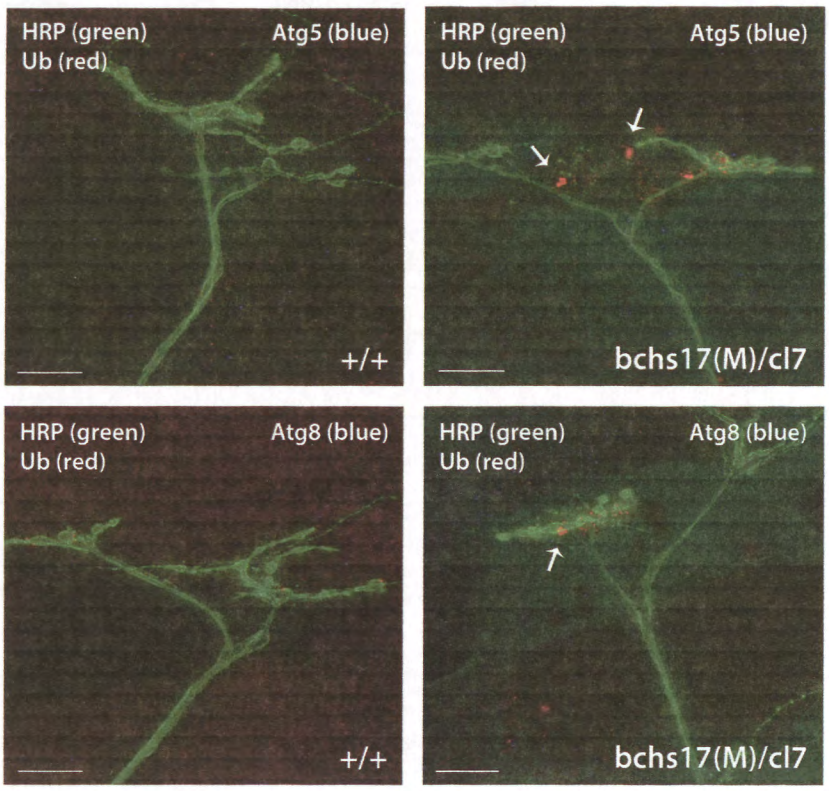


**Figure 34.** There is no detectable observation of Atg5-positive or Atg8-positive compartments in either wild-type or *bchs* NMJs. Dissected third instar larvae were immunostained with anti-HRP (*Drosophila* pan-neuronal membrane marker, green), monoclonal anti-ubiquitinated conjugates (red) and polyclonal anti-Atg5 or anti-Atg8 (blue). Although there is a notable deposition of ubiquitinated aggregates (arrows) in the synaptic termini of *bchs17(M)/cl7*, neither Atg5 nor Atg8 punctae are detected. Image projections were acquired at 40x magnification and the scale-bar represents 20 μm.

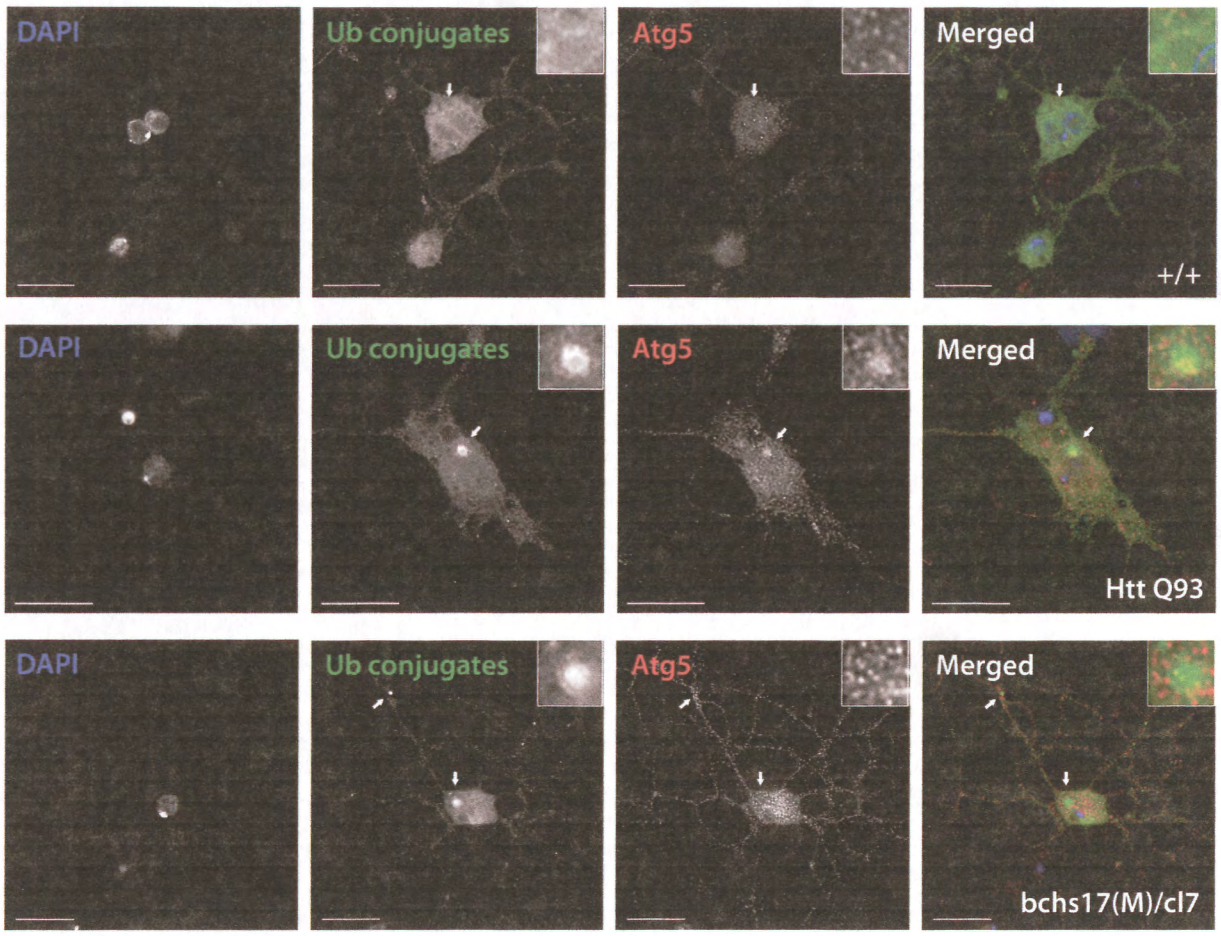


**Figure 35.** Atg5-positive compartments and ubiquitinated aggregates do not over-lap in *bchs* primary neurons, unlike in the control expressing Htt Q93. Primary neurons cultured from third instar larval brains of the indicated genotypes were immunostained for endogenous ubiquitinated conjugates and Atg5-positive autophagic vacuoles. These structures were also observed to accumulate in *bchs* mutant and in control expressing Htt Q93, but not in wild-type primary neurons. The scale-bar represents 10 µm. The top-right inset is a 5x digital zoom for the indicated region of interest by an arrow showing the deposition of ubiquitinated aggregate. Single-plane images were acquired at 100x magnification.

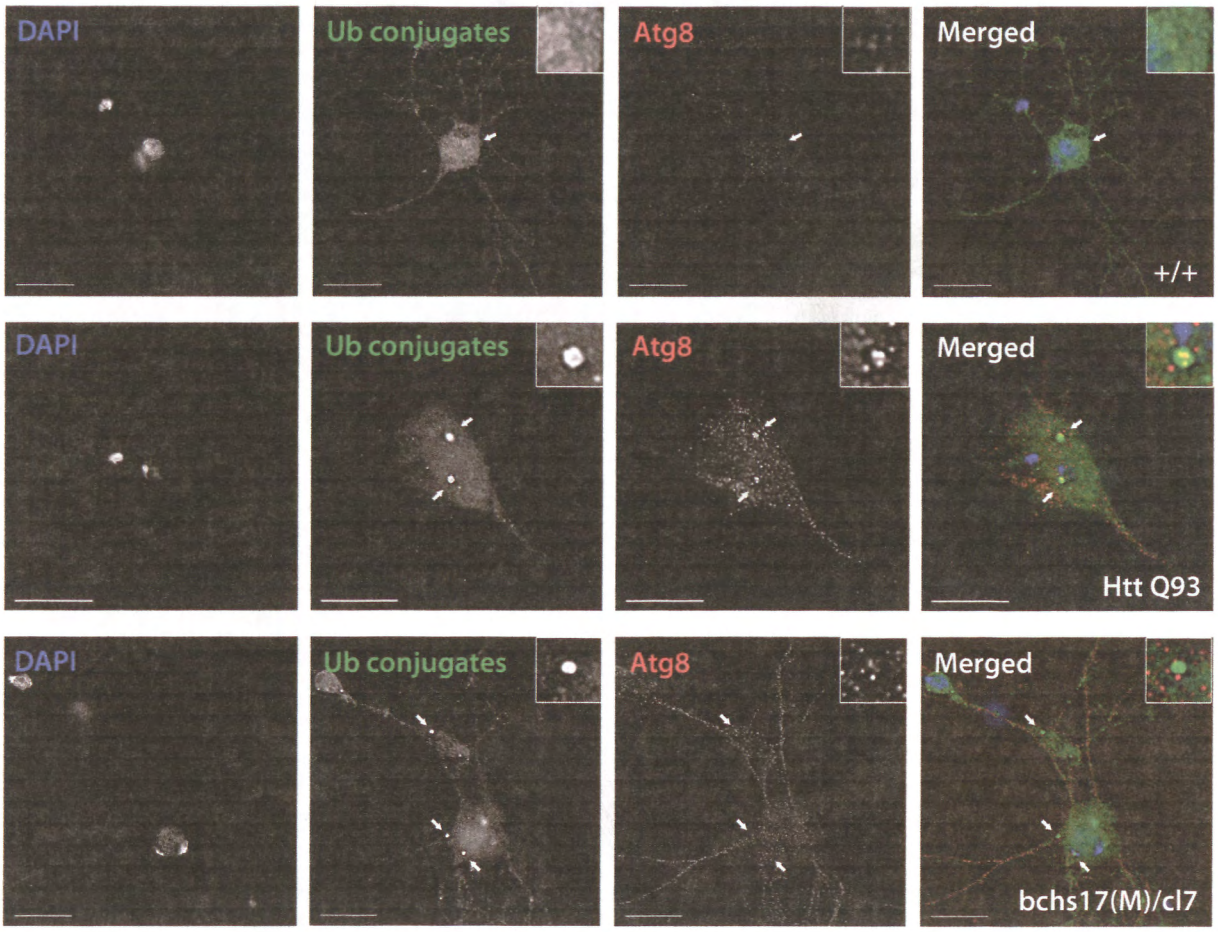


**Figure 36.** Atg8-positive compartments and ubiquitinated aggregates do not over-lap in *bchs* primary neurons, unlike in the control expressing Htt Q93. Primary neurons cultured from third instar larval brains of the indicated genotypes were immunostained for endogenous ubiquitinated conjugates and Atg8-positive autophagic vacuoles. These structures were also observed to accumulate in *bchs* mutant and in control expressing Htt Q93, but not in wild-type primary neurons. The scale-bar represents 10 µm. The top-right inset is a 5x digital zoom for the indicated region of interest by an arrow showing the deposition of ubiquitinated aggregate. Single-plane images were acquired at 100x magnification.

## B. Physiological roles in the presence of Bchs

### 3.14 Bchs associates more with Atg5 during selective autophagy and with Atg8 during non-selective autophagy

Bchs is a BEACH family protein with postulated functions in membrane vesicle transport. In order to study the physiological role of endogenous Bchs with different linked compartments of the autophagy process under comparison between selective and non-selective autophagy conditions, nutrient starvation, rapamycin treatment and Htt exon one polyQ expression were used for induction, and Bchs colocalization was assessed with each of the expressed markers labeling Atg5, Atg8, Rab11 and Spinster. Previous reports have found that Bchs homologue ALFY colocalizes with Atg5 and LC3 in HeLa cells under basal and starved conditions (Simonsen et al., 2004). Bchs was shown to partially colocalize with Rab11 and Spinster in *Drosophila* embryonic motor neurons under basal conditions (Lim and Kraut, 2009). However, no quantitative study has been conducted to investigate the spatio-temporal relationship of Bchs with different trafficking vesicles as a result of different types of autophagy.

After autophagy induction by different stimuli (starvation, rapamycin or Htt polyQ), it was observed generally that the size and number of individual Bchs, Atg5 and Atg8 punctae increased compared to non-treated primary neurons with basal level of autophagy **(Figures 37 and 38)**. Bchs was homogeneously distributed throughout the cell and, surprisingly in light of published reports, did not colocalize substantially with any single compartmental marker, including Atg5 (pre-autophagosome) and Atg8 (autophagosome), under either basal or induced autophagy **(Figures 37 and 38)**. Another notable observation was that in cases of over-lap between Bchs and the respective markers, the punctae do not completely colocalize with each other. An explanation for this observation could be that Bchs is a cytosolic adaptor protein which mediates the transient association with different vesicles in a manner reminiscent of vesicle recruitment and maturation.

In order to analyze quantitatively the colocalization of endogenous Bchs with exogenously expressed compartmental markers in response to different stimuli, Intensity Correlation Analysis from ImageJ was utilized (Li et al., 2004; Schneider et al., 2012). The colocalization

parameters produced from this analysis are $R_r$ (Pearson's correlation coefficient), Ch1 : Ch2 (the ratio of red pixels in Channel 1 to green pixels in Channel 2), M1 (the proportion of Channel 1 pixels that are also positive in Channel 2) and M2 (the proportion of Channel 2 pixels that are also positive in Channel 1). The M2-coloc of Bchs over-lapping with Atg5 decreased during nutrient starvation compared to non-treated control **(Figure 37A and 37D)**. Rapamycin treatment, another form of non-selective autophagy, did not show any difference in the colocalization between Bchs and Atg5, indicating that the dissociation is specific for starvation condition **(Figure 37B and 37D)**. The formation of expanded Htt Q93 led to a significant increase in M1-coloc of Atg5 over-lapping with Bchs and conversely, a significant increase in M2-coloc compared to Htt Q20 **(Figure 37C and 37D)**. Thus, the $R_r$ value between Bchs and Atg5 also increased when Htt Q93 was expressed. This suggests that Bchs associates preferentially with Atg5 during aggrephagy, however Bchs may dissociate from Atg5 during starvation-induced autophagy. The M1-coloc values for Atg5 are in general much higher than M2-coloc values for Bchs because the ratio of Ch1 (red pixels) : Ch2 (green pixels) is low **(Figure 37D)**. The increased association of Bchs with Atg5 may be due to the higher ratio of Atg5 : Bchs (Ch1 : Ch2) from the recruitment of cytosolic Atg5 into sites of autophagosome formation around aggregate-prone proteins.

The M2-coloc values of Bchs with Atg8 increased significantly after nutrient starvation and rapamycin treatment compared to non-treated control, possibly due to the corresponding increased Atg8 : Bchs (Ch1 : Ch2) ratios **(Figure 38A, 38B and 38D)**. The elevated levels of processed Atg8 during nutrient starvation and rapamycin treatment reflect the strength of autophagy induction by the type of stimulus, whereby both of the conditions represent non-selective autophagy. On the other hand, there was no significant increase in the proportion of Bchs (M2-coloc) over-lapping with Atg8 after Htt Q93 expression which represents a form of selective autophagy **(Figure 38C and 38D)**. A negative control to validate the specificity of Bchs and DsRed immunostaining was performed on *bchs17(M)/cl7* primary neurons not expressing the fluorophore-tagged compartmental markers **(Appendix Figure 1A)**.

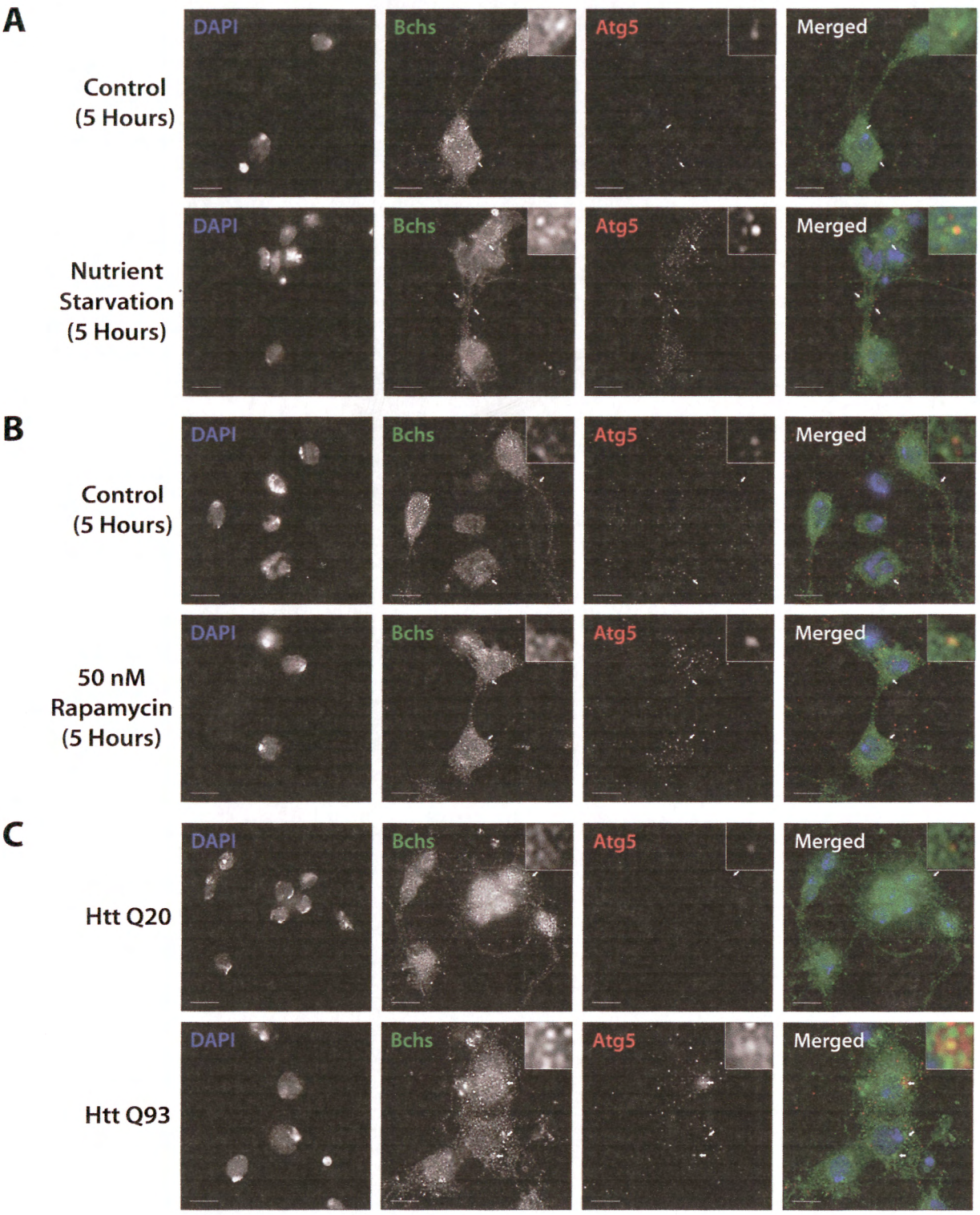


**Figure 37.** Continued on next page.

D

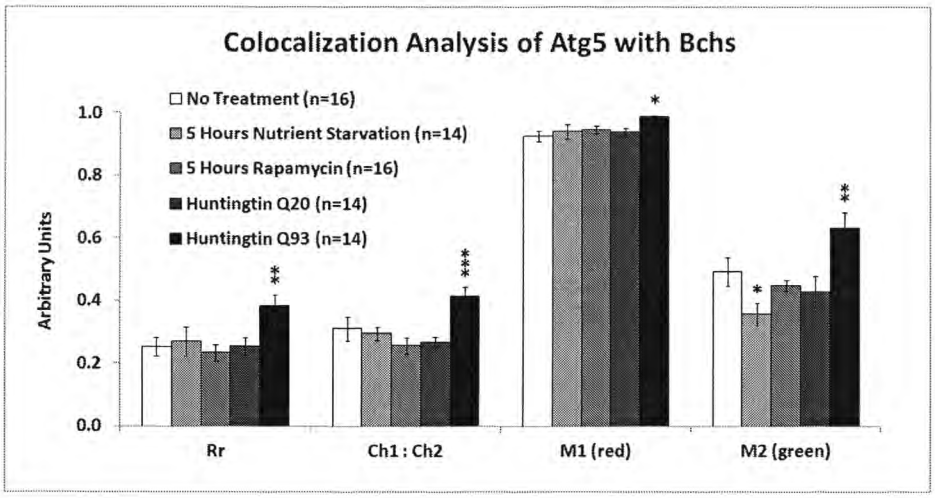


**Figure 37.** Bchs associates with Atg5 during aggrephagy and dissociates from Atg5 during starvation-induced autophagy. Third instar larval primary neurons were immunostained for endogenous Bchs and transgenic RFP-Atg5 using anti-Bchs and anti-DsRed antibodies after different conditions of autophagy induction: **(A)** five hours of nutrient starvation by incubation with serum-free hemolymph-like 3 (HL-3) buffer, **(B)** five hours of incubation with 50 nM rapamycin in complete medium and **(C)** Htt normal (Q20) and expanded (Q93) polyQ expression. 100x magnification, scale-bar represents 10 µm. Arrowheads indicate regions of close association between Bchs and Atg5. The top-right inset shows a 10x zoom of one of the indicated regions. **(D)** Colocalization analysis was performed using ImageJ to obtain Rr (Pearson's correlation coefficient), Ch1 : Ch2 ratio (red : green pixels ratio), M1 (Mander's colocalization coefficient for Channel 1) and M2 (Mander's colocalization coefficient for Channel 2). Error bars represent standard error of the mean for n = number of single-plane images. Unpaired Student's t-test is used for the statistical comparison between treatment and non-treatment groups. * $p < 0.05$, ** $p < 0.01$ and *** $p < 0.001$.

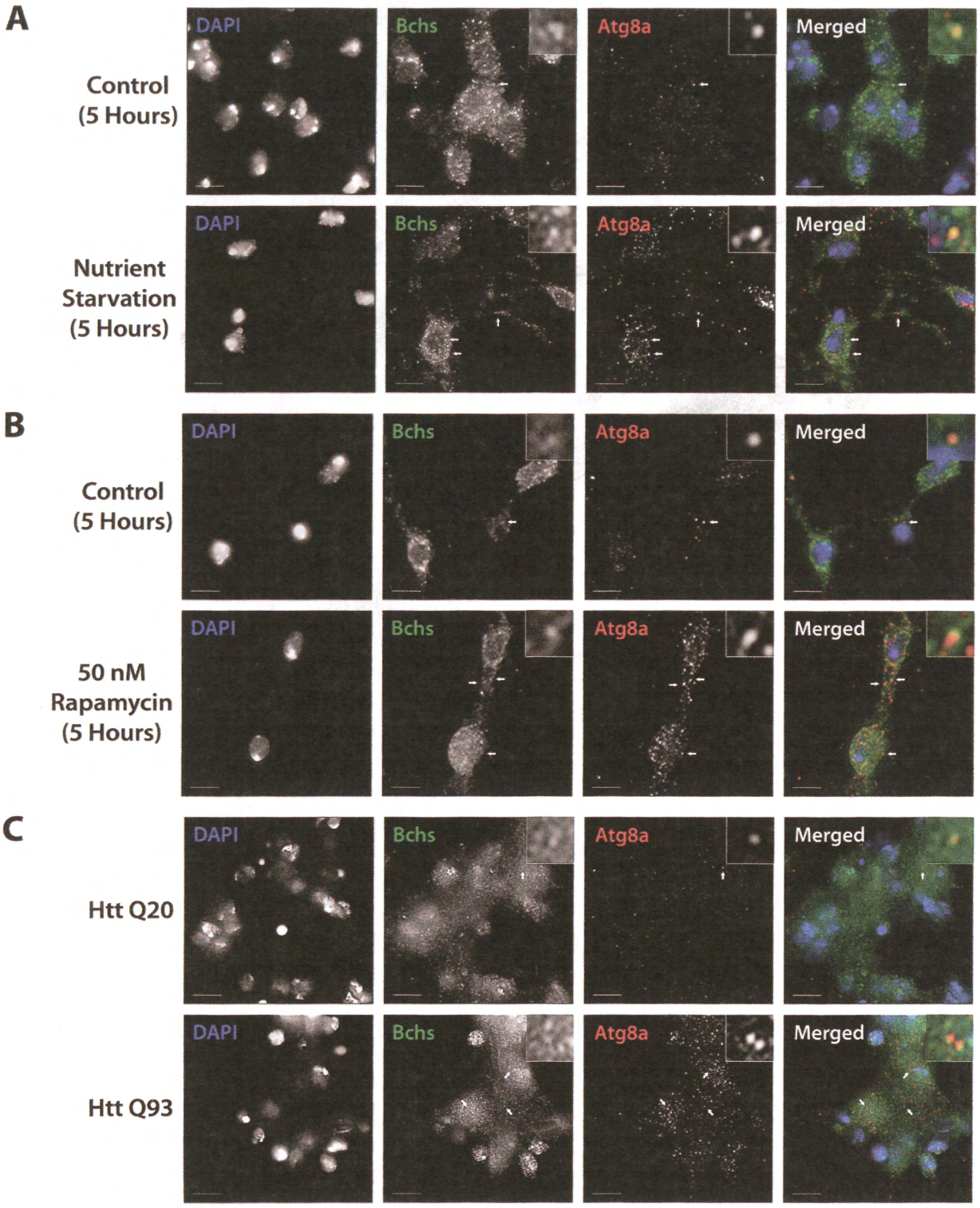


**Figure 38.** Continued on next page.

D

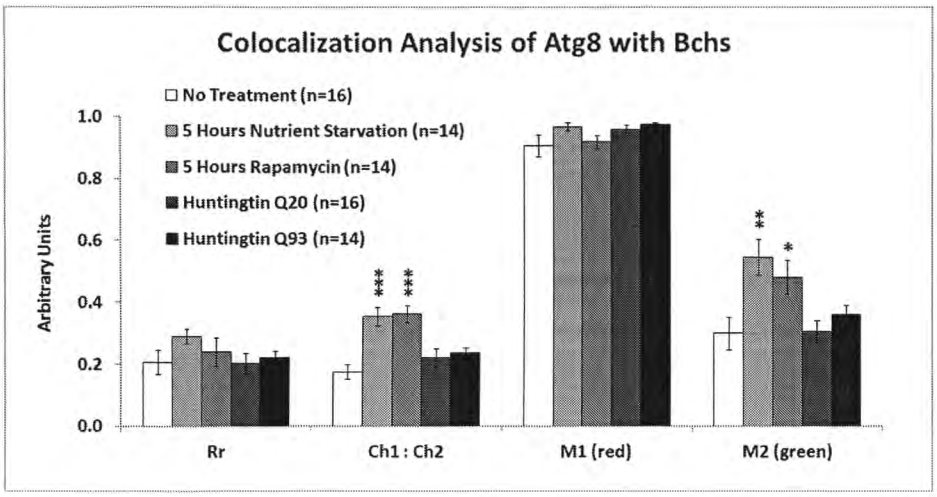


**Figure 38.** Bchs associates more with Atg8 during the induction of non-selective autophagic response. Third instar larval primary neurons were immunostained for endogenous Bchs and transgenic mCherry-Atg8a using anti-Bchs and anti-DsRed antibodies after different conditions of autophagy induction: **(A)** five hours of nutrient starvation by incubation with serum-free HL-3 buffer, **(B)** five hours of incubation with 50 nM rapamycin in complete medium and **(C)** Htt normal (Q20) and expanded (Q93) polyQ expression. 100x magnification, scale-bar represents 10 µm. Arrowheads indicate regions of close association between Bchs and Atg8. The top-right inset shows a 10x zoom of one of the indicated regions. **(D)** Colocalization analysis was performed using ImageJ to obtain Rr (Pearson's correlation coefficient), Ch1 : Ch2 ratio (red : green pixels ratio), M1 (Mander's colocalization coefficient for Channel 1) and M2 (Mander's colocalization coefficient for Channel 2). Error bars represent standard error of the mean for n = number of single-plane images. Unpaired Student's t-test is used for the statistical comparison between treatment and non-treatment groups. * $p < 0.05$, ** $p < 0.01$ and *** $p < 0.001$.

### 3.15 Bchs dissociates from Rab11 during selective autophagy and is not dependent on autophagy stimulus for association with Spinster

Rab11 localizes onto recycling endosomes and is required for early endocytic membrane trafficking and the recycling pathway (Ullrich et al., 1996; Wilcke et al., 2000). It was found that Bchs colocalizes partially with Rab11 in *Drosophila* embryonic motor neurons and Rab11 antagonizes Bchs function in synaptogenesis (Khodosh et al., 2006; Lim and Kraut, 2009). Therefore, the spatial relationship of Bchs with Rab11 was investigated in primary neurons in response to autophagy induction by different conditions. Bchs is generally distributed throughout the cell while Rab11 is concentrated at the perinuclear region as shown in **Figure 39**. After autophagy induction by nutrient starvation, rapamycin treatment and Htt polyQ expression, it was observed that there is a reduced colocalization between Bchs and Rab11 compared to non-treated control **(Figure 39A, 39B and 39C)**. Colocalization analysis also revealed decreased $R_r$ values after all conditions of autophagy induction **(Figure 39D)**. Interestingly, Htt Q20 expression resulted in a reduced $R_r$ value despite being the purportedly non-aggregating form, similar to the aggregating form Htt Q93. The M1-coloc values of the proportion of Bchs over-lapping with Rab11 decreased significantly for both Htt Q20 and Htt Q93 expression in agreement with the reduced $R_r$ values. In addition, the Bchs : Rab11 (Ch1 : Ch2) ratios increased, implying that elevated Bchs levels during Htt protein expression may contribute to the dissociation of Bchs from Rab11. These also suggest that Bchs preferentially dissociates from Rab11 during selective rather than non-selective autophagy, judging by the comparatively much lower $R_r$ values.

Spinster encodes a twelve-pass transmembrane sphingosine 1-phosphate (S1P) transporter localized on late endosomes and lysosomes (Fukuhara et al., 2012; Osborne et al., 2008; Sweeney and Davis, 2002). Spinster is required for the reactivation of TOR complex, a central nutrient sensor, following prolonged starvation and has been found to colocalize partially with Bchs in *Drosophila* embryonic motor neurons (Lim and Kraut, 2009; Rong et al., 2011). Both Bchs and Spinster are distributed throughout the cell as shown in **Figure 40** under basal and induced autophagy conditions; however Spinster levels seem to decrease and cluster at the cell periphery after Htt Q20 and Htt Q93 expression **(Figure 40C)**. One possible explanation is the

re-distribution of Spinster-positive amphisomes and autolysosomes around xenogeneic Htt protein, but not during starvation-induced autophagy or TOR inhibition. However, colocalization analysis did not demonstrate any significant differences in the levels and association between Bchs and Spinster under the various stimuli examined **(Figure 40D)**, indicating that the type of autophagy stimulus does not affect the association of Bchs with Spinster. Bchs may act as an adaptor for Spinster during sphingolipid signaling in a manner similar to FAN (factor activating neutral-sphingomyelinase) which is also a protein member of the BEACH family (Segui et al., 1999). As noted previously, Spinster is a S1P transporter and S1P can activate autophagy by inhibiting TORC1 directly (Bedia et al., 2011; Lavieu et al., 2006). In this way, the association between Bchs and Spinster may still participate in the regulation of autophagy function, albeit independent of the stimulation. A negative control to validate the specificity of Bchs and GFP immunostaining was performed on *bchs17(M)/cl7* primary neurons not expressing the fluorophore-tagged compartmental markers **(Appendix Figure 1B)**.

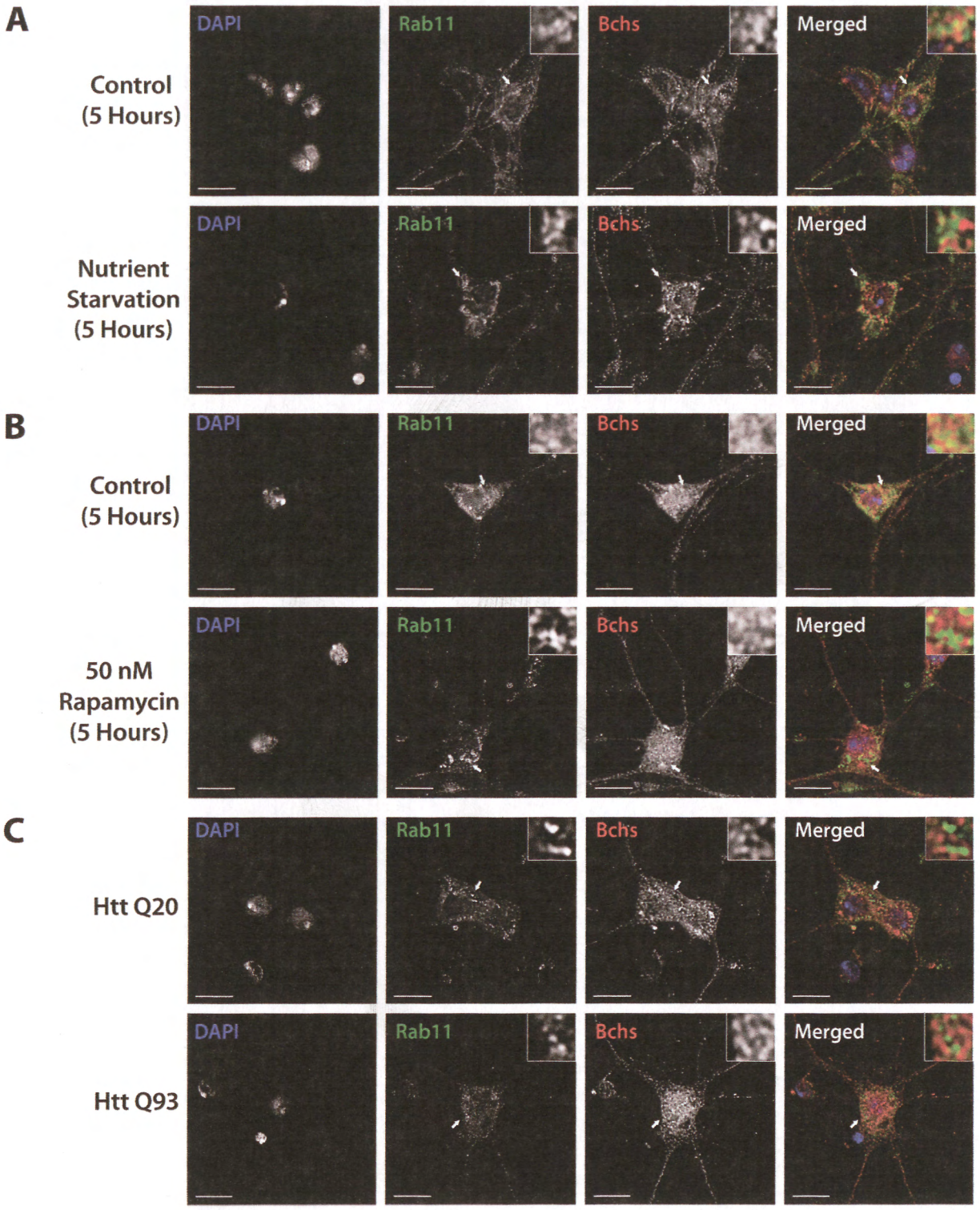


**Figure 39.** Continued on next page.

D

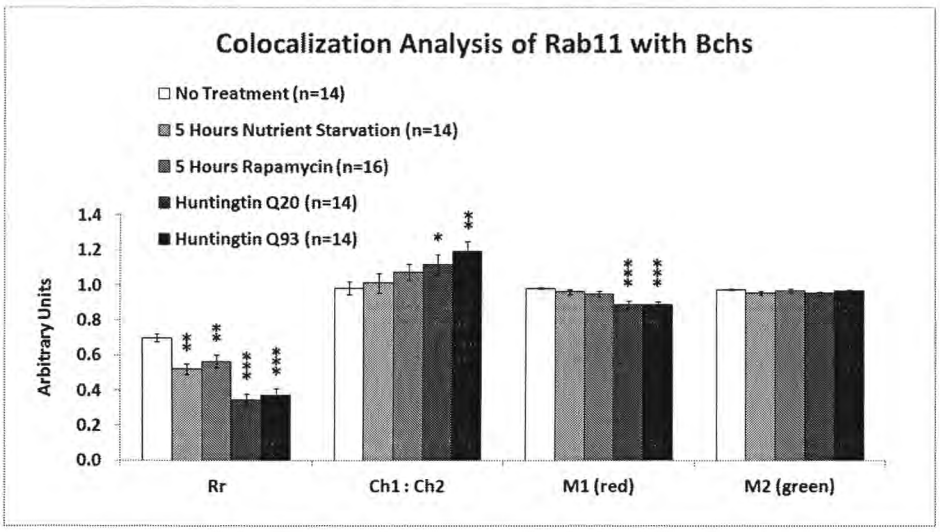


**Figure 39.** Bchs dissociates more from Rab11 during selective autophagy than non-selective autophagy. Third instar larval primary neurons were immunostained for endogenous Bchs and transgenic Rab11-GFP using anti-Bchs and anti-GFP antibodies after different conditions of autophagy induction: **(A)** five hours of nutrient starvation by incubation with serum-free HL-3 buffer, **(B)** five hours of incubation with 50 nM rapamycin in complete medium and **(C)** Htt normal (Q20) and expanded (Q93) polyQ expression. 100x magnification, scale-bar represents 10 µm. The top-right inset shows a 10x zoom of the region of interest indicated by an arrowhead. **(D)** Colocalization analysis was performed using ImageJ to obtain Rr (Pearson's correlation coefficient), Ch1 : Ch2 ratio (red : green pixels ratio), M1 (Mander's colocalization coefficient for Channel 1) and M2 (Mander's colocalization coefficient for Channel 2). Error bars represent standard error of the mean for n = number of single-plane images. Unpaired Student's t-test is used for the statistical comparison between treatment and non-treatment groups. * $p < 0.05$, ** $p < 0.01$ and *** $p < 0.001$.

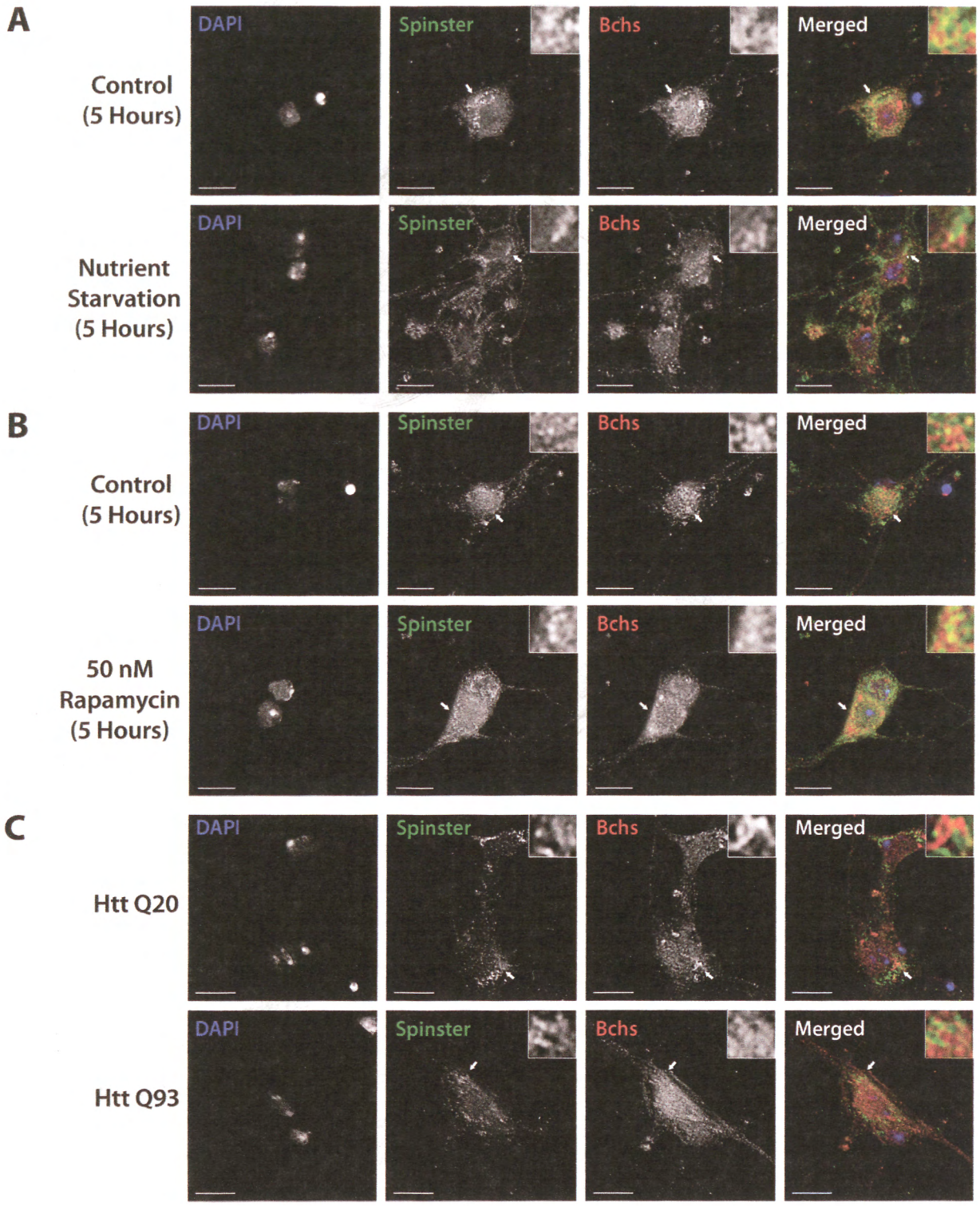


**Figure 40.** Continued on next page.

D

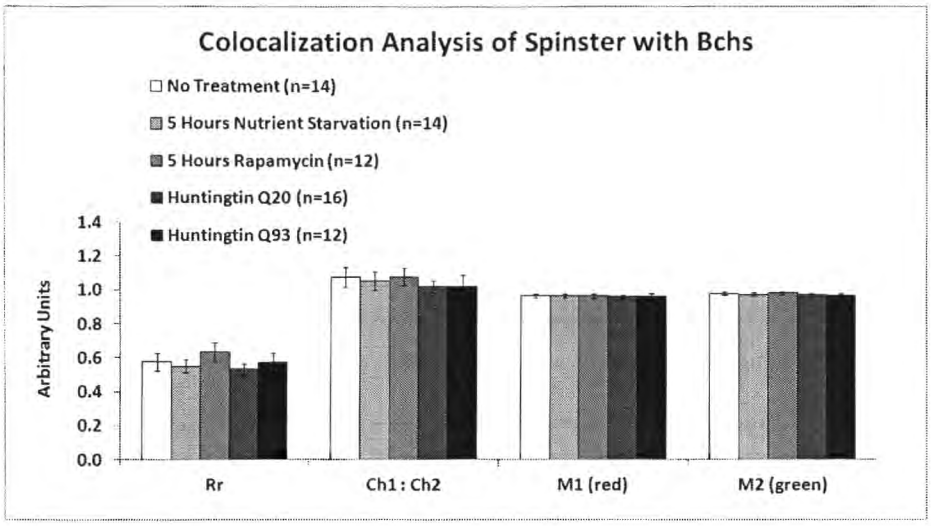


**Figure 40.** The association of Bchs with Spinster does not depend on autophagy stimulation. Third instar larval primary neurons were immunostained for endogenous Bchs and transgenic Spinster-GFP using anti-Bchs and anti-GFP antibodies after different conditions of autophagy induction: **(A)** five hours of nutrient starvation by incubation with serum-free HL-3 buffer, **(B)** five hours of incubation with 50 nM rapamycin in complete medium and **(C)** Htt normal (Q20) and expanded (Q93) polyQ expression. 100x magnification, scale-bar represents 10 µm. The top-right inset shows a 10x zoom of the region of interest indicated by an arrowhead. **(D)** Colocalization analysis was performed using ImageJ to obtain Rr (Pearson's correlation coefficient), Ch1 : Ch2 ratio (red : green pixels ratio), M1 (Mander's colocalization coefficient for Channel 1) and M2 (Mander's colocalization coefficient for Channel 2). Error bars represent standard error of the mean for n = number of single-plane images. Unpaired Student's t-test is used for the statistical comparison between treatment and non-treatment groups.

### 3.16 Live imaging of GFP-Bchs with RFP-Atg5 or mCherry-Atg8a during autophagy induction reveals similar behavior as colocalization study

In order to study the live trafficking of Bchs with autophagic vesicles under patho-physiological conditions, primary neurons cultured from third instar larval brains expressing transgenic GFP-Bchs and RFP-Atg5 or mCherry-Atg8a are utilized for live imaging. The GFP-Bchs construct consists of GFP fused to the N-terminal of the largest Bchs isoform and was cloned by Dr. Kathleen Osborne in the Kraut lab **(Figure 17)**. As shown in **Figure 41A**, GFP-Bchs punctae are localized adjacent to RFP-Atg5 punctae occasionally under basal autophagy. After induction by nutrient starvation, it was observed that there is a reduced association between GFP-Bchs and RFP-Atg5 **(Figure 41B)**. It is also interesting to note that RFP-Atg5 re-organizes itself to structures juxtaposed with the nuclear membrane which are reminiscent of the endoplasmic reticulum (ER) at 40 minutes of starvation. These structures are likely to be the phagophore assembly sites (PAS), consistent with earlier evidence that omegasomes on the ER contribute membrane source for the forming phagophore (Hayashi-Nishino et al., 2009; Yla-Anttila et al., 2009).

The expression of transfected Htt exon one Q15 resulted in the occasional localization of GFP-Bchs punctae adjacent to RFP-Atg5 punctae **(Figure 41C)** similar to basal (non-induced) autophagy conditions after incubation in complete medium. In contrast, the expression of transfected Htt exon one Q128 led to an increased association of GFP-Bchs and RFP-Atg5 in primary neurons **(Figure 41D)** which corresponds with the colocalization analysis performed on immunostained specimens **(Figure 37D)**. This provides support that Bchs associates preferentially with Atg5 during selective autophagy while Bchs may dissociate from Atg5 during non-selective autophagy. It is observed generally that cytosolic GFP-Bchs punctae are distributed throughout the cell which is in agreement with the immunostaining of endogenous Bchs.

Under basal autophagy conditions, some of the mCherry-Atg8a punctae had adjacent GFP-Bchs punctae **(Figure 42A)**. After two hours of nutrient starvation, there was a distinct formation of enlarged autophagosomes or autolysosomes as indicated by the growing mCherry-Atg8a punctae **(Figure 42B)**. These punctae had a "doughnut-like" structure and progressed to a

"bean-like" structure resembling the cross-section of vesicular compartments. The significantly larger punctae also correlate with the elevated level of processed Atg8 (or mammalian LC3-II) which is dependent on the strength of autophagy induction as reported previously (Wong and Cuervo, 2010; Xie et al., 2008). Starvation-induced autophagy, being an adaptive bulk degradation response to physiological insults, has the highest strength of autophagy stimulation. However, GFP-Bchs punctae were not observed in the vicinity of mCherry-Atg8a punctae during nutrient starvation **(Figure 42B)** although there was an increased M2-coloc value of Bchs over-lapping with Atg8a in immunostained specimens with corresponding treatment **(Figure 38D)**. This could be attributed to the engulfment of Bchs by autophagosomes which is non-detectable during live imaging.

When Htt Q15 was expressed, there is no observable over-lap between mCherry-Atg8a and GFP-Bchs similar to the basal conditions **(Figure 42C)**. The expression of Htt Q128 also did not lead to any changes in the association of mCherry-Atg8a and GFP-Bchs which corroborates the colocalization analysis **(Figure 42D)**. mCherry-Atg8a accumulated in a focal swelling along the axon (left arrow in **Figure 42D**) which is likely to be dysfunctional autophagic vesicles entrapped in the meshwork of expanded polyQ Htt aggregates. In addition, there was a mCherry-Atg8a streak which appeared to be moving in a retrograde direction towards the focal swelling but did not exit from it to transport to the cell soma. Therefore, the live imaging study shows the lack of interaction between Bchs and Atg8 under the various conditions of autophagy induction, suggesting that Bchs does not play a role with Atg8 during the autophagy process.

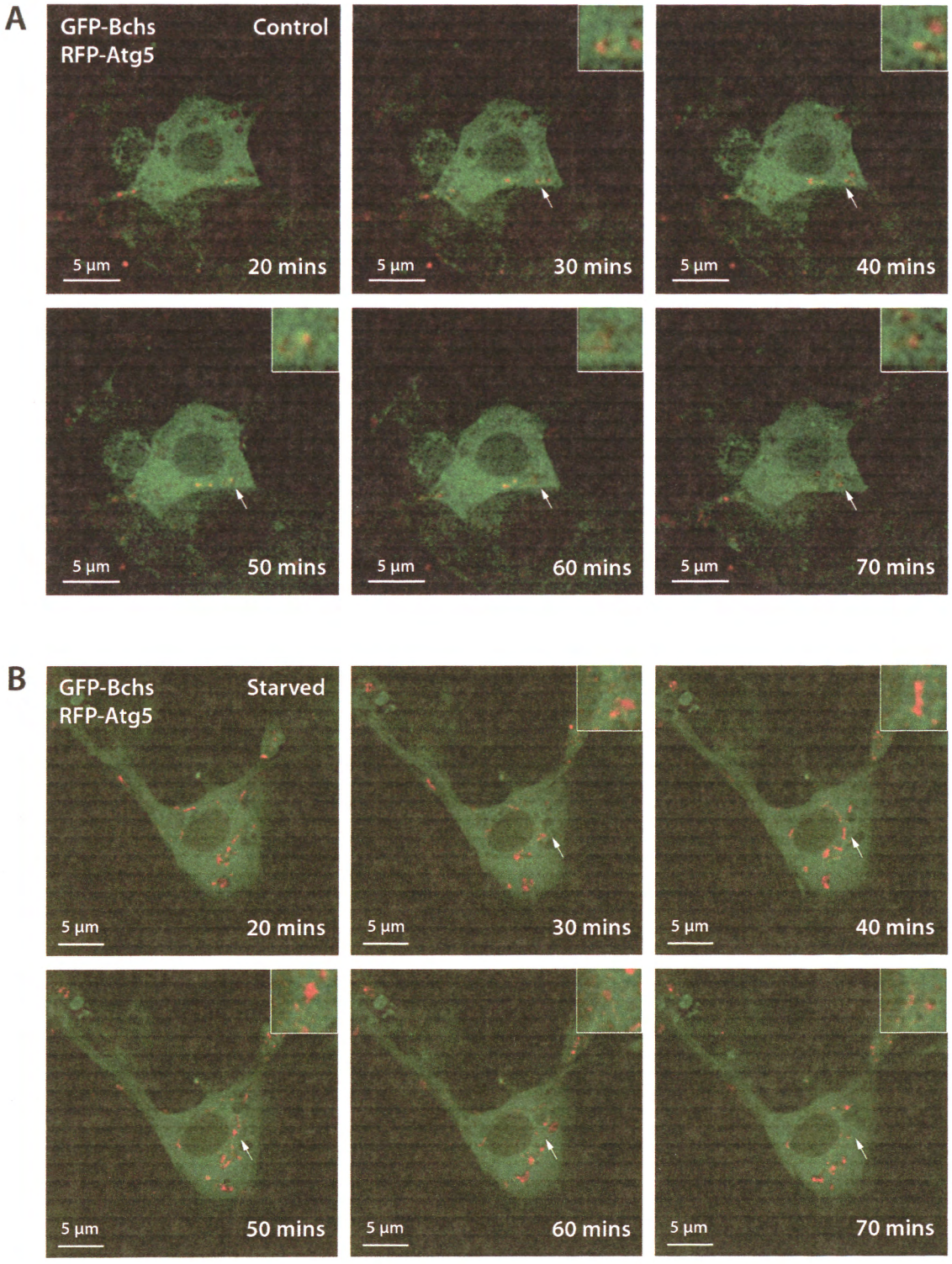


**Figure 41.** Continued on next page.

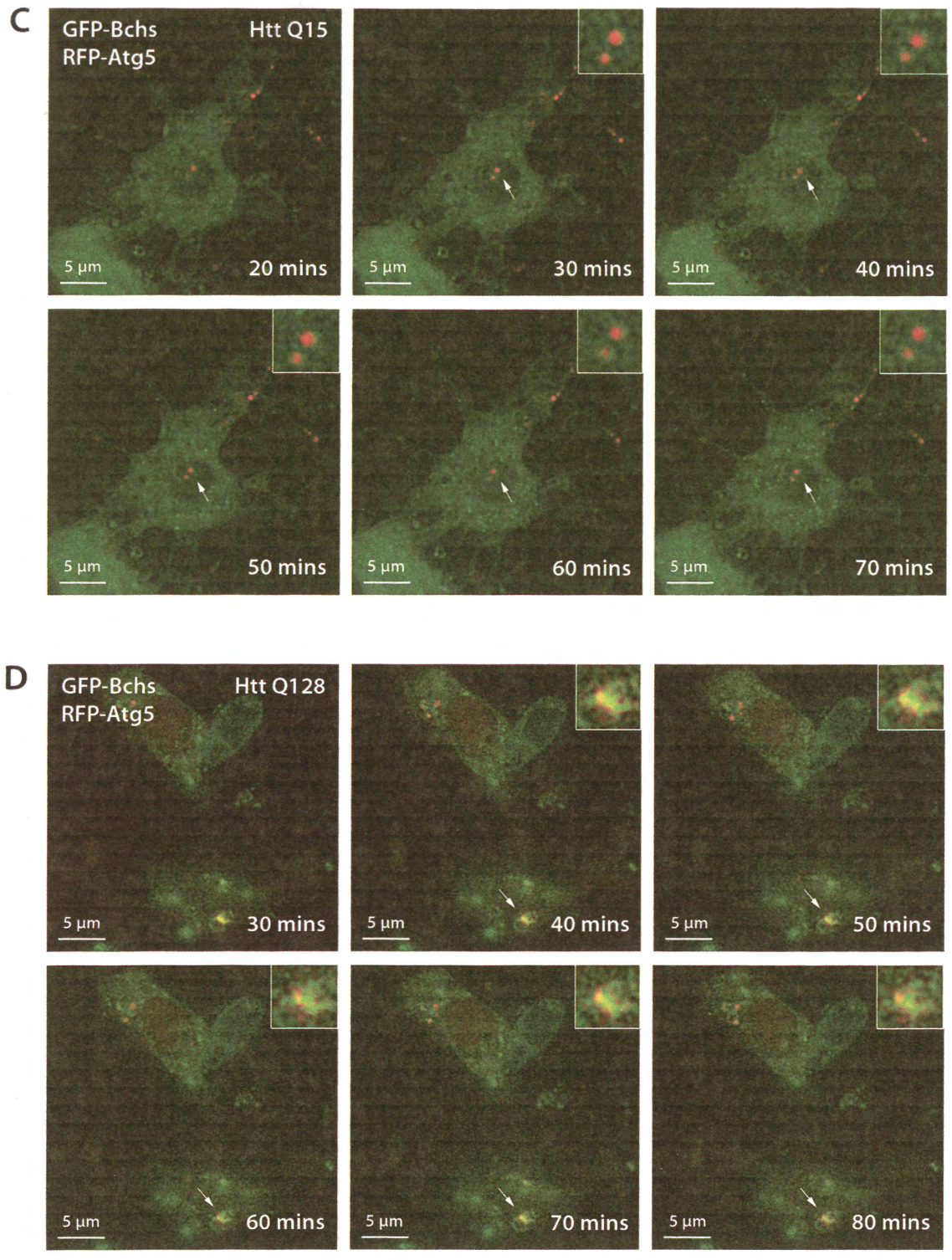


**Figure 41.** Continued on next page.

**Figure 41.** Live imaging shows GFP-Bchs associating with RFP-Atg5 during aggrephagy. Primary neurons cultured from third instar larval brains expressing GFP-Bchs and RFP-Atg5 were imaged live at time intervals of 10 minutes in the following conditions at room temperature: **(A)** incubation with complete medium, **(B)** incubation with HL-3 buffer, **(C)** 48 hours after transfection with Htt Q15 and **(D)** 48 hours after transfection with Htt Q128. The representative dimension for the scale-bar is as shown. The top-right inset shows a 5x digital zoom of the region of interest indicated by an arrow. Each single-plane image was acquired at 100x magnification.

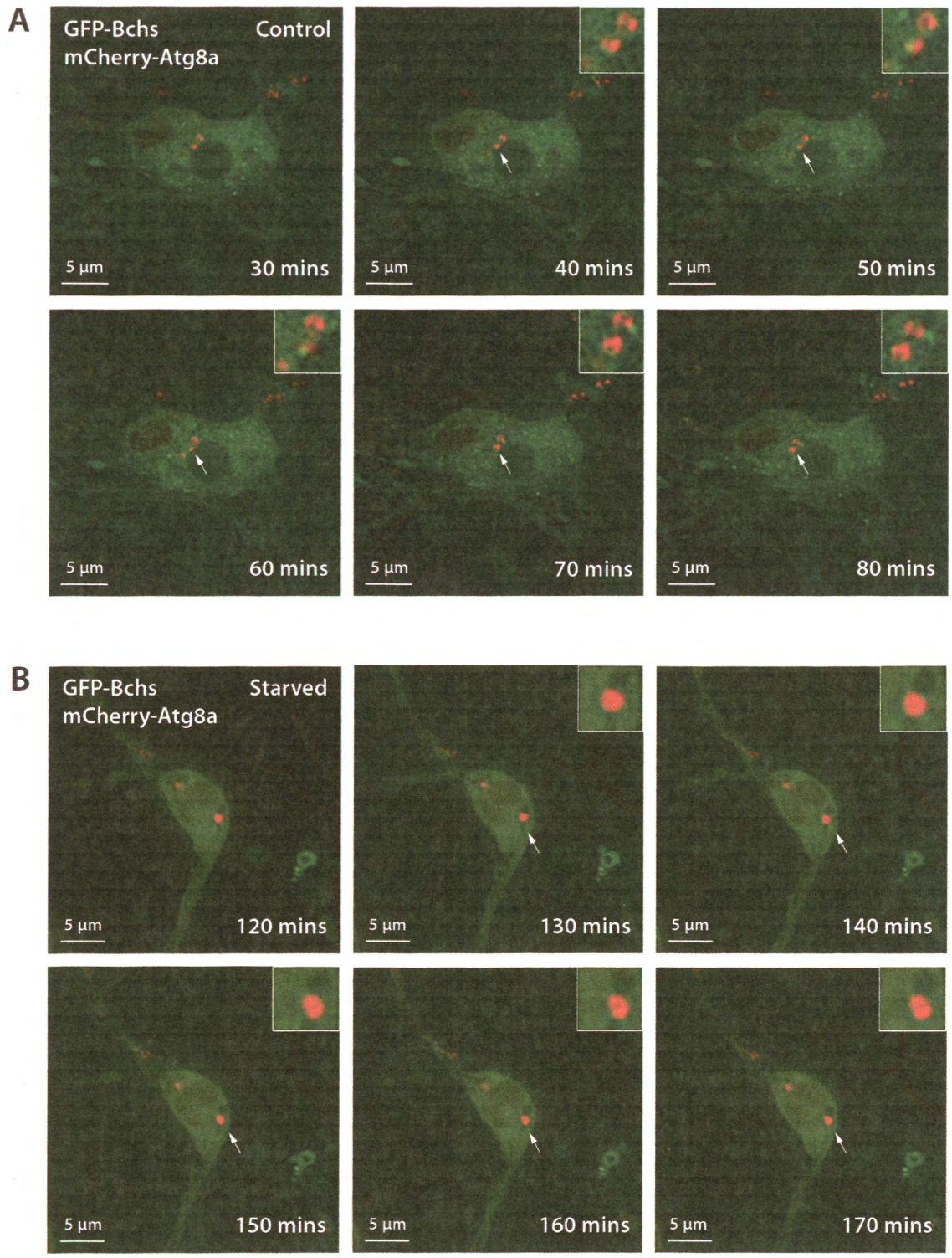


**Figure 42.** Continued on next page.

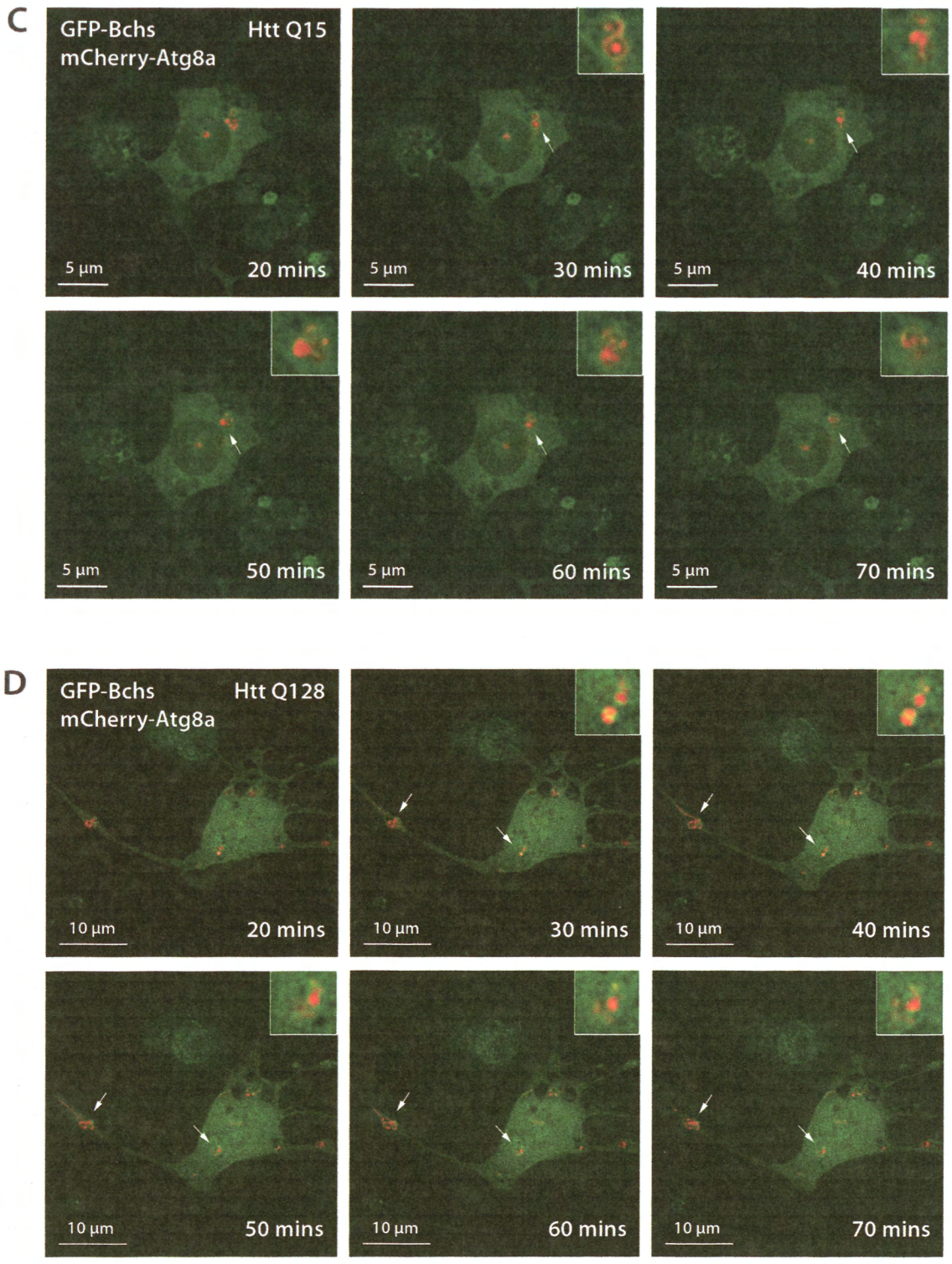


**Figure 42.** Continued on next page.

**Figure 42.** Live imaging does not show a difference in the association of GFP-Bchs with mCherry-Atg8 under any condition of autophagy induction. Primary neurons cultured from third instar larval brains expressing GFP-Bchs and mCherry-Atg8a were imaged live at time intervals of 10 minutes in the following conditions at room temperature: **(A)** incubation with complete medium, **(B)** incubation with HL-3 buffer, **(C)** 48 hours after transfection with Htt Q15 and **(D)** 48 hours after transfection with Htt Q128. The representative dimension for the scale-bar is as shown. The top-right inset shows a 5x digital zoom of the region of interest indicated by an arrow. Each single-plane image was acquired at 100x magnification.

### 3.17 Bchs does not form a complex with kinesin or dynein

We have shown in this work that Bchs associates and dissociates with different membrane vesicles, notably Atg5-positive phagophores and Rab11-positive recycling endosomes respectively, under induced selective autophagy conditions. It is also known that the anterograde transport of late endolysosomes is disrupted along motor neuron axons in *bchs* larvae (Lim and Kraut, 2009). Based on these observations, we were interested in investigating whether Bchs forms an adaptor for the motor protein assembly on microtubules with their designated cargo vesicles. Co-immunoprecipitation assay revealed that Bchs does not interact with kinesin heavy chain (KHC) and dynein heavy chain (DHC) either directly or indirectly **(Figure 43)**. However the APP-like interacting protein 1 (Aplip1), which is the *Drosophila* homologue of mammalian JNK interacting protein 1 (JIP1) and reported to bind to kinesin light chain (KLC) (Horiuchi et al., 2005), was shown as a positive control to interact with kinesin using Flag-Aplip1 for pull-down **(Figure 43)**.

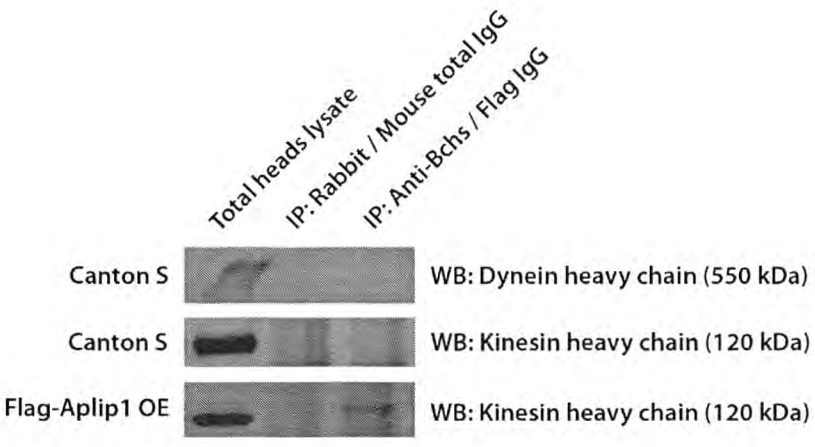


**Figure 43.** Bchs does not interact with the motor proteins kinesin or dynein. Rabbit anti-Bchs IgG was used for immunoprecipitation (IP) of endogenous Bchs in *Canton S* adult heads (top and middle panels) and subsequently probed for DHC or KHC in Western blots (WB). Over-expression (OE) of Flag-Aplip1 and using mouse anti-Flag IgG for IP (bottom panel) was shown as the positive control for interaction with kinesin. Total heads lysate and the negative control for IP using total rabbit or mouse IgG were also probed for the indicated proteins.

## 4. Discussion

The pathological manifestations of many neurodegenerative disorders are usually accompanied by the accumulation of cytotoxic aggregates such as amyloid plaques in Alzheimer's disease, Lewy bodies in Parkinson's disease, poly-glutamine tracts in Huntington's disease and ubiquitinated inclusions in amyotrophic lateral sclerosis (ALS). Many studies have established a link in the disruption of autophagy with these disorders (Boland et al., 2008; Levine and Kroemer, 2008; Ravikumar et al., 2002). Both the UPS and autophagy pathway play complementary important roles for maintaining metabolites turnover and intracellular homeostasis via different specificities for target substrates. When the UPS is defective, autophagy acts as a compensatory mechanism to eliminate ubiquitinated proteins that will otherwise aggregate. Autophagy function was also found to decline with age (Cuervo and Dice, 2000). Therefore, the accumulation of ubiquitinated inclusions in aged *bchs* brains compared to age-matched control (Finley et al., 2003) is likely due to a compromised autophagy function in *bchs* mutant.

The human ALFY protein, which is the orthologue of *Drosophila melanogaster* Bchs, was found to be required for the degradation of aggregate-prone proteins via the binding and recruitment of p62 through PH-BEACH domain and interaction with Atg5 through WD40 repeats in a cellular system (Clausen et al., 2010; Filimonenko et al., 2010). However, studies have not been reported to demonstrate impaired autophagy function in *bchs* animals. Although a genetic modifier screen for Bchs over-expressing rough eye phenotype showed several *atg* genes as genetic modifiers (Simonsen et al., 2007) and late endolysosomal transport was disrupted along motor neuron axons in *bchs* mutants (Lim and Kraut, 2009), the role of Bchs protein during the autophagy process has not been examined in neuronal tissues *in vivo*. In order to characterize the step at which Bchs is involved in the autophagy pathway, two main approaches under the absence (pathological effects) and presence (physiological roles) of functional Bchs are investigated.

## A. Pathological effects in the absence of Bchs

We initially measure the brain volume from third instar larvae to be utilized as a tool for the study of the modulation of *bchs* neurodegenerative phenotype from pharmacological interventions and genetic interactions. However, it was found that the genetic background of varying genotypes can have a significant contribution towards brain volume measurement **(Figure 13)**. One method of overcoming this is by performing isogenization to homogenize the genetic background of the chromosomes and remove any undesirable recessive lethal alleles which may interfere with the gene of interest (Ashburner et al., 2005). Isogenization involves the back-crossing of a relevant line to a balancer stock, which has balancer chromosome(s) on the first, second or third, for several generations. The balancer chromosome is a unique tool of *Drosophila* genetics that has multiple regional inversions in order to suppress random homologous recombination.

Unfortunately, this was not practically feasible in our study for the genetic interactions between different *bchs* and *atg* alleles due to the involvement of multiple genotypes that will need to be back-crossed to a common stock. It is nevertheless possible to infer based on appropriate comparison with the respective background controls, that the loss of Bchs led to 15% - 17% reduction in larval brain volume **(Figure 13)**, a similar trend observed in aged *bchs* adult brains which had an estimated 40% reduction in brain volume based on linear dimensions (Finley et al., 2003). Conversely, the over-expression of Bchs resulted in a 15% increase of larval brain volume compared to the respective background control. This is possibly due to one of the downstream effects of autophagy function to inhibit apoptosis, although the debate is controversial as excessive autophagy could also promote apoptosis (Boya et al., 2005; Pattingre et al., 2005; Scott et al., 2007).

Therefore, we went back to the previous assay to measure the neurodegenerative penetrance through a GFP reporter expressed in only a subset of the ~ 30 motor neurons in the larval CNS, the identified neurons aCC and RP2 (Lim and Kraut, 2009). These motor neurons are two of a number of embryonic neurons that express relatively higher endogenous level of Bchs (Lim and Kraut, 2009). When there is a *bchs* mutation, RP2 motor neurons exhibit a significantly reduced

viability, but this is not in the case for aCC motor neurons which are often present. However, aCC motor neurons are completely absent after Atg1 over-expression. The discrepancy between the viability of RP2 and aCC motor neurons may be due to their innate characteristics – RP2 being a fast-twitch neuron and aCC being a slow-twitch neuron. Fast-twitch neurons have more mitochondria than slow-twitch neurons, to provide sufficient ATP production; oxidative phosphorylation in mitochondria produces ATP faster and more efficiently than cytosolic glycolysis (Kuznetsov et al., 1996; Wallace and Fan, 2010). It is hypothesized that selective autophagy (i.e. in the case of mitophagy) may play a more prominent role in RP2 rather than aCC motor neuron and thus in the absence of Bchs function which promotes autophagy, RP2 is susceptible to neuronal atrophy. Although the assay based on RP2 motor neuron death may not be representative of neurodegenerative severity as a whole, since this has never been rigorously proven by other assays done in parallel (e.g. whole brain ubiquitin content, climbing assay etc.), it provides a useful tool for studying the effects of pharmacological modulations and genetic interactions on the *bchs* phenotype.

Using this assay of scoring for the percentage of RP2 motor neuron survival, it was found that the penetrance of *bchs* degenerative phenotype was influenced by autophagy-modulating drugs. After feeding with 1 μM rapamycin, *bchs58(O)/cl7* showed the highest rescue of RP2 motor neuron death, followed by *bchs58(M)/cl7* **(Figure 18)**. *bchs17(M)/cl7* showed only a small elevation in the rescue of RP2 death when fed with rapamycin, suggesting that a rate-limiting step of autophagy initiation downstream of TORC1 in *bchs17(M)* may be inhibited. The differential responses of these *bchs* mutants may reflect the presence of alternatively spliced Bchs isoforms. Both *bchs58(O)* and *bchs58(M)* alleles are hypomorphic mutations that remove the largest Bchs isoform while *bchs17(M)* affects the largest and intermediate Bchs isoforms **(Figure 17)**. As a result, *bchs17(M)/cl7* is observed to have the least response towards autophagy-modulating drugs. *bchs58(O)/cl7* has a more severe RP2 degeneration than *bchs58(M)/cl7* due to the insertion of an EP element in *bchs58(O)* that can drive the expression of a truncated dominant negative Bchs protein. The *in vivo* rescue of RP2 degenerative phenotype in *bchs* mutants by rapamycin suggests that autophagy function is deficient in *bchs* mutants. In addition to promoting autophagy, rapamycin may also suppress protein synthesis

through TORC1 inhibition, thereby alleviating the protein load imposed upon the cellular quality control system and preventing the formation of cytotoxic aggregates (Huo et al., 2011).

On the other hand, inhibition of autophagy through the PI3K inhibitors wortmannin and 3-MA led to RP2 loss in wild-type which did not worsen with increasing drug concentration. In contrast, an exacerbation of RP2 death in *bchs58(O)/cl7* and *bchs58(M)/cl7* in a dose-dependent manner was seen **(Figures 19 and 20)**. This indicates that autophagy function is sufficiently robust in wild-type to cope with increased pharmacological inhibition while the *bchs* hypomorphs are sensitive towards autophagy inhibition. *bchs17(M)/cl7* did not worsen after wortmannin and 3-MA feeding, suggesting that the loss of two Bchs isoforms abolished not the PI3K activity *per se* but its downstream effect of PI3P. This may be due to the inability to recruit and organize PI3P at sites of phagophore assembly through the FYVE domain in Bchs. Although the third and smallest Bchs isoform has FYVE domain but lacks the PH-BEACH domain which binds to Ref(2)P (*Drosophila* homologue of mammalian p62) **(Figure 17)**, we postulate that this Bchs isoform does not play a role in autophagy. These experiments indicate that Bchs is likely to function downstream of the targets for the drugs, namely TORC1 and class III PI3K. It is also important to note that wortmannin and 3-MA may affect endocytic trafficking through PI3-P levels, subsequently impeding the maturation and fusion of autophagosomes with late endosomes.

To further demonstrate that autophagy is deficient in *bchs* mutants, the over-expression of Atg7 strikingly rescued RP2 survival to almost 100% in *bchs17(M)/cl7* and *bchs58(M)/cl7* **(Figure 26)**. Atg7 is an E1-like ubiquitin activating enzyme that participates in the two parallel ubiquitin-like conjugation systems of Atg8 and Atg12 during autophagosome biogenesis (Geng and Klionsky, 2008; Ichimura et al., 2000). This finding shows for the first time that augmenting autophagy through Atg7 over-expression can promote neuronal survival and ameliorate death in a neurodegenerative disease model, and that there is a positive genetic interaction between Atg proteins and Bchs demonstrated by rescue in a loss-of-function *bchs* background. Previous work from other groups has reported that *Drosophila atg7-/-* adults also accumulate ubiquitinated aggregates in neurons and mouse brain-specific ablation of *atg5* or *atg7* leads to

a massive loss of pyramidal neurons in cerebral cortex and Purkinje cells in cerebellar cortex (Hara et al., 2006; Juhasz et al., 2007; Komatsu et al., 2006).

Likewise, in this study, a single copy deletion of *atg7* resulted in a similar percentage of RP2 death as the hypomorphic *bchs58(M)/cl7*. The recombination of *atg7[d77]* with *bchs58(M)* slightly exacerbated RP2 death in a non-additive manner while the recombination of *atg7[d77]* with *bchs17(M)* did not exacerbate RP2 death. This is consistent with the observation that autophagy suppression by wortmannin and 3-MA feeding also did not exacerbate the *bchs17(M)/cl7* phenotype. The above results provide support for the notion that *bchs17(M)/cl7* behaves as a null with respect to autophagy function and that Bchs may act upstream of Atg7 in the same pathway due to the rescue by Atg7 over-expression. Unfortunately, another *atg7* deletion *atg7[d14]* was not able to be recombined with *cl7* in order to examine the effect of homozygous *atg7* deletion on *bchs* mutants. Both *atg7[d14]* and *cl7* are regional deletions on opposite arms of chromosome two, suggesting that the inability to recombine these two alleles is not because of cytological proximity, but instead may be due to synthetic lethality, further supportive of an agonistic interaction between the *atg* gene and *bchs*. Therefore, the neurodegenerative phenotype caused by *bchs* mutation is mediated through a loss of function in autophagy that is required for its neuro-protective effects under basal homeostasis and in response to cellular stress.

As the nervous system consists of a major population of post-mitotic neurons and glial cells, it is important that protein quality control occurs in a constitutive manner to cope with the high protein translational and turnover activity. Ubiquitinated aggregates were found along photoreceptor axons in *bchs* over-expressing late pupae and *bchs* loss-of-function adult brains (Finley et al., 2003; Simonsen et al., 2007). In this study, further evidence is provided for the accumulation of ubiquitinated aggregates in different parts of the neuron, specifically the synaptic termini of *bchs* motor neurons in third instar larvae, cytoplasmic processes, and perikarya of *bchs* primary larval brain neurons **(Figures 29, 35 and 36)**. This indicates that Bchs is required for the degradation of target substrates throughout the cell, and indeed low levels of Bchs are found throughout the ventral ganglion and brain of third instar larvae in fully

differentiated neurons (Dr. Kathleen Osborne, personal communication), although Bchs had been reported to be enriched in synaptic boutons of axon terminals (Khodosh et al., 2006).

To demonstrate that the ubiquitinated aggregates in synaptic termini of *bchs* larval NMJs can be removed via autophagy, rapamycin feeding suppresses the number and size of ubiquitinated aggregates in NMJs, corresponding with an improved RP2 motor neuron survival **(Figure 31)**. Although 3-MA resulted in the deposition of ubiquitinated aggregates in wild-type NMJs, both wortmannin and 3-MA did not cause a growth in the number of ubiquitinated aggregates in *bchs* mutant, despite exacerbating RP2 death **(Figures 32 and 33)**. This underscores the fact that the percentage of RP2 survival is not necessarily correlated with the detectable level of ubiquitinated aggregates in NMJs, and thereby also suggests that mechanisms of death may be multi-factorial (i.e. aggregate-related and -unrelated). Thus, even though the degree of RP2 degeneration in the order of increasing severity is *bchs58(M)/cl7*, *bchs17(M)/cl7* and *bchs58(O)/cl7*, the distribution of the size of ubiquitinated aggregates is in the reverse order. Nonetheless, *bchs* mutants in general accumulate more and larger ubiquitinated aggregates in neuronal termini than wild-type control animals due to an impairment of autophagy function.

The conditional knockout of *atg7* in mouse brain led to the pre-synaptic accumulation of α-synuclein and leucine-rich repeat kinase 2 (LRRK2), both of which are PD-related proteins (Friedman et al., 2012). Thus, Bchs and Atg7 may cooperate in the same pathway to eliminate unwanted proteins that potentially accumulate in synaptic termini. Interestingly, a recent study showed that the early initiation steps of autophagosome formation occur distally and constitutively in the neurite tips of mouse primary neurons which mature as the autophagosomes are transported retrogradely towards the cell soma in a dynein-dependent manner (Maday et al., 2012). Therefore, the enrichment of Bchs protein in vesicular structures at synaptic boutons of axon endings as reported by Khodosh and co-workers suggests that Bchs may play a more prominent role during the initiation of autophagosome biogenesis at neuronal termini. However, this does not imply that autophagic substrates are only degraded at neuronal termini, because the internalization of organelles and soluble cargoes by autophagosomes can occur along axons (Maday et al., 2012). Our observation of ubiquitinated aggregates in cell soma, neurites and synaptic termini of *bchs* mutant also suggests that the autophagy defect is

not limited to a failure of clearance at termini, but may arise from deficits occurring throughout the cell.

In this study, Atg5-positive compartments were also elevated throughout the cell bodies and axons of primary neurons while Atg8-positive compartments were elevated predominantly along axons of primary neurons in *bchs* mutant **(Figures 35 and 36)**. This correlates with the earlier report that autophagic vacuoles transport retrogradely along axons and they had been found to accumulate in dystrophic neurites of AD brain (Lee et al., 2011; Maday et al., 2012; Nixon et al., 2005). In addition, the accumulation of Atg5-marked pre-autophagosomes throughout the cell suggests that there is a blockage in the biogenesis and thus downstream maturation of autophagosomes because Atg5 leaves the latter once the double-membrane compartment is sealed and formed completely (Mizushima et al., 2001; Suzuki et al., 2001). Atg5 accumulation is unlikely to be due to an increase of autophagy induction but rather an inhibition of autophagy flux, based on the complementary role between Bchs and Atg7 in the genetic interaction study, and the accumulation of ubiquitinated aggregates in *bchs* mutants. Stronger evidence could have been provided through the use of Ref(2)P (or p62), which is an autophagy receptor, to measure the turnover activity; unfortunately, this was not possible as we were unable to obtain Ref(2)P antibody (Nezis et al., 2008). The inhibition of autophagy flux in *bchs* mutants may lead to a compensatory mechanism by the cell to up-regulate the expression level of Atg5, thus resulting in its accumulation throughout the cell and causing a greater load on the autophagy pathway in a manner similar to lysosomal storage disorders (LSDs), in which the abundance of compartments along the autophagic-endocytic-lysosomal system is increased, depending on the LSDs sub-type (Platt et al., 2012).

Why is there an inhibition of autophagy flux in *bchs* mutants caused by the upstream blockage at the biogenesis of complete autophagosome and not just attributed to a disruption in autophagosomal maturation steps with endosomes and subsequent fusion with lysosomes? In addition to the observable accumulation of autophagic vacuoles, these compartments do not colocalize with ubiquitinated aggregates in *bchs* mutant unlike those in wild-type primary neurons expressing expanded polyQ Htt protein. This suggests that there is a failure in the recognition of ubiquitinated substrates by components of the autophagy machinery and points

to a disruption in the involvement of autophagy receptors and adaptors that function as molecular bridges **(Figure 44)**. As a result, autophagic vacuoles are not able to be recruited to target substrates for the sequestration of double membrane-bound cargoes. It was reported that ALFY protein functions as an autophagy adaptor by binding to p62-positive inclusion bodies and Atg5-Atg12-Atg16L multimeric complex directly to promote the clearance of aggresomes (Clausen et al., 2010; Filimonenko et al., 2010). In the absence of Bchs, Ref(2)P is still able to aid in the polymerization of ubiquitinated substrates through the PB1 (Phox and Bem1) domain (Bjorkoy et al., 2005; Nezis et al., 2008) but they cannot be degraded via macroautophagy in a similar way as that mediated by ALFY.

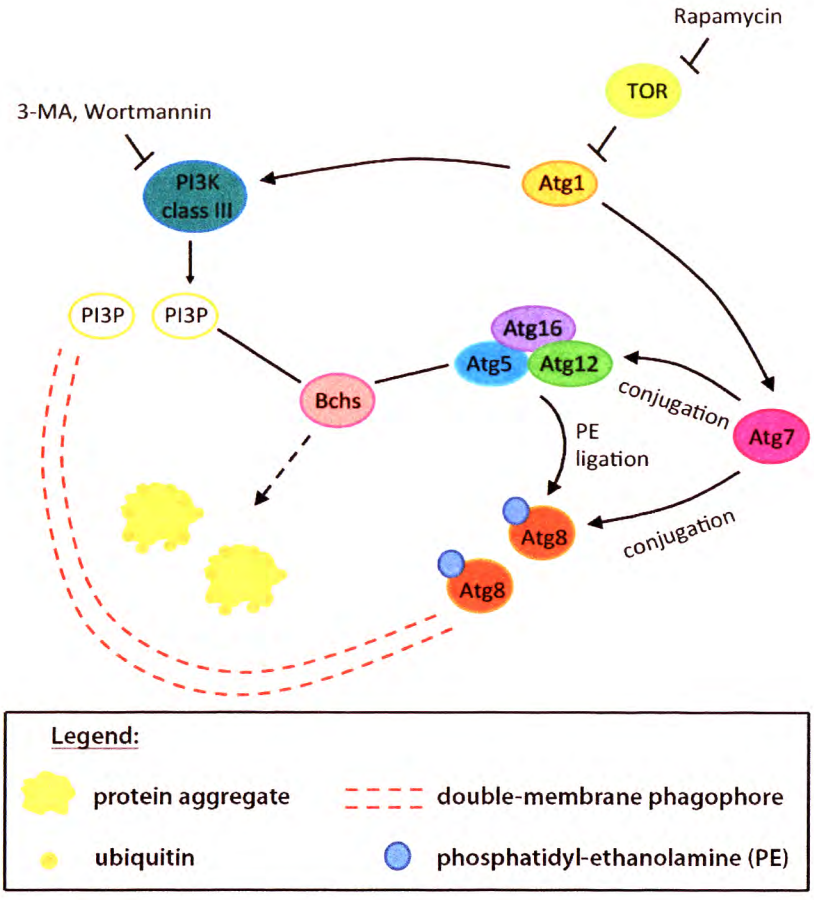


**Figure 44.** A schematic diagram showing the relationship of Bchs and autophagy pathway in the clearance of aggregate-prone proteins. Bchs associates with Atg5 during the induction of aggrephagy and plays a role in recruiting components of the autophagy machinery to sites of autophagosome formation around ubiquitinated aggregates. Future studies could be aimed at investigating whether Bchs interacts with a selective autophagy receptor, such as Ref(2)P, in order to recognize target substrates for degradation. Based on pharmacological modulations which partially rescues *bchs* degenerative phenotype with autophagy inducers and exacerbates correspondingly with autophagy inhibitors, it is proposed that Bchs acts downstream of the TOR complex and PI3K class III. Genetic interaction revealed that the over-expression of Atg7 rescues *bchs* degenerative phenotype, thus Atg7 is likely to function downstream of or in a parallel pathway as Bchs. Although Atg5 is required to undergo conjugation reaction by Atg7 and Bchs associates with Atg5, Bchs adaptor protein can still act upstream of Atg7 by "priming" target substrates for the autophagy machinery.

## B. Physiological roles in the presence of Bchs

Bchs protein contains both BEACH and FYVE domains with regulatory roles in vesicle trafficking and membrane dynamics (Kutateladze, 2010; Shiflett et al., 2002). A structural crystallography study revealed strong interaction between the PH domain, which binds to phosphoinositides, and the BEACH domain via a groove at the interface that is likely to be involved in the interaction with their partner proteins (Jogl et al., 2002). There is also a concanavalin A-like lectin domain in the N-terminus of Bchs that binds to oligosaccharide moieties possibly on the membrane periphery in order to promote vesicle fusion (Burgess et al., 2009). Only the WD40 repeats in Bchs do not have a role in binding to membrane sites. With such a strong biochemical linkage to membrane vesicles, the idea of dissecting the spatial-temporal relationship of Bchs to different processive compartments in vesicle trafficking of the autophagy pathway, in the background of various patho-physiological environments is enticing.

In this study, quantitative colocalization analysis was performed on the subcellular distribution of endogenous Bchs and expressed compartmental markers, namely Atg5, Atg8, Rab11 and Spinster, in response to non-selective and selective forms of autophagy. There is a greater association between Bchs and Atg5 after the expression of Htt Q93 based on the increased colocalization values of $R_r$, M1 and M2 parameters **(Figure 37)**, indicating that Bchs may interact with Atg5 to promote the clearance of aggregate-prone proteins during selective autophagy similarly to ALFY. Live imaging study using GFP-Bchs and RFP-Atg5 expressed in primary neurons transfected with Htt Q128 also revealed their increased association **(Figure 41D)**, thus supporting the hypothesis. Interestingly, the M2 value which annotates the proportion of green channel pixels over-lapping with red channel pixels showed a reduction in the association between Bchs and Atg5 during starvation-induced autophagy that was also corroborated by the live imaging study. This suggests that Bchs dissociates from Atg5 under nutrient starvation and is likely to be not required for non-selective autophagy. Therefore, a possible scenario arises whereby Bchs can compete for the binding of Atg5 for autophagosome biogenesis around specific targets and results in a reduced efficiency of bulk cytoplasmic degradation to recycle macromolecules during nutrient starvation.

In the case for ALFY, this protein is localized specifically on nuclear membrane in HeLa cells and only translocates out to cytoplasmic structures in the presence of aggregate-prone proteins, proposing a mechanism for the spatial restriction of ALFY activity (Filimonenko et al., 2010). However, immunostaining of endogenous Bchs revealed homogeneous distribution throughout primary neurons, including their nuclei. Bchs was observed to be more concentrated on the nuclear membranes and nuclei in primary neurons occasionally under basal autophagy condition **(Appendix Figure 2)**. The expression pattern of Bchs and ALFY is also highest in neuronal tissues compared to other tissue types (Finley et al., 2003; Khodosh et al., 2006; Simonsen et al., 2004). This implies that the activity for both proteins is greatest in neuronal tissues wherein a constitutively high level of quality control (or selective) autophagy is crucial to eliminate unwanted proteins in post-mitotic cells. Starvation-induced autophagy may not play a prominent physiological role in the brain being the primary organ for a constant supply of glucose and based on a study using GFP-LC3 autophagosomal marker expressed in transgenic mice which showed that *in vivo* autophagy level was elevated in various tissues except the brain after starving (Mizushima et al., 2004).

The M2-coloc value of Bchs over-lapping with Atg8 increased during nutrient starvation and rapamycin treatment, both of which are non-selective forms of autophagy induction **(Figure 38)**. This coincides with higher Ch1 : Ch2 ratios respectively and it is postulated that the increased association between Bchs and Atg8 during non-selective autophagy could be due to a higher protein turnover rate in general, including Bchs. It is important to note that the reverse scenario with respect to the proportion of Atg8 over-lapping with Bchs (M1-coloc) and the $R_r$ values did not increase correspondingly, supporting the earlier hypothesis. The elevated level of autophagy induction as measured by Atg8-positive compartments reflects the strength of autophagy stimuli in the increasing order – aggregate-prone protein expression, TOR complex inhibition and nutrient starvation – which helps to explain why there is no increase of the association between Bchs and Atg8 during aggrephagy compared to non-selective autophagy. This is corroborated by the live imaging study on primary neurons whereby there is no observation of GFP-Bchs and mCherry-Atg8a over-lapping with each other during Htt Q128 expression and the significant growth of mCherry-Atg8a vesicular structures after nutrient

starvation **(Figure 42)**. Therefore, Bchs associates with Atg5 during aggrephagy and may be released together once the autophagosomes are completely formed **(Figure 45)**.

Bchs and Rab11 colocalize partially in synaptic boutons of larval NMJs and embryonic motor neurons; however they perform antagonistic roles towards each other (Khodosh et al., 2006; Lim and Kraut, 2009). Bchs promotes synaptogenesis while Rab11 inhibits it and another study reported that autophagy function is required for synaptic development, suggesting that the involvement of Bchs in synaptogenesis is mediated by its function in selective autophagy (Khodosh et al., 2006; Shen and Ganetzky, 2009). Indeed, it was shown that the Highwire (Hiw) protein, an E3 ubiquitin ligase which suppresses synaptic growth, is degraded by autophagy in synaptic termini. It is possible that Rab11 antagonizes Bchs through competitive routing of recycling endosomal membrane to different target sites, for example, Rab11-positive recycling endosomes are mainly trafficked to the plasma membrane under fed condition and only extensively contribute membrane to nascent phagophores under amino acid starvation (Longatti et al., 2012). Coincidentally, this is when Bchs dissociates from Atg5-positive phagophores during starvation-induced autophagy.

In this study, quantitative colocalization analysis showed decreased $R_r$ values between Bchs and Rab11 for all the various conditions of autophagy induction; this was even more significant when normal and expanded polyQ Htt protein was expressed **(Figure 39)**. Firstly, this provides support that Rab11 antagonizes the autophagy function of Bchs and secondly, that Bchs is selectively employed for the degradation of xenogenic proteins as opposed to non-selective autophagy. The higher Ch1 : Ch2 ratios after the expression of Htt protein also demonstrated an increased level of Bchs expression relative to Rab11 and was more significant for Htt Q93. Although Htt Q20 itself is the non-aggregating form, however this may still be selectively removed via autophagy induced on a smaller scale than the aggregating form of Htt Q93. In addition, the reduced M1-coloc values of the proportion of Bchs over-lapping with Rab11 indicate that Bchs dissociates from Rab11 during selective autophagy. Therefore, Rab11 associates with and Bchs dissociates from phagophores during starvation-induced autophagy while on the other hand, Rab11 likely dissociates from and Bchs associates with phagophores during aggrephagy. This implies that there is a specific stimulus-dependent regulation at the

step of phagophore assembly and elongation mediated by both Bchs and Rab11 which are antagonistic **(Figure 45)**. It will be interesting to elucidate the exact mechanism of how the two proteins antagonize the function of each other at this particular step and how they may serve as a checkpoint for switching between non-selective and selective autophagy.

Spinster is a late endolysosomal protein that encodes a twelve-pass transmembrane nutrient efflux transporter and helps in the process of autophagic lysosome reformation (ALR) by re-activating the TOR complex after prolonged starvation (Rong et al., 2011; Sweeney and Davis, 2002). In the absence of Spinster, enlarged autolysosomes and increased oxidative stress resulted due to the inability to regulate the size of lysosomes containing degradative cathepsins and hydrolases (Dermaut et al., 2005; Milton et al., 2011). The quantitative colocalization analysis of Spinster with Bchs did not reveal any difference in the colocalization parameters of $R_r$, Ch1 : Ch2, M1-coloc and M2-coloc values between basal and induced autophagy, suggesting that the association of Bchs with Spinster does not depend on autophagy stimulation **(Figure 40)**. This is similar to the colocalization analysis with Atg8 whereby there is no increase in the overall association between Bchs and Atg8 even under nutrient starvation and rapamycin treatment. Therefore, Bchs does not play a role with vesicular compartments belonging to the late autophagy process but instead plays a more important role during the early steps of autophagy initiation when Bchs dissociates from Rab11-positive recycling endosomes and associates with Atg5-positive phagophores under selective autophagy conditions.

However, Spinster-positive lysosomal vesicles fail to be transported in an anterograde direction towards motor neuron termini in *bchs* larvae (Lim and Kraut, 2009). Thus, subsequent investigation was performed to determine whether Bchs may act as a motor protein adaptor that binds to both vesicle cargo and motor protein, particularly kinesin, thereby enabling the regulation of Bchs by kinases or other signaling proteins to mediate cargo-motor complex assembly on microtubules and axonal transport. For example, Aplip1 (*Drosophila* homologue of JIP1) interacts with APPL (APP like)-bound vesicles, KLC (kinesin light chain) and Hemipterous (*Drosophila* homologue of MKK7) whose phosphorylated active form leads to conformational change and dissociation of the cargo-motor complex (Horiuchi et al., 2007). Unc76 is another adaptor protein that interacts with synaptic vesicles and KHC (kinesin heavy chain) and

phosphorylation by ULK1 (Unc51-like kinase 1) results in a greater affinity to membrane proteins on synaptic vesicle, such as synaptotagmin 1 (Toda et al., 2008). The co-immunoprecipitation assay showed that Bchs does not form a complex with kinesin or dynein **(Figure 43)**. This suggests that Bchs is not a motor protein adaptor and the defect in anterograde transport of Spinster-positive late endolysosomes in *bchs* mutant could be due to a secondary effect from blockage in the maturation process by fusion of late endolysosomes with completed autophagosomes.

The exocytic Q-SNAREs, Sso1 and Sec9, endosomal Q-SNARE Tlg2, and R-SNAREs, Sec22 and Ykt6, have been found to be required at the step of autophagosome biogenesis by promoting Atg9 recycling through tubulo-vesicular clustering and membrane fusion at PAS (Nair et al., 2011). In addition, the Q-SNARE Syntaxin 17 (Stx17) localizes onto the outer membrane of completed autophagosomes and mediates the fusion with both late endosomes and lysosomes in mammalian cells and *Drosophila melanogaster* (Itakura et al., 2012; Takats et al., 2013). Interestingly, the BEACH protein LYST was reported to bind to SNARE proteins (Tchernev et al., 2002) and this raises the possibility of Bchs interacting with SNARE proteins to promote vesicle fusion. Alternatively, the absence of Bchs leads to incompletely formed autophagosomes which fail to envelop target substrates, thus causing a subsequent defect in the maturation process and inability to fuse with late endolysosomes. It is important to note that the *de novo* formation of autophagosomes *per se* does not depend on Bchs, for example during starvation-induced autophagy, but the selective recognition of ubiquitinated substrates and sequestration by sealed autophagosomes for clearance requires the Bchs adaptor protein.

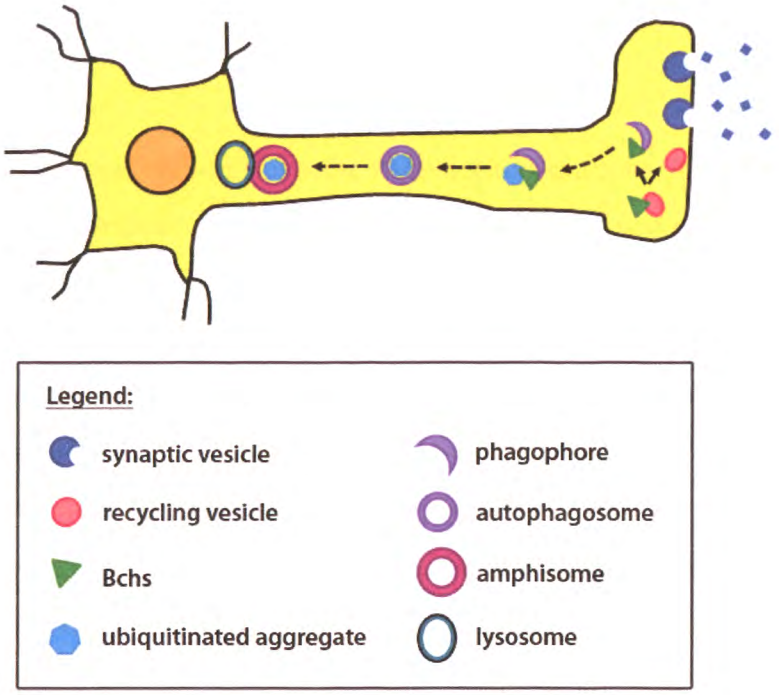


**Figure 45.** A proposed model of the physiological function of Bchs for protein quality control in neurons. As both Bchs vesicular compartments and Rab11-positive recycling endosomes are found to be enriched in synaptic boutons and partially colocalize with each other, we hypothesize that they play regulatory roles which are antagonistic during the initiation of autophagosome biogenesis in neuronal termini. Autophagy enhances synapse development and Bchs is required for maintaining synaptic morphology while Rab11 inhibits synaptic growth. Aggregate-prone proteins which are modified by ubiquitination and marked for autophagic removal send a signal promoting the dissociation of Bchs and Rab11, thus enabling Bchs to bind to Atg5-positive phagophores in neuronal termini. Alternatively, Bchs adaptor protein which has dissociated from Rab11 subsequently interacts with an autophagy receptor localized onto target substrates distributed throughout the cell in order to recruit Atg5-positive phagophores. The association of Bchs and Rab11 may interfere with the interaction between Bchs and Atg5 competitively, especially during selective autophagy. These phagophores, with the aid of Bchs, sequester ubiquitinated aggregates to form cargo-bound autophagosomes which transport along the axon retrogradely to mature into amphisomes and fuse with lysosomes in perikarya for degradation.

## 5. Future Work

The identity of accumulated Atg5-positive and Atg8-positive autophagic vacuoles can be further elucidated through transmission electron microscopy (TEM) coupled with immuno-labeling on *bchs* whole-brain slices and motor neuron synaptic termini in order to determine specifically which stage of the autophagy process has been disrupted. Motility of *bchs* third instar larvae and climbing assay for *bchs* adult flies can be performed to provide behavioral assays and supplement the degenerative assay measured by motor neuron survival. The potential interaction of Bchs with Ref(2)P can be investigated via colocalization analysis or co-immunoprecipitation assay under basal and induced autophagy conditions. In addition, the dissociation between Bchs and Rab11 during selective autophagy remains to be studied for its function and regulatory mechanism. The potential interaction of Bchs with SNARE complex proteins should also be examined by using a yeast two-hybrid screening library. It will be a challenge to study whether there is an inter-relationship between Bchs, Rab11 (or other Rab GTPases) and Q-SNARE (or R-SNARE) that mediates directionality in vesicle trafficking and downstream target membrane docking with fusion events which have an effect on the autophagy pathway because Rab proteins aid in the assembly of the SNARE complex between specific membrane vesicles (Grosshans et al., 2006; Sogaard et al., 1994).

## 6. Conclusion

In this study, it is shown that the neurodegenerative phenotype caused by *bchs* mutation is mediated through a loss of autophagy function based on pharmacological modulations and genetic interactions. Bchs participates in the early steps of autophagy initiation by acting as an adaptor protein that recruits components of the autophagy machinery and target substrates. In particular, this study provides evidence that Bchs is involved in selective autophagy and not during starvation-induced autophagy. Bchs associates with Atg5 and dissociates from Rab11 significantly upon the expression of aggregate-prone proteins. Atg5 and Rab11 have been reported to participate in autophagosome biogenesis, but Rab11 is found to be involved during starvation-induced autophagy, which supports the antagonistic roles between Bchs and Rab11. In addition, this study shows that Bchs is required for the association of Atg5 and Atg8 with ubiquitinated substrates, supporting selective cargo recognition. A loss of function in Bchs results in the accumulation of ubiquitinated aggregates in various parts of the neuron.

Therefore, we propose a hypothesis whereby Bchs mainly resides on Rab11-positive recycling endosomes in synaptic termini of neurons under physiological conditions, possibly participating in exocytic or membrane recycling pathway. Upon the induction of selective autophagy by aggregate-prone proteins, Bchs leaves recycling endosomes and recruits Atg5-Atg12-Atg16 E3-like ligase complex for the initiation of autophagosome biogenesis in neurite tips. These pre-autophagosomes can transport retrogradely along axons to sequester target substrates and seal to form autophagosomes which then mature and fuse with lysosomes concentrated in the perikarya **(Figure 45)**.

# 7. References


Abramoff, M., P. Magelhaes, and S. Ram. 2004. Image processing with ImageJ. *Biophotonics international*. 11:36-42.

Adams, R., and L. Bischof. 2002. Seeded region growing. *Pattern Analysis and Machine Intelligence, IEEE Transactions on*. 16:641-647.

Agarraberes, F.A., and J.F. Dice. 2001. A molecular chaperone complex at the lysosomal membrane is required for protein translocation. *Journal of Cell Science*. 114:2491-2499.

Alberti, S. 1998. A phosphoinositide-binding sequence is shared by PH domain target molecules - A model for the binding of PH domains to proteins. *Proteins-Structure Function and Genetics*. 31:1-9.

Ashburner, M., K.G. Golic, and R.S. Hawley. 2005. Drosophila: a laboratory handbook. Cold Spring Harbor Laboratory Press Cold Spring Harbor, NY.

Axe, E.L., S.A. Walker, M. Manifava, P. Chandra, H.L. Roderick, A. Habermann, G. Griffiths, and N.T. Ktistakis. 2008. Autophagosome formation from membrane compartments enriched in phosphatidylinositol 3-phosphate and dynamically connected to the endoplasmic reticulum. *Journal of Cell Biology*. 182:685-701.

Bandyopadhyay, U., S. Kaushik, L. Varticovski, and A.M. Cuervo. 2008. The chaperone-mediated autophagy receptor organizes in dynamic protein complexes at the lysosomal membrane. *Molecular and Cellular Biology*. 28:5747-5763.

Barbosa, M., Q.A. Nguyen, V.T. Tchernev, J.A. Ashley, J.C. Detter, S.M. Blaydes, S.J. Brandt, D. Chotai, C. Hodgman, R.C.E. Solari, M. Lovett, and S.F. Kingsmore. 1996. Identification of the homologous beige and Chediak-Higashi syndrome genes. *Nature*. 382:262-265.

Bedia, C., T. Levade, and P. Codogno. 2011. Regulation of Autophagy by Sphingolipids. *Anti-Cancer Agents in Medicinal Chemistry*. 11:844-853.

Berg, T.O., M. Fengsrud, P.E. Stromhaug, T. Berg, and P.O. Seglen. 1998. Isolation and characterization of rat liver amphisomes - Evidence for fusion of autophagosomes with both early and late endosomes. *Journal of Biological Chemistry*. 273:21883-21892.

Bernstein, E., A.A. Caudy, S.M. Hammond, and G.J. Hannon. 2001. Role for a bidentate ribonuclease in the initiation step of RNA interference. *Nature*. 409:363-366.

Birmingham, C.L., A.C. Smith, M.A. Bakowski, T. Yoshimori, and J.H. Brumell. 2006. Autophagy controls Salmonella infection in response to damage to the Salmonella-containing vacuole. *J. Biol. Chem.* 281:11374-11383.

Bjorkoy, G., T. Lamark, A. Brech, H. Outzen, M. Perander, A. Overvatn, H. Stenmark, and T. Johansen. 2005. p62/SQSTM1 forms protein aggregates degraded by autophagy and has a protective effect on huntingtin-induced cell death. *Journal of Cell Biology*. 171:603-614.

Blommaart, E.F.C., U. Krause, J.P.M. Schellens, H. VreelingSindelarova, and A.J. Meijer. 1997. The phosphatidylinositol 3-kinase inhibitors wortmannin and LY294002 inhibit autophagy in isolated rat hepatocytes. *European Journal of Biochemistry*. 243:240-246.

Boland, B., A. Kumar, S. Lee, F.M. Platt, J. Wegiel, W.H. Yu, and R.A. Nixon. 2008. Autophagy induction and autophagosome clearance in neurons: Relationship to autophagic pathology in Alzheimer's disease. *Journal of Neuroscience*. 28:6926-6937.

Bove, J., M. Martinez-Vicente, and M. Vila. 2011. Fighting neurodegeneration with rapamycin: mechanistic insights. *Nature Reviews Neuroscience*. 12:437-452.

Boya, P., R.A. Gonzalez-Polo, N. Casares, J.L. Perfettini, P. Dessen, N. Larochette, D. Metivier, D. Meley, S. Souquere, T. Yoshimori, G. Pierron, P. Codogno, and G. Kroemer. 2005. Inhibition of macroautophagy triggers apoptosis. *Molecular and Cellular Biology*. 25:1025-1040.

Brookmeyer, R., S. Gray, and C. Kawas. 1998. Projections of Alzheimer's disease in the United States and the public health impact of delaying disease onset. *Am J Public Health*. 88:1337-1342.

Bruijn, L.I., M.K. Houseweart, S. Kato, K.L. Anderson, S.D. Anderson, E. Ohama, A.G. Reaume, R.W. Scott, and D.W. Cleveland. 1998. Aggregation and motor neuron toxicity of an ALS-linked SOD1 mutant independent from wild-type SOD1. *Science*. 281:1851-1854.

Budovskaya, Y.V., J.S. Stephan, F. Reggiori, D.J. Klionsky, and P.K. Herman. 2004. The Ras/cAMP-dependent protein kinase signaling pathway regulates an early step of the autophagy process in Saccharomyces cerevisiae. *J. Biol. Chem.* 279:20663-20671.

Bukau, B., J. Weissman, and A. Horwich. 2006. Molecular chaperones and protein quality control. *Cell*. 125:443-451.

Burgess, A., J.P. Mornon, G. de Saint-Basile, and I. Callebaut. 2009. A concanavalin A-like lectin domain in the CHS1/LYST protein, shared by members of the BEACH family. *Bioinformatics*. 25:1219-1222.

Casso, D., F.A. Ramirez-Weber, and T.B. Kornberg. 1999. GFP-tagged balancer chromosomes for Drosophila melanogaster. *Mechanisms of Development*. 88:229-232.

Cataldo, A.M., D.J. Hamilton, J.L. Barnett, P.A. Paskevich, and R.A. Nixon. 1996. Properties of the endosomal-lysosomal system in the human central nervous system: Disturbances mark most neurons in populations at risk to degenerate in Alzheimer's disease. *Journal of Neuroscience*. 16:186-199.

Chang, Y.Y., and T.P. Neufeld. 2009. An Atg1/Atg13 complex with multiple roles in TOR-mediated autophagy regulation. *Mol Biol Cell*. 20:2004-2014.

Cheong, H., U. Nair, J.F. Geng, and D.J. Klionsky. 2008. The Atg1 kinase complex is involved in the regulation of protein recruitment to initiate sequestering vesicle formation for nonspecific autophagy in Saccharomyces cerevisiae. *Molecular Biology of the Cell*. 19:668-681.

Chiu, M.I., H. Katz, and V. Berlin. 1994. RAPT1, a mammalian homolog of yeast Tor, interacts with the FKBP12/rapamycin complex. *Proc Natl Acad Sci U S A*. 91:12574-12578.

Ciechanover, A., A. Orian, and A.L. Schwartz. 2000. Ubiquitin-mediated proteolysis: biological regulation via destruction. *Bioessays*. 22:442-451.

Clausen, T.H., T. Lamark, P. Isakson, K. Finley, K.B. Larsen, A. Brech, A. Overvatn, H. Stenmark, G. Bjorkoy, A. Simonsen, and T. Johansen. 2010. p62/SQSTM1 and ALFY interact to facilitate the formation of p62 bodies/ALIS and their degradation by autophagy. *Autophagy*. 6:330-344.

Cuervo, A.M. 2004. Autophagy: in sickness and in health. *Trends in Cell Biology*. 14:70-77.

Cuervo, A.M., E. Bergamini, U.T. Brunk, W. Droge, M. Ffrench, and A. Terman. 2005. Autophagy and aging - The importance of maintaining "clean" cells. *Autophagy*. 1:131-140.

Cuervo, A.M., and J.F. Dice. 1996. A receptor for the selective uptake and degradation of proteins by lysosomes. *Science*. 273:501-503.

Cuervo, A.M., and J.F. Dice. 2000. Age-related decline in chaperone-mediated autophagy. *Journal of Biological Chemistry*. 275:31505-31513.

Cuervo, A.M., L. Stefanis, R. Fredenburg, P.T. Lansbury, and D. Sulzer. 2004. Impaired degradation of mutant alpha-synuclein by chaperone-mediated autophagy. *Science*. 305:1292-1295.

Dall'Armi, C., K.A. Devereaux, and G. Di Paolo. 2013. The role of lipids in the control of autophagy. *Curr Biol*. 23:R33-45.

De Lozanne, A. 2003. The role of BEACH proteins in Dictyostelium. *Traffic*. 4:6-12.

Degenhardt, K., R. Mathew, B. Beaudoin, K. Bray, D. Anderson, G.H. Chen, C. Mukherjee, Y.F. Shi, C. Gelinas, Y.J. Fan, D.A. Nelson, S.K. Jin, and E. White. 2006. Autophagy promotes tumor cell survival and restricts necrosis, inflammation, and tumorigenesis. *Cancer Cell*. 10:51-64.

Dermaut, B., K.K. Norga, A. Kania, P. Verstreken, H. Pan, Y. Zhou, P. Callaerts, and H.J. Bellen. 2005. Aberrant lysosomal carbohydrate storage accompanies endocytic defects and neurodegeneration in Drosophila benchwarmer. *J Cell Biol*. 170:127-139.

Di Bartolomeo, S., M. Corazzari, F. Nazio, S. Oliverio, G. Lisi, M. Antonioli, V. Pagliarini, S. Matteoni, C. Fuoco, L. Giunta, M. D'Amelio, R. Nardacci, A. Romagnoli, M. Piacentini, F. Cecconi, and G.M. Fimia. 2010. The dynamic interaction of AMBRA1 with the dynein motor complex regulates mammalian autophagy. *Journal of Cell Biology*. 191:155-168.

Dice, J.F. 1990. PEPTIDE SEQUENCES THAT TARGET CYTOSOLIC PROTEINS FOR LYSOSOMAL PROTEOLYSIS. *Trends in Biochemical Sciences*. 15:305-309.

Dietzl, G., D. Chen, F. Schnorrer, K.C. Su, Y. Barinova, M. Fellner, B. Gasser, K. Kinsey, S. Oppel, S. Scheiblauer, A. Couto, V. Marra, K. Keleman, and B.J. Dickson. 2007. A genome-wide transgenic RNAi library for conditional gene inactivation in Drosophila. *Nature*. 448:151-U151.

Dunn, W.A., Jr. 1990. Studies on the mechanisms of autophagy: formation of the autophagic vacuole. *J Cell Biol*. 110:1923-1933.

Eisenberg, T., H. Knauer, A. Schauer, S. Buttner, C. Ruckenstuhl, D. Carmona-Gutierrez, J. Ring, S. Schroeder, C. Magnes, L. Antonacci, H. Fussi, L. Deszcz, R. Hartl, E. Schraml, A. Criollo, E. Megalou, D. Weiskopf, P. Laun, G. Heeren, M. Breitenbach, B. Grubeck-Loebenstein, E. Herker, B. Fahrenkrog, K.U. Frohlich, F. Sinner, N. Tavernarakis, N. Minois, G. Kroemer, and F. Madeo. 2009. Induction of autophagy by spermidine promotes longevity. *Nature Cell Biology*. 11:1305-U1102.

Fader, C.M., and M.I. Colombo. 2009. Autophagy and multivesicular bodies: two closely related partners. *Cell Death and Differentiation*. 16:70-78.

Farre, J.C., and S. Subramani. 2004. Peroxisome turnover by micropexophagy: an autophagy-related process. *Trends in Cell Biology*. 14:515-523.

Feany, M.B., and W.W. Bender. 2000. A Drosophila model of Parkinson's disease. *Nature*. 404:394-398.

Filimonenko, M., P. Isakson, K.D. Finley, M. Anderson, H. Jeong, T.J. Melia, B.J. Bartlett, K.M. Myers, H.C.G. Birkeland, T. Lamark, D. Krainc, A. Brech, H. Stenmark, A. Simonsen, and A. Yamamoto. 2010. The Selective Macroautophagic Degradation of Aggregated Proteins Requires the PI3P-Binding Protein Alfy. *Molecular Cell*. 38:265-279.

Filimonenko, M., S. Stuffers, C. Raiborg, A. Yamamoto, L. Malerod, E.M.C. Fisher, A. Isaacs, A. Brech, H. Stenmark, and A. Simonsen. 2007. Functional multivesicular bodies are required for autophagic clearance of protein aggregates associated with neurodegenerative disease. *Journal of Cell Biology*. 179:485-500.

Finley, K.D., P.T. Edeen, R.C. Cumming, M.D. Mardahl-Dumesnil, B.J. Taylor, M.H. Rodriguez, C.E. Hwang, M. Benedetti, and M. McKeown. 2003. blue cheese mutations define a novel, conserved gene involved in progressive neural degeneration. *Journal of Neuroscience*. 23:1254-1264.

Friedman, L.G., M.L. Lachenmayer, J. Wang, L.Q. He, S.M. Poulose, M. Komatsu, G.R. Holstein, and Z.Y. Yue. 2012. Disrupted Autophagy Leads to Dopaminergic Axon and Dendrite Degeneration and Promotes Presynaptic Accumulation of alpha-Synuclein and LRRK2 in the Brain. *Journal of Neuroscience*. 32:7585-7593.

Fujioka, M., B.C. Lear, M. Landgraf, G.L. Yusibova, J. Zhou, K.M. Riley, N.H. Patel, and J.B. Jaynes. 2003. Even-skipped, acting as a repressor, regulates axonal projections in Drosophila. *Development*. 130:5385-5400.

Fukuhara, S., S. Simmons, S. Kawamura, A. Inoue, Y. Orba, T. Tokudome, Y. Sunden, Y. Arai, K. Moriwaki, J. Ishida, A. Uemura, H. Kiyonari, T. Abe, A. Fukamizu, M. Hirashima, H. Sawa, J. Aoki, M. Ishii, and N. Mochizuki. 2012. The sphingosine-1-phosphate transporter Spns2 expressed on endothelial cells regulates lymphocyte trafficking in mice. *Journal of Clinical Investigation*. 122:1416-1426.

Garami, A., F.J.T. Zwartkruis, T. Nobukuni, M. Joaquin, M. Roccio, H. Stocker, S.C. Kozma, E. Hafen, J.L. Bos, and G. Thomas. 2003. Insulin activation of Rheb, a mediator of mTOR/S6K/4E-BP signaling, is inhibited by TSC1 and 2. *Molecular Cell*. 11:1457-1466.

Geetha, T., and M.W. Wooten. 2002. Structure and functional properties of the ubiquitin binding protein p62. *Febs Letters*. 512:19-24.

Geng, J.F., and D.J. Klionsky. 2008. The Atg8 and Atg12 ubiquitin-like conjugation systems in macroautophagy. *Embo Reports*. 9:859-864.

Ginet, V., J. Puyal, P.G. Clarke, and A.C. Truttmann. 2009. Enhancement of autophagic flux after neonatal cerebral hypoxia-ischemia and its region-specific relationship to apoptotic mechanisms. *Am J Pathol*. 175:1962-1974.

Glickman, M.H., and A. Ciechanover. 2002. The ubiquitin-proteasome proteolytic pathway: Destruction for the sake of construction. *Physiological Reviews*. 82:373-428.

Greeve, I., D. Kretzschmar, J.A. Tschape, A. Beyn, C. Brellinger, M. Schweizer, R.M. Nitsch, and R. Reifegerste. 2004. Age-dependent neurodegeneration and Alzheimer-amyloid plaque formation in transgenic Drosophila. *Journal of Neuroscience*. 24:3899-3906.

Grosshans, B.L., D. Ortiz, and P. Novick. 2006. Rabs and their effectors: Achieving specificity in membrane traffic. *Proceedings of the National Academy of Sciences of the United States of America*. 103:11821-11827.

Guenther, G.G., E.R. Peralta, K.R. Rosales, S.Y. Wong, L.J. Siskind, and A.L. Edinger. 2008. Ceramide starves cells to death by downregulating nutrient transporter proteins. *Proceedings of the National Academy of Sciences of the United States of America*. 105:17402-17407.

Hailey, D.W., A.S. Rambold, P. Satpute-Krishnan, K. Mitra, R. Sougrat, P.K. Kim, and J. Lippincott-Schwartz. 2010. Mitochondria Supply Membranes for Autophagosome Biogenesis during Starvation. *Cell*. 141:656-667.

Hanada, T., N.N. Noda, Y. Satomi, Y. Ichimura, Y. Fujioka, T. Takao, F. Inagaki, and Y. Ohsumi. 2007. The Atg12-Atg5 conjugate has a novel E3-like activity for protein lipidation in autophagy. *Journal of Biological Chemistry*. 282:37298-37302.

Hara, K., Y. Maruki, X.M. Long, K. Yoshino, N. Oshiro, S. Hidayat, C. Tokunaga, J. Avruch, and K. Yonezawa. 2002. Raptor, a binding partner of target of rapamycin (TOR), mediates TOR action. *Cell*. 110:177-189.

Hara, T., K. Nakamura, M. Matsui, A. Yamamoto, Y. Nakahara, R. Suzuki-Migishima, M. Yokoyama, K. Mishima, I. Saito, H. Okano, and N. Mizushima. 2006. Suppression of basal autophagy in neural cells causes neurodegenerative disease in mice. *Nature*. 441:885-889.

Hardie, D.G. 2007. AMP-activated/SNF1 protein kinases: conserved guardians of cellular energy. *Nature Reviews Molecular Cell Biology*. 8:774-785.

Haucke, V., and G. Di Paolo. 2007. Lipids and lipid modifications in the regulation of membrane traffic. *Curr Opin Cell Biol*. 19:426-435.

Hay, N., and N. Sonenberg. 2004. Upstream and downstream of mTOR. *Genes & Development*. 18:1926-1945.

Hayashi-Nishino, M., N. Fujita, T. Noda, A. Yamaguchi, T. Yoshimori, and A. Yamamoto. 2009. A subdomain of the endoplasmic reticulum forms a cradle for autophagosome formation. *Nat Cell Biol*. 11:1433-1437.

He, C.C., H. Song, T. Yorimitsu, I. Monastyrska, W.L. Yen, J.E. Legakis, and D.J. Klionsky. 2006. Recruitment of Atg9 to the preautophagosomal structure by Atg11 is essential for selective autophagy in budding yeast. *Journal of Cell Biology*. 175:925-935.

Hofmann, K., and L. Falquet. 2001. A ubiquitin-interacting motif conserved in components of the proteasomal and lysosomal protein degradation systems. *Trends in Biochemical Sciences*. 26:347-350.

Horiuchi, D., R.V. Barkus, A.D. Pilling, A. Gassman, and W.M. Saxton. 2005. APLIP1, a Kinesin binding JIP-1/JNK scaffold protein, influences the axonal transport of both vesicles and mitochondria in Drosophila. *Current Biology*. 15:2137-2141.

Horiuchi, D., C.A. Collins, P. Bhat, R.V. Barkus, A. DiAntonio, and W.M. Saxton. 2007. Control of a kinesin-cargo linkage mechanism by JNK pathway kinases. *Current Biology*. 17:1313-1317.

Huo, Y.L., V. Iadevaia, and C.G. Proud. 2011. Differing effects of rapamycin and mTOR kinase inhibitors on protein synthesis. *Biochemical Society Transactions*. 39:446-450.

Ichimura, Y., T. Kirisako, T. Takao, Y. Satomi, Y. Shimonishi, N. Ishihara, N. Mizushima, I. Tanida, E. Kominami, M. Ohsumi, T. Noda, and Y. Ohsumi. 2000. A ubiquitin-like system mediates protein lipidation. *Nature*. 408:488-492.

Ikenoue, T., K. Inoki, Q. Yang, X. Zhou, and K.L. Guan. 2008. Essential function of TORC2 in PKC and Akt turn motif phosphorylation, maturation and signalling. *Embo Journal*. 27:1919-1931.

Inoki, K., Y. Li, T. Xu, and K.L. Guan. 2003. Rheb GTPase is a direct target of TSC2 GAP activity and regulates mTOR signaling. *Genes Dev*. 17:1829-1834.

Inoki, K., Y. Li, T.Q. Zhu, J. Wu, and K.L. Guan. 2002. TSC2 is phosphorylated and inhibited by Akt and suppresses mTOR signalling. *Nature Cell Biology*. 4:648-657.

Inoki, K., H. Ouyang, T.Q. Zhu, C. Lindvall, Y. Wang, X.J. Zhang, Q. Yang, C. Bennett, Y. Harada, K. Stankunas, C.Y. Wang, X. He, O.A. MacDougald, M. You, B.O. Williams, and K.L. Guan. 2006. TSC2 integrates Wnt and energy signals via a coordinated phosphorylation by AMPK and GSK3 to regulate cell growth. *Cell*. 126:955-968.

Itakura, E., C. Kishi, K. Inoue, and N. Mizushima. 2008. Beclin 1 Forms Two Distinct Phosphatidylinositol 3-Kinase Complexes with Mammalian Atg14 and UVRAG. *Molecular Biology of the Cell*. 19:5360-5372.

Itakura, E., C. Kishi-Itakura, and N. Mizushima. 2012. The Hairpin-type Tail-Anchored SNARE Syntaxin 17 Targets to Autophagosomes for Fusion with Endosomes/Lysosomes. *Cell*. 151:1256-1269.

Itakura, E., and N. Mizushima. 2009. Atg14 and UVRAG Mutually exclusive subunits of mammalian Beclin 1-PI3K complexes. *Autophagy*. 5:534-536.

Itakura, E., and N. Mizushima. 2010. Characterization of autophagosome formation site by a hierarchical analysis of mammalian Atg proteins. *Autophagy*. 6:764-776.

Iwata, A., B.E. Riley, J.A. Johnston, and R.R. Kopito. 2005. HDAC6 and microtubules are required for autophagic degradation of aggregated Huntingtin. *Journal of Biological Chemistry*. 280:40282-40292.

Jacinto, E., R. Loewith, A. Schmidt, S. Lin, M.A. Ruegg, A. Hall, and M.N. Hall. 2004. Mammalian TOR complex 2 controls the actin cytoskeleton and is rapamycin insensitive. *Nature Cell Biology*. 6:1122-U1130.

Jacinto, E., and A. Lorberg. 2008. TOR regulation of AGC kinases in yeast and mammals. *Biochemical Journal*. 410:19-37.

Jia, K.L., and B. Levine. 2007. Autophagy is required for dietary restriction-mediated life span extension in C-elegans. *Autophagy*. 3:597-599.

Jogl, G., Y. Shen, D. Gebauer, J. Li, K. Wiegmann, H. Kashkar, M. Kronke, and L. Tong. 2002. Crystal structure of the BEACH domain reveals an unusual fold and extensive association with a novel PH domain. *Embo Journal*. 21:4785-4795.

Juhasz, G., B. Erdi, M. Sass, and T.P. Neufeld. 2007. Atg7-dependent autophagy promotes neuronal health, stress tolerance, and longevity but is dispensable for metamorphosis in Drosophila. *Genes & Development*. 21:3061-3066.

Juhasz, G., J.H. Hill, Y. Yan, M. Sass, E.H. Baehrecke, J.M. Backer, and T.P. Neufeld. 2008. The class III PI(3)K Vps34 promotes autophagy and endocytosis but not TOR signaling in Drosophila. *Journal of Cell Biology*. 181:655-666.

Jung, C.H., C.B. Jun, S.H. Ro, Y.M. Kim, N.M. Otto, J. Cao, M. Kundu, and D.H. Kim. 2009. ULK-Atg13-FIP200 Complexes Mediate mTOR Signaling to the Autophagy Machinery. *Molecular Biology of the Cell*. 20:1992-2003.

Kabeya, Y., N. Mizushima, T. Ueno, A. Yamamoto, T. Kirisako, T. Noda, E. Kominami, Y. Ohsumi, and T. Yoshimori. 2000. LC3, a mammalian homologue of yeast Apg8p, is localized in autophagosome membranes after processing. *EMBO J*. 19:5720-5728.

Kamada, Y., K. Yoshino, C. Kondo, T. Kawamata, N. Oshiro, K. Yonezawa, and Y. Ohsumi. 2010. Tor Directly Controls the Atg1 Kinase Complex To Regulate Autophagy. *Molecular and Cellular Biology*. 30:1049-1058.

Kang, R., H.J. Zeh, M.T. Lotze, and D. Tang. 2011. The Beclin 1 network regulates autophagy and apoptosis. *Cell Death Differ*.

Kanki, T., K. Wang, Y. Cao, M. Baba, and D.J. Klionsky. 2009. Atg32 Is a Mitochondrial Protein that Confers Selectivity during Mitophagy. *Developmental Cell*. 17:98-109.

Kapahi, P., D. Chen, A.N. Rogers, S.D. Katewa, P.W.L. Li, E.L. Thomas, and L. Kockel. 2010. With TOR, Less Is More: A Key Role for the Conserved Nutrient-Sensing TOR Pathway in Aging. *Cell Metab.* 11:453-465.

Kaushik, S., A.C. Massey, and A.M. Cuervo. 2006. Lysosome membrane lipid microdomains: novel regulators of chaperone-mediated autophagy. *Embo Journal*. 25:3921-3933.

Kaushik, S., A.C. Massey, N. Mizushima, and A.M. Cuervo. 2008. Constitutive activation of chaperone-mediated autophagy in cells with impaired macroautophagy. *Mol. Biol. Cell*. 19:2179-2192.

Kawamata, T., Y. Kamada, Y. Kabeya, T. Sekito, and Y. Ohsumi. 2008. Organization of the pre-autophagosomal structure responsible for autophagosome formation. *Molecular Biology of the Cell*. 19:2039-2050.

Khodosh, R., A. Augsburger, T.L. Schwarz, and P.A. Garrity. 2006. Bchs, a BEACH domain protein, antagonizes Rab11 in synapse morphogenesis and other developmental events. *Development*. 133:4655-4665.

Kihara, A., T. Noda, N. Ishihara, and Y. Ohsumi. 2001. Two distinct Vps34 phosphatidylinositol 3-kinase complexes function in autophagy and carboxypeptidase Y sorting in Saccharomyces cerevisiae. *Journal of Cell Biology*. 152:519-530.

Kim, D.H., D.D. Sarbassov, S.M. Ali, J.E. King, R.R. Latek, H. Erdjument-Bromage, P. Tempst, and D.M. Sabatini. 2002. mTOR interacts with raptor to form a nutrient-sensitive complex that signals to the cell growth machinery. *Cell*. 110:163-175.

Kim, E., P. Goraksha-Hicks, L. Li, T.P. Neufeld, and K.L. Guan. 2008. Regulation of TORC1 by Rag GTPases in nutrient response. *Nat Cell Biol*. 10:935-945.

Kim, J., and K.L. Guan. 2011. Amino Acid Signaling in TOR Activation. *In* Annual Review of Biochemistry, Vol 80. Vol. 80. R.D. Kornberg, C.R.H. Raetz, J.E. Rothman, and J.W. Thorner, editors. 1001-1032.

Kim, J., M. Kundu, B. Viollet, and K.L. Guan. 2011. AMPK and mTOR regulate autophagy through direct phosphorylation of Ulk1. *Nature Cell Biology*. 13:132-U171.

Kirisako, T., Y. Ichimura, H. Okada, Y. Kabeya, N. Mizushima, T. Yoshimori, M. Ohsumi, T. Takao, T. Noda, and Y. Ohsumi. 2000. The reversible modification regulates the membrane-binding state of Apg8/Aut7 essential for autophagy and the cytoplasm to vacuole targeting pathway. *Journal of Cell Biology*. 151:263-275.

Kirkin, V., T. Lamark, Y.S. Sou, G. Bjorkoy, J.L. Nunn, J.A. Bruun, E. Shvets, D.G. McEwan, T.H. Clausen, P. Wild, I. Bilusic, J.P. Theurillat, A. Overvatn, T. Ishii, Z. Elazar, M. Komatsu, I. Dikic, and T. Johansen. 2009a. A Role for NBR1 in Autophagosomal Degradation of Ubiquitinated Substrates. *Molecular Cell*. 33:505-516.

Kirkin, V., D.G. McEwan, I. Novak, and I. Dikic. 2009b. A Role for Ubiquitin in Selective Autophagy. *Molecular Cell*. 34:259-269.

Knaevelsrud, H., and A. Simonsen. 2012. Lipids in autophagy: Constituents, signaling molecules and cargo with relevance to disease. *Biochimica Et Biophysica Acta-Molecular and Cell Biology of Lipids*. 1821:1133-1145.

Koga, H., S. Kaushik, and A.M. Cuervo. 2010. Altered lipid content inhibits autophagic vesicular fusion. *Faseb Journal*. 24:3052-3065.

Komatsu, M., S. Waguri, T. Chiba, S. Murata, J. Iwata, I. Tanida, T. Ueno, M. Koike, Y. Uchiyama, E. Kominami, and K. Tanaka. 2006. Loss of autophagy in the central nervous system causes neurodegeneration in mice. *Nature*. 441:880-884.

Kondo, Y., T. Kanzawa, R. Sawaya, and S. Kondo. 2005. The role of autophagy in cancer development and response to therapy. *Nature Reviews Cancer*. 5:726-734.

Korolchuk, V.I., S. Saiki, M. Lichtenberg, F.H. Siddiqi, E.A. Roberts, S. Imarisio, L. Jahreiss, S. Sarkar, M. Futter, F.M. Menzies, C.J. O'Kane, V. Deretic, and D.C. Rubinsztein. 2011. Lysosomal positioning coordinates cellular nutrient responses. *Nature Cell Biology*. 13:453-U242.

Kraft, R., M.M. Escobar, M.L. Narro, J.L. Kurtis, A. Efrat, K. Barnard, and L.L. Restifo. 2006. Phenotypes of Drosophila brain neurons in primary culture reveal a role for fascin in neurite shape and trajectory. *J Neurosci*. 26:8734-8747.

Kraut, R., K. Menon, and K. Zinn. 2001. A gain-of-function screen for genes controlling motor axon guidance and synaptogenesis in Drosophila. *Current Biology*. 11:417-430.

Kriston-Vizi, J., N.W. Thong, C.L. Poh, K.C. Yee, J.S. Ling, R. Kraut, and M. Wasser. 2011. Gebiss: an ImageJ plugin for the specification of ground truth and the performance evaluation of 3D segmentation algorithms. *BMC Bioinformatics*. 12:232.

Kuma, A., N. Mizushima, N. Ishihara, and Y. Ohsumi. 2002. Formation of the approximately 350-kDa Apg12-Apg5.Apg16 multimeric complex, mediated by Apg16 oligomerization, is essential for autophagy in yeast. *J Biol Chem*. 277:18619-18625.

Kundu, M., and C.B. Thompson. 2008. Autophagy: basic principles and relevance to disease. *Annu Rev Pathol*. 3:427-455.

Kutateladze, T.G. 2010. Translation of the phosphoinositide code by PI effectors. *Nature Chemical Biology*. 6:507-513.

Kuznetsov, A.V., T. Tiivel, P. Sikk, T. Kaambre, L. Kay, Z. Daneshrad, A. Rossi, L. Kadaja, N. Peet, E. Seppet, and V.A. Saks. 1996. Striking differences between the kinetics of regulation of respiration by ADP in slow-twitch and fast-twitch muscles in vivo. *European Journal of Biochemistry*. 241:909-915.

Lamark, T., V. Kirkin, I. Dikic, and T. Johansen. 2009. NBR1 and p62 as cargo receptors for selective autophagy of ubiquitinated targets. *Cell Cycle*. 8:1986-1990.

Lamark, T., M. Perander, H. Outzen, K. Kristiansen, A. Overvatn, E. Michaelsen, G. Bjorkoy, and T. Johansen. 2003. Interaction codes within the family of mammalian Phox and Bem1p domain-containing proteins. *Journal of Biological Chemistry*. 278:34568-34581.

Lavieu, G., F. Scarlatti, G. Sala, S. Carpentier, T. Levade, R. Ghidoni, J. Botti, and P. Codogno. 2006. Regulation of autophagy by sphingosine kinase 1 and its role in cell survival during nutrient starvation. *Journal of Biological Chemistry*. 281:8518-8527.

Lawrence, B.P., and W.J. Brown. 1993. Inhibition of protein synthesis separates autophagic sequestration from the delivery of lysosomal enzymes. *J Cell Sci*. 105 ( Pt 2):473-480.

Lee, J.A., A. Beigneux, S.T. Ahmad, S.G. Young, and F.B. Gao. 2007a. ESCRT-III dysfunction causes autophagosome accumulation and neurodegeneration. *Current Biology*. 17:1561-1567.

Lee, J.W., S. Park, Y. Takahashi, and H.G. Wang. 2010a. The Association of AMPK with ULK1 Regulates Autophagy. *Plos One*. 5.

Lee, J.Y., H. Koga, Y. Kawaguchi, W.X. Tang, E. Wong, Y.S. Gao, U.B. Pandey, S. Kaushik, E. Tresse, J.R. Lu, J.P. Taylor, A.M. Cuervo, and T.P. Yao. 2010b. HDAC6 controls autophagosome maturation essential for ubiquitin-selective quality-control autophagy. *Embo Journal*. 29:969-980.

Lee, S., Y. Sato, and R.A. Nixon. 2011. Lysosomal Proteolysis Inhibition Selectively Disrupts Axonal Transport of Degradative Organelles and Causes an Alzheimer's-Like Axonal Dystrophy. *Journal of Neuroscience*. 31:7817-7830.

Lee, S.B., S. Kim, J. Lee, J. Park, G. Lee, Y. Kim, J.M. Kim, and J. Chung. 2007b. ATG1, an autophagy regulator, inhibits cell growth by negatively regulating S6 kinase. *Embo Reports*. 8:360-365.

Lee, Y.S., K. Nakahara, J.W. Pham, K. Kim, Z.Y. He, E.J. Sontheimer, and R.W. Carthew. 2004. Distinct roles for Drosophila Dicer-1 and Dicer-2 in the siRNA/miRNA silencing pathways. *Cell*. 117:69-81.

Levine, B., and D.J. Klionsky. 2004. Development by self-digestion: Molecular mechanisms and biological functions of autophagy. *Developmental Cell*. 6:463-477.

Levine, B., and G. Kroemer. 2008. Autophagy in the pathogenesis of disease. *Cell*. 132:27-42.

Levine, B., N. Mizushima, and H.W. Virgin. 2011. Autophagy in immunity and inflammation. *Nature*. 469:323-335.

Li, Q., A. Lau, T.J. Morris, L. Guo, C.B. Fordyce, and E.F. Stanley. 2004. A syntaxin 1, Galpha(o), and N-type calcium channel complex at a presynaptic nerve terminal: analysis by quantitative immunocolocalization. *J Neurosci*. 24:4070-4081.

Lim, A., and R. Kraut. 2009. The Drosophila BEACH family protein, blue cheese, links lysosomal axon transport with motor neuron degeneration. *J Neurosci*. 29:951-963.

Longatti, A., C.A. Lamb, M. Razi, S. Yoshimura, F.A. Barr, and S.A. Tooze. 2012. TBC1D14 regulates autophagosome formation via Rab11- and ULK1-positive recycling endosomes. *J Cell Biol*. 197:659-675.

Lum, J.J., R.J. DeBerardinis, and C.B. Thompson. 2005. Autophagy in metazoans: Cell survival in the land of plenty. *Nature Reviews Molecular Cell Biology*. 6:439-448.

Lynch-Day, M.A., and D.J. Klionsky. 2010. The Cvt pathway as a model for selective autophagy. *Febs Letters*. 584:1359-1366.

Ma, A.D., L.F. Brass, and C.S. Abrams. 1997. Pleckstrin associates with plasma membranes and induces the formation of membrane projections: Requirements for phosphorylation and the NH2-terminal PH domain. *Journal of Cell Biology*. 136:1071-1079.

Maday, S., K.E. Wallace, and E.L.F. Holzbaur. 2012. Autophagosomes initiate distally and mature during transport toward the cell soma in primary neurons. *Journal of Cell Biology*. 196:407-417.

Maiuri, M.C., E. Zalckvar, A. Kimchi, and G. Kroemer. 2007. Self-eating and self-killing: crosstalk between autophagy and apoptosis. *Nature Reviews Molecular Cell Biology*. 8:741-752.

Marsh, J.L., and L.M. Thompson. 2004. Can flies help humans treat neurodegenerative diseases? *Bioessays*. 26:485-496.

Marsh, J.L., and L.M. Thompson. 2006. Drosophila in the study of neurodegenerative disease. *Neuron*. 52:169-178.

Martinez-Vicente, M., and A.M. Cuervo. 2007. Autophagy and neurodegeneration: when the cleaning crew goes on strike. *Lancet Neurology*. 6:352-361.

Massey, A.C., C. Zhang, and A.M. Cuervo. 2006. Chaperone-mediated autophagy in aging and disease. *Current Topics in Developmental Biology, Vol 73*. 73:205-+.

Mathew, R., V. Karantza-Wadsworth, and E. White. 2007a. Role of autophagy in cancer. *Nature Reviews Cancer*. 7:961-967.

Mathew, R., S. Kongara, B. Beaudoin, C.M. Karp, K. Bray, K. Degenhardt, G.H. Chen, S.K. Jin, and E. White. 2007b. Autophagy suppresses tumor progression by limiting chromosomal instability. *Genes & Development*. 21:1367-1381.

Matsunaga, K., E. Morita, T. Saitoh, S. Akira, N.T. Ktistakis, T. Izumi, T. Noda, and T. Yoshimori. 2010. Autophagy requires endoplasmic reticulum targeting of the PI3-kinase complex via Atg14L. *Journal of Cell Biology*. 190:511-521.

Meley, D., C. Bauvy, J. Houben-Weerts, P.F. Dubbelhuis, M.T.J. Helmond, P. Codogno, and A.J. Meijer. 2006. AMP-activated protein kinase and the regulation of autophagic proteolysis. *J. Biol. Chem.* 281:34870-34879.

Milton, V.J., H.E. Jarrett, K. Gowers, S. Chalak, L. Briggs, I.M. Robinson, and S.T. Sweeney. 2011. Oxidative stress induces overgrowth of the Drosophila neuromuscular junction. *Proc Natl Acad Sci U S A*. 108:17521-17526.

Misra, S., G.J. Miller, and J.H. Hurley. 2001. Recognizing phosphatidylinositol 3-phosphate. *Cell*. 107:559-562.

Mizushima, N. 2010. The role of the Atg1/ULK1 complex in autophagy regulation. *Current Opinion in Cell Biology*. 22:132-139.

Mizushima, N., and M. Komatsu. 2011. Autophagy: Renovation of Cells and Tissues. *Cell*. 147:728-741.

Mizushima, N., A. Kuma, Y. Kobayashi, A. Yamamoto, M. Matsubae, T. Takao, T. Natsume, Y. Ohsumi, and T. Yoshimori. 2003. Mouse Apg16L, a novel WD-repeat protein, targets to the autophagic isolation membrane with the Apg12-Apg5 conjugate. *J Cell Sci*. 116:1679-1688.

Mizushima, N., B. Levine, A.M. Cuervo, and D.J. Klionsky. 2008. Autophagy fights disease through cellular self-digestion. *Nature*. 451:1069-1075.

Mizushima, N., A. Yamamoto, M. Hatano, Y. Kobayashi, Y. Kabeya, K. Suzuki, T. Tokuhisa, Y. Ohsumi, and T. Yoshimori. 2001. Dissection of autophagosome formation using Apg5-deficient mouse embryonic stem cells. *Journal of Cell Biology*. 152:657-667.

Mizushima, N., A. Yamamoto, M. Matsui, T. Yoshimori, and Y. Ohsumi. 2004. In vivo analysis of autophagy in response to nutrient starvation using transgenic mice expressing a fluorescent autophagosome marker. *Molecular Biology of the Cell*. 15:1101-1111.

Mizushima, N., T. Yoshimori, and Y. Ohsumi. 2011. The Role of Atg Proteins in Autophagosome Formation. *In* Annual Review of Cell and Developmental Biology, Vol 27. Vol. 27. R. Schekman, L. Goldstein, and R. Lehmann, editors. 107-132.

Mortimore, G.E., B.R. Lardeux, and C.E. Adams. 1988. REGULATION OF MICROAUTOPHAGY AND BASAL PROTEIN-TURNOVER IN RAT-LIVER - EFFECTS OF SHORT-TERM STARVATION. *Journal of Biological Chemistry*. 263:2506-2512.

Mostowy, S., V. Sancho-Shimizu, M.A. Hamon, R. Simeone, R. Brosch, T. Johansen, and P. Cossart. 2011. p62 and NDP52 Proteins Target Intracytosolic Shigella and Listeria to Different Autophagy Pathways. *J. Biol. Chem.* 286:26987-26995.

Motley, A.M., J.M. Nuttall, and E.H. Hettema. 2012. Pex3-anchored Atg36 tags peroxisomes for degradation in Saccharomyces cerevisiae. *Embo Journal*. 31:2852-2868.

Nagle, D.L., M.A. Karim, E.A. Woolf, L. Holmgren, P. Bork, D.J. Misumi, S.H. McGrail, B.J. Dussault, C.M. Perou, R.E. Boissy, G.M. Duyk, R.A. Spritz, and K.J. Moore. 1996. Identification and mutation analysis of the complete gene for Chediak-Higashi syndrome. *Nature Genetics*. 14:307-311.

Nair, U., A. Jotwani, J.F. Geng, N. Gammoh, D. Richerson, W.L. Yen, J. Griffith, S. Nag, K. Wang, T. Moss, M. Baba, J.A. McNew, X.J. Jiang, F. Reggiori, T.J. Melia, and D.J. Klionsky. 2011. SNARE Proteins Are Required for Macroautophagy. *Cell*. 146:290-302.

Nakatogawa, H., Y. Ichimura, and Y. Ohsumi. 2007. Atg8, a ubiquitin-like protein required for autophagosome formation, mediates membrane tethering and hemifusion. *Cell*. 130:165-178.

Nakatogawa, H., K. Suzuki, Y. Kamada, and Y. Ohsumi. 2009. Dynamics and diversity in autophagy mechanisms: lessons from yeast. *Nature Reviews Molecular Cell Biology*. 10:458-467.

Navarro, J.A.R., and A.M. Cuervo. 2012. Dietary lipids and aging compromise chaperone-mediated autophagy by similar mechanisms. *Autophagy*. 8:1152-1154.

Nedelsky, N.B., P.K. Todd, and J.P. Taylor. 2008. Autophagy and the ubiquitin-proteasome system: Collaborators in neuroprotection. *Biochimica Et Biophysica Acta-Molecular Basis of Disease*. 1782:691-699.

Neer, E.J., C.J. Schmidt, R. Nambudripad, and T.F. Smith. 1994. The ancient regulatory-protein family of WD-repeat proteins. *Nature*. 371:297-300.

Nezis, I.P., A. Simonsen, A.P. Sagona, K. Finley, S. Gaumer, D. Contamine, T.E. Rusten, H. Stenmark, and A. Brech. 2008. Ref(2) P, the Drosophila melanogaster homologue of mammalian p62, is required for the formation of protein aggregates in adult brain. *Journal of Cell Biology*. 180:1065-1071.

Nixon, R.A., J. Wegiel, A. Kumar, W.H. Yu, C. Peterhoff, A. Cataldo, and A.M. Cuervo. 2005. Extensive involvement of autophagy in Alzheimer disease: An immuno-electron microscopy study. *Journal of Neuropathology and Experimental Neurology*. 64:113-122.

Noda, N.N., Y. Ohsumi, and F. Inagaki. 2010a. Atg8-family interacting motif crucial for selective autophagy. *Febs Letters*. 584:1379-1385.

Noda, T., K. Matsunaga, N. Taguchi-Atarashi, and T. Yoshimori. 2010b. Regulation of membrane biogenesis in autophagy via PI3P dynamics. *Semin. Cell Dev. Biol.* 21:671-676.

Noda, T., and Y. Ohsumi. 1998. Tor, a phosphatidylinositol kinase homologue, controls autophagy in yeast. *Journal of Biological Chemistry*. 273:3963-3966.

Ohsumi, Y. 2001. Molecular dissection of autophagy: two ubiquitin-like systems. *Nat Rev Mol Cell Biol.* 2:211-216.

Okamoto, K., N. Kondo-Okamoto, and Y. Ohsumi. 2009. Mitochondria-Anchored Receptor Atg32 Mediates Degradation of Mitochondria via Selective Autophagy. *Developmental Cell*. 17:87-97.

Osborne, N., K. Brand-Arzamendi, E.A. Ober, S.W. Jin, H. Verkade, N.G. Holtzman, D. Yelon, and D.Y.R. Stainierl. 2008. The Spinster Homolog, Two of Hearts, Is Required for Sphingosine 1-Phosphate Signaling in Zebrafish. *Current Biology*. 18:1882-1888.

Pandey, U.B., Z.P. Nie, Y. Batlevi, B.A. McCray, G.P. Ritson, N.B. Nedelsky, S.L. Schwartz, N.A. DiProspero, M.A. Knight, O. Schuldiner, R. Padmanabhan, M. Hild, D.L. Berry, D. Garza, C.C. Hubbert, T.P. Yao, E.H. Baehrecke, and J.P. Taylor. 2007. HDAC6 rescues neurodegeneration and provides an essential link between autophagy and the UPS. *Nature*. 447:859-863.

Pankiv, S., T.H. Clausen, T. Lamark, A. Brech, J.A. Bruun, H. Outzen, A. Overvatn, G. Bjorkoy, and T. Johansen. 2007. p62/SQSTM1 binds directly to Atg8/LC3 to facilitate degradation of ubiquitinated protein aggregates by autophagy. *Journal of Biological Chemistry*. 282:24131-24145.

Pattingre, S., C. Bauvy, S. Carpentier, T. Levade, B. Levine, and P. Codogno. 2009. Role of JNK1-dependent Bcl-2 Phosphorylation in Ceramide-induced Macroautophagy. *J. Biol. Chem.* 284:2719-2728.

Pattingre, S., A. Tassa, X.P. Qu, R. Garuti, X.H. Liang, N. Mizushima, M. Packer, M.D. Schneider, and B. Levine. 2005. Bcl-2 antiapoptotic proteins inhibit Beclin 1-dependent autophagy. *Cell*. 122:927-939.

Petiot, A., E. Ogier-Denis, E.F.C. Blommaart, A.J. Meijer, and P. Codogno. 2000. Distinct classes of phosphatidylinositol 3 '-kinases are involved in signaling pathways that control macroautophagy in HT-29 cells. *Journal of Biological Chemistry*. 275:992-998.

Platt, F.M., B. Boland, and A.C. van der Spoel. 2012. The cell biology of disease: Lysosomal storage disorders: The cellular impact of lysosomal dysfunction. *J Cell Biol*. 199:723-734.

Powis, G., R. Bonjouklian, M.M. Berggren, A. Gallegos, R. Abraham, C. Ashendel, L. Zalkow, W.F. Matter, J. Dodge, G. Grindey, and et al. 1994. Wortmannin, a potent and selective inhibitor of phosphatidylinositol-3-kinase. *Cancer Res*. 54:2419-2423.

Price, J.L., P.B. Davis, J.C. Morris, and D.L. White. 1991. The distribution of tangles, plaques and related immunohistochemical markers in healthy aging and Alzheimer's disease. *Neurobiol Aging*. 12:295-312.

Ptacek, J., G. Devgan, G. Michaud, H. Zhu, X.W. Zhu, J. Fasolo, H. Guo, G. Jona, A. Breitkreutz, R. Sopko, R.R. McCartney, M.C. Schmidt, N. Rachidi, S.J. Lee, A.S. Mah, L. Meng, M.J.R. Stark, D.F. Stern, C.

De Virgilio, M. Tyers, B. Andrews, M. Gerstein, B. Schweitzer, P.F. Predki, and M. Snyder. 2005. Global analysis of protein phosphorylation in yeast. *Nature*. 438:679-684.

Rajawat, Y.S., and I. Bossis. 2008. Autophagy in aging and in neurodegenerative disorders. *Hormones-International Journal of Endocrinology and Metabolism*. 7:46-61.

Ravikumar, B., R. Duden, and D.C. Rubinsztein. 2002. Aggregate-prone proteins with polyglutamine and polyalanine expansions are degraded by autophagy. *Human Molecular Genetics*. 11:1107-1117.

Reggiori, F., K.A. Tucker, P.E. Stromhaug, and D.J. Klionsky. 2004. The Atg1-Atg13 complex regulates Atg9 and Atg23 retrieval transport from the pre-autophagosomal structure. *Developmental Cell*. 6:79-90.

Reiter, L.T., L. Potocki, S. Chien, M. Gribskov, and E. Bier. 2001. A systematic analysis of human disease-associated gene sequences in Drosophila melanogaster. *Genome Res*. 11:1114-1125.

Rodriguez-Navarro, J.A., S. Kaushik, H. Koga, C. Dall'Armi, G.H. Shui, M.R. Wenk, G. Di Paolo, and A.M. Cuervo. 2012. Inhibitory effect of dietary lipids on chaperone-mediated autophagy. *Proceedings of the National Academy of Sciences of the United States of America*. 109:E705-E714.

Rong, Y.G., C. McPhee, S.S. Deng, L. Huang, L.L. Chen, M. Liu, K. Tracy, E.H. Baehreck, L. Yu, and M.J. Lenardo. 2011. Spinster is required for autophagic lysosome reformation and mTOR reactivation following starvation. *Proceedings of the National Academy of Sciences of the United States of America*. 108:7826-7831.

Rorth, P. 1996. A modular misexpression screen in Drosophila detecting tissue-specific phenotypes. *Proc Natl Acad Sci U S A*. 93:12418-12422.

Rubinsztein, D.C., G. Marino, and G. Kroemer. 2011. Autophagy and Aging. *Cell*. 146:682-695.

Rubinsztein, D.C., and R.A. Nixon. 2010. Rapamycin induces autophagic flux in neurons. *Proceedings of the National Academy of Sciences of the United States of America*. 107:E181-E181.

Sancak, Y., T.R. Peterson, Y.D. Shaul, R.A. Lindquist, C.C. Thoreen, L. Bar-Peled, and D.M. Sabatini. 2008. The Rag GTPases bind raptor and mediate amino acid signaling to mTORC1. *Science*. 320:1496-1501.

Sarbassov, D.D., S.M. Ali, and D.M. Sabatini. 2005. Growing roles for the mTOR pathway. *Curr. Opin. Cell Biol.* 17:596-603.

Sarkar, S., B. Ravikumar, R.A. Floto, and D.C. Rubinsztein. 2009. Rapamycin and mTOR-independent autophagy inducers ameliorate toxicity of polyglutamine-expanded huntingtin and related proteinopathies. *Cell Death and Differentiation*. 16:46-56.

Scarlatti, F., C. Bauvy, A. Ventruti, G. Sala, F. Cluzeaud, A. Vandewalle, R. Ghidoni, and P. Codogno. 2004. Ceramide-mediated macroautophagy involves inhibition of protein kinase B and up-regulation of beclin 1. *J. Biol. Chem.* 279:18384-18391.

Schaefer, A.M., J.R. Sanes, and J.W. Lichtman. 2005. A compensatory subpopulation of motor neurons in a mouse model of amyotrophic lateral sclerosis. *Journal of Comparative Neurology*. 490:209-219.

Scherzinger, E., R. Lurz, M. Turmaine, L. Mangiarini, B. Hollenbach, R. Hasenbank, G.P. Bates, S.W. Davies, H. Lehrach, and E.E. Wanker. 1997. Huntingtin-encoded polyglutamine expansions form amyloid-like protein aggregates in vitro and in vivo. *Cell*. 90:549-558.

Schindelin, J. 2008. Fiji is just ImageJ—batteries included. *In* Proceedings of the ImageJ User and Developer Conference. Centre de Recherche Public Henri Tudor, Luxembourg. 99-104.

Schmelzle, T., and M.N. Hall. 2000. TOR, a central controller of cell growth. *Cell*. 103:253-262.

Schmid, A., A. Chiba, and C.Q. Doe. 1999. Clonal analysis of Drosophila embryonic neuroblasts: neural cell types, axon projections and muscle targets. *Development*. 126:4653-4689.

Schneider, C.A., W.S. Rasband, and K.W. Eliceiri. 2012. NIH Image to ImageJ: 25 years of image analysis. *Nat Methods*. 9:671-675.

Scott, R.C., G. Juhasz, and T.P. Neufeld. 2007. Direct induction of autophagy by Atg1 inhibits cell growth and induces apoptotic cell death. *Current Biology*. 17:1-11.

Scott, S.V., J. Guan, M.U. Hutchins, J. Kim, and D.J. Klionsky. 2001. Cvt19 is a receptor for the cytoplasm-to-vacuole targeting pathway. *Molecular Cell*. 7:1131-1141.

Seglen, P.O., and P.B. Gordon. 1982. 3-Methyladenine: specific inhibitor of autophagic/lysosomal protein degradation in isolated rat hepatocytes. *Proc Natl Acad Sci U S A*. 79:1889-1892.

Segui, B., N. Andrieu-Abadie, S. Adam-Klages, O. Meilhac, D. Kreder, V. Garcia, A.P. Bruno, J.P. Jaffrezou, R. Salvayre, M. Kronke, and T. Levade. 1999. CD40 signals apoptosis through FAN-regulated activation of the sphingomyelin-ceramide pathway. *J. Biol. Chem.* 274:37251-37258.

Shah, O.J., Z.Y. Wang, and T. Hunter. 2004. Inappropriate activation of the TSC/Rheb/mTOR/S6K cassette induces IRS1/2 depletion, insulin resistance, and cell survival deficiencies. *Current Biology*. 14:1650-1656.

Shen, W., and B. Ganetzky. 2009. Autophagy promotes synapse development in Drosophila. *Journal of Cell Biology*. 187:71-79.

Shiflett, S.L., J. Kaplan, and D.M. Ward. 2002. Chediak-Higashi syndrome: A rare disorder of lysosomes and lysosome related organelles. *Pigm. Cell. Res.* 15:251-257.

Shintani, T., W.P. Huang, P.E. Stromhaug, and D.J. Klionsky. 2002. Mechanism of cargo selection in the cytoplasm to vacuole targeting pathway. *Developmental Cell*. 3:825-837.

Shulman, J.M., and M.B. Feany. 2003. Genetic modifiers of tauopathy in Drosophila. *Genetics*. 165:1233-1242.

Simonsen, A., H.C.G. Birkeland, D.J. Gillooly, N. Mizushima, A. Kuma, T. Yoshimori, T. Slagsvold, A. Brech, and H. Stenmark. 2004. Alfy, a novel FYVE-domain-containing protein associated with protein granules and autophagic membranes. *Journal of Cell Science*. 117:4239-4251.

Simonsen, A., R.C. Cumming, K. Lindmo, V. Galaviz, S. Cheng, T.E. Rusten, and K.D. Finley. 2007. Genetic modifiers of the Drosophila blue cheese gene link defects in lysosomal transport with decreased life span and altered ubiquitinated-protein profiles. *Genetics*. 176:1283-1297.

Simonsen, A., and S.A. Tooze. 2009. Coordination of membrane events during autophagy by multiple class III PI3-kinase complexes. *Journal of Cell Biology*. 186:773-782.

Singh, R., and A.M. Cuervo. 2011. Autophagy in the Cellular Energetic Balance. *Cell Metab.* 13:495-504.

Singh, R., S. Kaushik, Y.J. Wang, Y.Q. Xiang, I. Novak, M. Komatsu, K. Tanaka, A.M. Cuervo, and M.J. Czaja. 2009. Autophagy regulates lipid metabolism. *Nature*. 458:1131-U1164.

Slagsvold, T., K. Pattni, L. Malerod, and H. Stenmark. 2006. Endosomal and non-endosomal functions of ESCRT proteins. *Trends in Cell Biology*. 16:317-326.

Sogaard, M., K. Tani, R.R. Ye, S. Geromanos, P. Tempst, T. Kirchhausen, J.E. Rothman, and T. Sollner. 1994. A rab protein is required for the assembly of SNARE complexes in the docking of transport vesicles. *Cell*. 78:937-948.

Spillantini, M.G., R.A. Crowther, R. Jakes, M. Hasegawa, and M. Goedert. 1998. alpha-synuclein in filamentous inclusions of Lewy bodies from Parkinson's disease and dementia with Lewy bodies. *Proceedings of the National Academy of Sciences of the United States of America*. 95:6469-6473.

Stephan, J.S., Y.Y. Yeh, V. Ramachandran, S.J. Deminoff, and P.K. Herman. 2009. The Tor and PKA signaling pathways independently target the Atg1/Atg13 protein kinase complex to control autophagy. *Proceedings of the National Academy of Sciences of the United States of America*. 106:17049-17054.

Suzuki, K., T. Kirisako, Y. Kamada, N. Mizushima, T. Noda, and Y. Ohsumi. 2001. The pre-autophagosomal structure organized by concerted functions of APG genes is essential for autophagosome formation. *Embo Journal*. 20:5971-5981.

Suzuki, K., Y. Kubota, T. Sekito, and Y. Ohsumi. 2007. Hierarchy of Atg proteins in pre-autophagosomal structure organization. *Genes Cells*. 12:209-218.

Sweeney, S.T., and G.W. Davis. 2002. Unrestricted synaptic growth in spinster - A late endosomal protein implicated in TGF-beta-mediated synaptic growth regulation. *Neuron*. 36:403-416.

Takats, S., P. Nagy, A. Varga, K. Pircs, M. Karpati, K. Varga, A.L. Kovacs, K. Hegedus, and G. Juhasz. 2013. Autophagosomal Syntaxin17-dependent lysosomal degradation maintains neuronal function in Drosophila. *J Cell Biol*. 201:531-539.

Tan, J.M.M., E.S.P. Wong, V.L. Dawson, T.M. Dawson, and K.L. Lim. 2008. Lysine 63-linked polyubiquitin potentially partners with p62 to promote the clearance of protein inclusions by autophagy. *Autophagy*. 4:251-253.

Tang, H.W., Y.B. Wang, S.L. Wang, M.H. Wu, S.Y. Lin, and G.C. Chen. 2011. Atg1-mediated myosin II activation regulates autophagosome formation during starvation-induced autophagy. *Embo Journal*. 30:636-651.

Tanida, I., N. Minematsu-Ikeguchi, T. Ueno, and E. Kominami. 2005. Lysosomal turnover, but not a cellular level, of endogenous LC3 is a marker for autophagy. *Autophagy*. 1:84-91.

Tanida, I., Y.S. Sou, J. Ezaki, N. Minematsu-Ikeguchi, T. Ueno, and E. Kominami. 2004. HsAtg4B/HsApg4B/autophagin-1 cleaves the carboxyl termini of three human Atg8 homologues and delipidates microtubule-associated protein light chain 3-and GABA(A) receptor-associated protein-phospholipid conjugates. *Journal of Biological Chemistry*. 279:36268-36276.

Tchernev, V.T., T.A. Mansfield, L. Giot, A.M. Kumar, K. Nandabalan, Y. Li, V.S. Mishra, J.C. Detter, J.M. Rothberg, M.R. Wallace, F.S. Southwick, and S.F. Kingsmore. 2002. The Chediak-Higashi protein interacts with SNARE complex and signal transduction proteins. *Mol. Med.* 8:56-64.

Toda, H., H. Mochizuki, R. Flores, R. Josowitz, T.B. Krasieva, V.J. LaMorte, E. Suzuki, J.G. Gindhart, K. Furukubo-Tokunaga, and T. Tomoda. 2008. UNC-51/ATG1 kinase regulates axonal transport by mediating motor-cargo assembly. *Genes & Development*. 22:3292-3307.

Ullrich, O., S. Reinsch, S. Urbe, M. Zerial, and R.G. Parton. 1996. Rab11 regulates recycling through the pericentriolar recycling endosome. *Journal of Cell Biology*. 135:913-924.

Vadlamudi, R.K., I. Joung, J.L. Strominger, and J. Shin. 1996. p62, a phosphotyrosine-independent ligand of the SH2 domain of p56(lck), belongs to a new class of ubiquitin-binding proteins. *Journal of Biological Chemistry*. 271:20235-20237.

Vlahos, C.J., W.F. Matter, K.Y. Hui, and R.F. Brown. 1994. A specific inhibitor of phosphatidylinositol 3-kinase, 2-(4-morpholinyl)-8-phenyl-4H-1-benzopyran-4-one (LY294002). *J Biol Chem*. 269:5241-5248.

von Muhlinen, N., M. Akutsu, B.J. Ravenhill, A. Foeglein, S. Bloor, T.J. Rutherford, S.M.V. Freund, D. Komander, and F. Randow. 2012. LC3C, Bound Selectively by a Noncanonical LIR Motif in NDP52, Is Required for Antibacterial Autophagy. *Molecular Cell*. 48:329-342.

Wallace, D.C., and W.W. Fan. 2010. Energetics, epigenetics, mitochondrial genetics. *Mitochondrion*. 10:12-31.

Wang, J.W., J.J. Gamsby, S.L. Highfill, L.B. Mora, G.C. Bloom, T.J. Yeatman, T.C. Pan, A.L. Ramne, L.A. Chodosh, W.D. Cress, J.D. Chen, and W.G. Kerr. 2004. Deregulated expression of LRBA facilitates cancer cell growth. *Oncogene*. 23:4089-4097.

Wang, N., W.I. Wu, and A. De Lozanne. 2002. BEACH family of proteins: Phylogenetic and functional analysis of six Dictyostelium BEACH proteins. *Journal of Cellular Biochemistry*. 86:561-570.

Wang, X.L., F.W. Herberg, M.M. Laue, C. Wullner, B. Hu, E. Petrasch-Parwez, and M.W. Kilimann. 2000. Neurobeachin: A protein kinase A-anchoring, beige/Chediak-Higashi protein homolog implicated in neuronal membrane traffic. *Journal of Neuroscience*. 20:8551-8565.

Warrick, J.M., H.L. Paulson, G.L. Gray-Board, Q.T. Bui, K.H. Fischbeck, R.N. Pittman, and N.M. Bonini. 1998. Expanded polyglutamine protein forms nuclear inclusions and causes neural degeneration in Drosophila. *Cell*. 93:939-949.

Wilcke, M., L. Johannes, T. Galli, V. Mayau, B. Goud, and J. Salamero. 2000. Rab11 regulates the compartmentalization of early endosomes required for efficient transport from early endosomes to the trans-golgi network. *Journal of Cell Biology*. 151:1207-1220.

Wild, P., H. Farhan, D.G. McEwan, S. Wagner, V.V. Rogov, N.R. Brady, B. Richter, J. Korac, O. Waidmann, C. Choudhary, V. Dotsch, D. Bumann, and I. Dikic. 2011. Phosphorylation of the Autophagy Receptor Optineurin Restricts Salmonella Growth. *Science*. 333:228-233.

Williams, A., S. Sarkar, P. Cuddon, E.K. Ttofi, S. Saiki, F.H. Siddiqi, L. Jahreiss, A. Fleming, D. Pask, P. Goldsmith, C.J. O'Kane, A. Floto, and D.C. Rubinsztein. 2008. Novel targets for Huntington's disease in an mTOR-independent autophagy pathway. *Nature Chemical Biology*. 4:295-305.

Williams, R.L., and S. Urbe. 2007. The emerging shape of the ESCRT machinery. *Nature Reviews Molecular Cell Biology*. 8:355-368.

Wong, E., and A.M. Cuervo. 2010. Autophagy gone awry in neurodegenerative diseases. *Nature Neuroscience*. 13:805-811.

Wullschleger, S., R. Loewith, and M.N. Hall. 2006. TOR signaling in growth and metabolism. *Cell*. 124:471-484.

Xie, Z.P., and D.J. Klionsky. 2007. Autophagosome formation: Core machinery and adaptations. *Nature Cell Biology*. 9:1102-1109.

Xie, Z.P., U. Nair, and D.J. Klionsky. 2008. Atg8 controls phagophore expansion during autophagosome formation. *Mol. Biol. Cell*. 19:3290-3298.

Xiong, X., R. Tao, R.A. Depinho, and X.C. Dong. 2012. The Autophagy-related Gene 14 (Atg14) Is Regulated by Forkhead Box O Transcription Factors and Circadian Rhythms and Plays a Critical Role in Hepatic Autophagy and Lipid Metabolism. *J Biol Chem*. 287:39107-39114.

Yang, Z.F., and D.J. Klionsky. 2010. Mammalian autophagy: core molecular machinery and signaling regulation. *Curr. Opin. Cell Biol.* 22:124-131.

Yla-Anttila, P., H. Vihinen, E. Jokita, and E.L. Eskelinen. 2009. 3D tomography reveals connections between the phagophore and endoplasmic reticulum. *Autophagy*. 5:1180-1185.

Yorimitsu, T., and D.J. Klionsky. 2005. Atg11 links cargo to the vesicle-forming machinery in the cytoplasm to vacuole targeting pathway. *Mol. Biol. Cell*. 16:1593-1605.

Yousefi, S., R. Perozzo, I. Schmid, A. Ziemiecki, T. Schaffner, L. Scapozza, T. Brunner, and H.U. Simon. 2006. Calpain-mediated cleavage of Atg5 switches autophagy to apoptosis. *Nature Cell Biology*. 8:1124-U1146.

Yu, L., A. Alva, H. Su, P. Dutt, E. Freundt, S. Welsh, E.H. Baehrecke, and M.J. Lenardo. 2004. Regulation of an ATG7-beclin 1 program of autophagic cell death by caspase-8. *Science*. 304:1500-1502.

Zhao, Z., D.J. Ni, I. Ghozalli, S.D. Pirooz, B.Y. Ma, and C.Y. Liang. 2012. UVRAG At the crossroad of autophagy and genomic stability. *Autophagy*. 8:1392-1393.

Zhong, Y., Q.J. Wang, X.T. Li, Y. Yan, J.M. Backer, B.T. Chait, N. Heintz, and Z.Y. Yue. 2009. Distinct regulation of autophagic activity by Atg14L and Rubicon associated with Beclin 1-phosphatidylinositol-3-kinase complex. *Nature Cell Biology*. 11:468-U262.

# 8. Appendix

| Allele | Primers | PCR product (bp) | Application |
|---|---|---|---|
| *bchs17(M)* | 5' CAGTGCTCCAAGTTTGCGTA 3' | 526 | Sequencing |
| | 5' AGAGTGGGACGATCCGCACG 3' | | |
| *bchs58(M)* | 5' CTGGACGTTCCGGAGTTGTAC 3' | 429 | Sequencing |
| | 5' ACAGACGATACGGGAAGCAGC 3' | | |
| *atg7[EY]* | 5' CCTGCAGCCAAGCTTATGAG 3' | 922 | Gel Electrophoresis |
| | 5' TTCTGTGACTCAGTGGGTAAG 3' | | |
| *atg7[d77]* | 5' TGAACATCGATGACAGCCTTG 3' | 752 | Gel Electrophoresis |
| | 5' GTTGCACAGCATTCCACGGA 3' | | |
| *UAS-atg1[6A]* | 5' TCAAACAAGCAAAGTGAACACG 3' | 715 | Gel Electrophoresis |
| | 5' AGAGCCACCACATTCTCATG 3' | | |
| *UAS-bchsRNAi* (VDRC 45028) | 5' TCAAACAAGCAAAGTGAACACG 3' | 595 | Gel Electrophoresis |
| | 5' CAGACGATACGGGAAGCAGC 3' | | |
| *UAS-bchsRNAi* (VDRC 110785) | 5' TCAAACAAGCAAAGTGAACACG 3' | 492 | Gel Electrophoresis |
| | 5' CGACGACATGCTGCACATACT 3' | | |
| *UAS-dicer2* | 5' TTCGTGAATTTCCAGGAGAGC 3' | 597 | Gel Electrophoresis |
| | 5' CACAGAAGTAAGGTTCCTTCACAAAGATCC 3' | | |

**Table 3.** PCR primers and applications to verify positive recombinants. The alleles for different genes used during homologous recombination and their specific primer pairs to perform PCR are shown. The respective PCR product sizes and downstream applications for detection are indicated.

Third instar larval brain volume measurement

1. Canton S
2. C155
3. yw
4. yw; bchs58(O)
5. yw; bchs58(O)/Df(2L)clot7
6. C155/yw
7. C155/yw; EP2299/+

RP2 motor neuron viability assay

A) Drug feedings
   1. yw; +; RRaCD8GFP
   2. yw; bchs58(O)/Df(2L)clot7; RRaCD8GFP
   3. yw; bchs58(M)/Df(2L)clot7; RRaCD8GFP
   4. yw; bchs17(M)/Df(2L)clot7; RRaCD8GFP
B) Genetic interactions
   1. yw; +; RRaCD8GFP
   2. yw; bchs58(M)/Df(2L)clot7; RRaCD8GFP
   3. yw; bchs17(M)/Df(2L)clot7; RRaCD8GFP
   4. yw; atg7[EY]/+; RRaCD8GFP
   5. yw; atg7[d77]/+; RRaCD8GFP
   6. yw; bchs58(M), atg7[EY]/Df(2L)clot7; RRaCD8GFP
   7. yw; bchs58(M), atg7[d77]/Df(2L)clot7; RRaCD8GFP
   8. yw; bchs17(M), atg7[EY]/Df(2L)clot7; RRaCD8GFP
   9. yw; bchs17(M), atg7[d77]/Df(2L)clot7; RRaCD8GFP
   10. yw; UAS-bchsRNAi (45028), UAS-dicer2/Df(2L)clot7; RRaCD8GFP

Ubiquitinated aggregates size measurement in larval NMJs

A) Fed on standard food
   1. yw
   2. yw; bchs58(O)/Df(2L)clot7
   3. yw; bchs58(M)/Df(2L)clot7
   4. yw; bchs17(M)/Df(2L)clot7
B) Fed on standard food containing autophagy-modulating drugs
   1. yw
   2. yw; bchs58(M)/Df(2L)clot7
   3. yw; bchs17(M)/Df(2L)clot7

Colocalization analysis of endogenous Bchs with expressed compartmental markers

A) Nutrient starvation
   1. C155/+; +; UAS-RFP-Atg5/+
   2. C155/+; +; UAS-mCherry-Atg8a/+
   3. C155/+; UAS-Rab11-GFP/+
   4. C155/+; +; UAS-Spinster-GFP/+
B) Rapamycin treatment
   1. C155/+; +; UAS-RFP-Atg5/+
   2. C155/+; +; UAS-mCherry-Atg8a/+
   3. C155/+; UAS-Rab11-GFP/+
   4. C155/+; +; UAS-Spinster-GFP/+
C) Huntingtin exon one poly-glutamine Q20 expression
   1. C155/+; UAS-Htt exon1-Q20/+; UAS-RFP-Atg5/+
   2. C155/+; UAS-Htt exon1-Q20/+; UAS-mCherry-Atg8a/+
   3. C155/+; UAS-Htt exon1-Q20/UAS-Rab11-GFP
   4. C155/+; UAS-Htt exon1-Q20/+; UAS-Spinster-GFP/+
D) Huntingtin exon one poly-glutamine Q93 expression
   1. C155/+; UAS-Htt exon1-Q93/+; UAS-RFP-Atg5/+
   2. C155/+; UAS-Htt exon1-Q93/+; UAS-mCherryAtg8a/+
   3. C155/+; UAS-Htt exon1-Q93/UAS-Rab11-GFP
   4. C155/+; UAS-Htt exon1-Q93/+; UAS-Spinster-GFP/+

Immunocytochemistry for autophagic structures and ubiquitinated conjugates

1. yw
2. yw; bchs17(M)/Df(2L)clot7
3. C155/+; UAS-Htt exon1-Q93/+

Live trafficking studies of GFP-Bchs with RFP-Atg5 or mCherry-Atg8a

1. C155/+; UAS-GFP-Bchs/+; UAS-RFP-Atg5/+
2. C155/+; UAS-GFP-Bchs/+; UAS-mCherry-Atg8a/+

**Table 4.** A complete list of final *Drosophila melanogaster* genotypes used in each of the different experiments in this study.

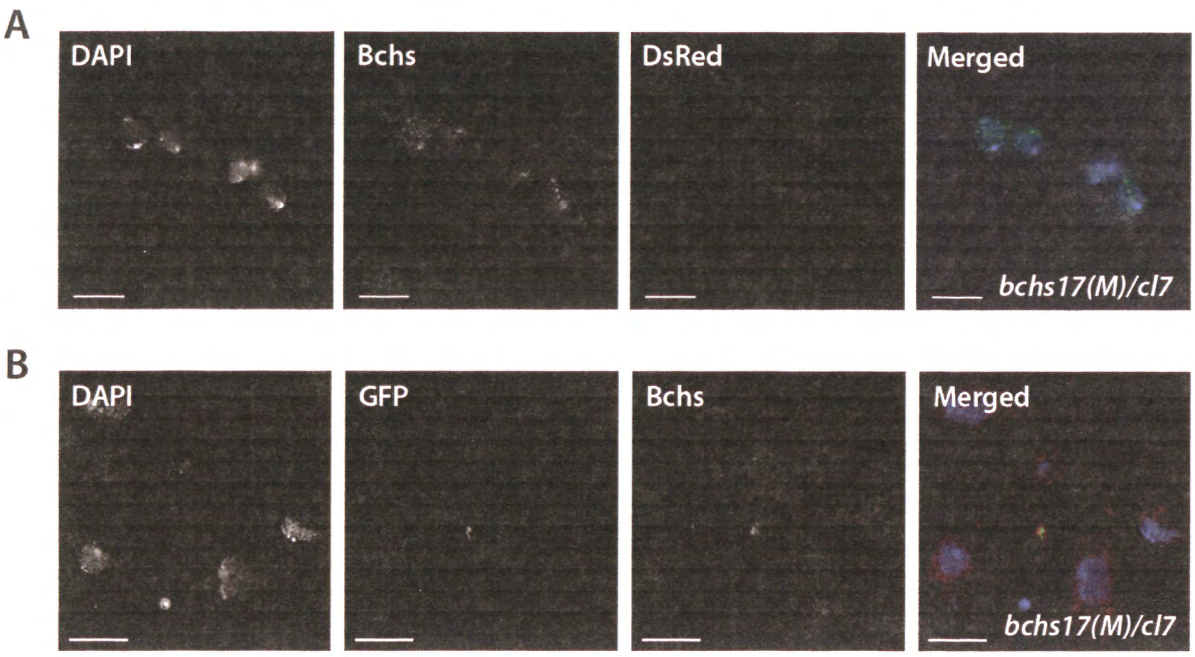


**Appendix Figure 1.** Negative control to validate the specificity of Bchs and fluorophore-tagged compartmental markers immunostaining. Third instar larval primary neurons from *bchs17(M)/cl7* (putative *bchs* null) genotype were **(A)** incubated with anti-Bchs and anti-DsRed antibodies or **(B)** incubated with anti-GFP and anti-Bchs antibodies in the absence of RFP-Atg5, mCherry-Atg8a, Rab11-GFP and Spinster-GFP expression. Images were acquired at 100x magnification and the scale-bar represents 10 µm.

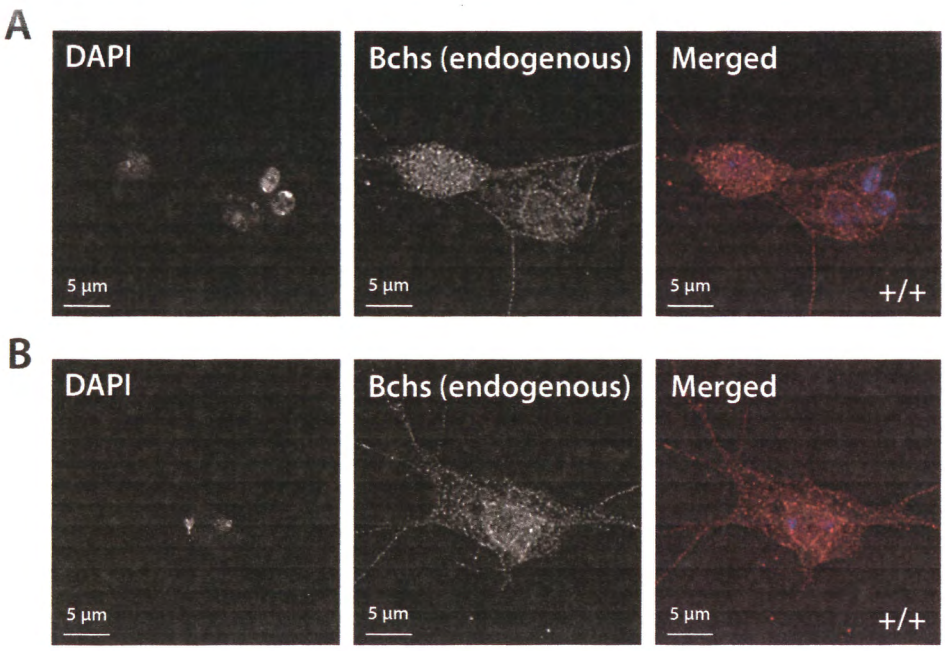


**Appendix Figure 2.** Bchs protein localizes occasionally onto nuclear membrane and nuclei under basal autophagy. Wild-type primary neurons from third instar larval brains were cultured in complete medium and immunostained for endogenous Bchs. Out of an estimated 150 single-plane images acquired, one image shows the distinct localization of Bchs **(A)** on nuclear membrane and another image **(B)** in nucleus other than the general observation of a homogeneous Bchs punctate distribution throughout the cell.

## 9. Author's Publications

Kriston-Vizi, J., N.W. Thong, C.L. Poh, K.C. Yee, J.Sim, R. Kraut, and M. Wasser. 2011. Gebiss: an ImageJ plugin for the specification of ground truth and the performance evaluation of 3D segmentation algorithms. *BMC Bioinformatics*. 12:232.

Mok, S., M. Imwong, M.J. Mackinnon, J. Sim, R. Ramadoss, P. Yi, M. Mayxay, K. Chotivanich, K.Y. Liong, B. Russell, D. Socheat, P.N. Newton, N.P. Day, N.J. White, P.R. Preiser, F. Nosten, A.M. Dondorp, and Z. Bozdech. 2011. Artemisinin resistance in Plasmodium falciparum is associated with an altered temporal pattern of transcription. *BMC Genomics*. 12:391.

Sim, P.L., and K. Heese. 2010. Ligand-dependent activation of the chimeric tumor necrosis factor receptor-amyloid precursor protein (APP) reveals increased APP processing and suppressed neuronal differentiation. *Neurosignals*. 18:9-23.

## 10. Posters

Poster Presenter at the 6$^{th}$ International Symposium on Autophagy (ISA) 2012, Okinawa, Japan

Poster Presenter at the 6$^{th}$ Forum of European Neuroscience (FENS) 2008, Geneva, Switzerland